

**COOPERATIVE MAGNETOPHORESIS OF  
MAGNETIC NANOPARTICLES UNDER  
HYDRODYNAMIC REGIME: EXPERIMENTAL  
AND THEORETICAL STUDY**

**WONG YI XUAN**

**UNIVERSITI TUNKU ABDUL RAHMAN**

**COOPERATIVE MAGNETOPHORESIS OF MAGNETIC  
NANOPARTICLES UNDER HYDRODYNAMIC REGIME:  
EXPERIMENTAL AND THEORETICAL STUDY**

**WONG YI XUAN**


**A project report submitted in partial fulfilment of the  
requirements for the award of  
Bachelor of Engineering (Honours) Petrochemical Engineering**

**Faculty of Engineering and Green Technology  
Universiti Tunku Abdul Rahman**

**MAY 2023**

**DECLARATION**

I hereby declare that this project report is based on my original work except for citation and quotation which have been duly acknowledged. I also declare that it has not been previously and concurrently submitted for any other degree or award at UTAR or other institutions.

Signature :  \_\_\_\_\_

Name : \_\_\_ WONG YI XUAN \_\_\_\_\_

ID No. : \_\_\_ 18AGB04492 \_\_\_\_\_

Date : \_\_\_ 29/4/2023 \_\_\_\_\_

**APPROVAL FOR SUBMISSION**

I certify that this project report entitled “**COOPERATIVE MAGNETOPHORESIS OF MAGNETIC NANOPARTICLES: EXPERIMENTAL AND THEORETICAL STUDY**” was prepared by **WONG YI XUAN** have met the required standard for submission in partial fulfilment of the requirements for the award of Bachelor of Engineering (Honours) Petrochemical Engineering at Universiti Tunku Abdul Rahman.

Approved by,

Signature : \_\_\_\_\_

Supervisor : \_\_\_\_\_

Date : \_\_\_\_\_

The copyright of this report belongs to the author under the terms of the copyright Act 1987 as qualified by Intellectual Property Policy of Universiti Tunku Abdul Rahman. Due acknowledgement shall always be made of the use of any material contained in, or derived from, this report.

© 2023, Wong Yi Xuan, All right reserved.

Specially dedicated to  
my beloved, father, mother and all my friends.

## ACKNOWLEDGEMENTS

I would like to express my deepest gratitude to all those who have contributed to the successful completion of this project. I extend my heartfelt thanks to my research supervisors, Dr. Yeoh Wei Ming, Dr. Leong Sim Siong, and Dr. Toh Pey Yi for their invaluable advice, guidance, and unwavering support throughout the development of this research.

Their dedication and expertise have been instrumental in shaping my understanding of the subject matter and have helped me to navigate through the various challenges that arose during the research process. Their constant encouragement, patience, and constructive criticism have been invaluable in shaping the direction of this project

In addition, I would also like to express my gratitude to my loving parent and friends who had helped and given me encouragement to face every challenge and come out better and wiser than before.

## **COOPERATIVE MAGNETOPHORESIS OF MAGNETIC NANOPARTICLES: THEORETICAL AND EXPERIMENTAL STUDY**

### **ABSTRACT**

This project focuses on modelling of the magnetophoresis kinetics of magnetic nanoparticles (MNPs) under the cooperative and hydrodynamic regimes so that the understanding towards the transport mechanism of this separation process can be further enhanced. The study begins with the functionalization of MNPs with poly(sodium 4-styrenesulfonate) (PSS) at different mass ratios, with the aim to identify the optimal MNP to PSS mass ratio during the functionalization process to produce MNPs with the highest colloidal stability. Here, the MNP system functionalized under the MNP to PSS ratio of 1:1 is found to be exhibiting the highest colloidal stability among all MNP system produced in this study, hence, it is chosen as the model system to be used in the subsequent magnetophoresis experiments. According to the experimental results of the magnetophoresis kinetics measurement, the cooperative effect is found to be more apparent during the higher MNP concentration, in which the separation time reduced by 66 % when the MNP concentration is increased from 50 mg/L (separation time of 162 s) to 300 mg/L (separation time of 54 s). In addition, the hydrodynamic effect is also revealed to be dominating the magnetophoresis experiment that is conducted in this study due to the continuity homogeneity of the MNP solution throughout the entire timescale of the experiment, owing to the consistent agitation of induced convective current within the MNP solution. The final objective of this study is to develop a mathematical model that can predict the magnetophoresis kinetic profile under the simultaneous presence of both cooperative and hydrodynamic effects. The modelling was conducted by assuming the continuous homogeneity of the MNP solution (by incorporating the hydrodynamic effect) and occurrence of tip-to-tip aggregation (by incorporating the cooperative effect), which



results in prediction results that are in good agreement with the experimental results. For instance, the model prediction is also showing a consistent trend in which the separation rate is more rapid for the magnetophoresis conducted under the higher MNP concentration. This study has successfully developed a mathematical model that is able to predict the magnetophoresis kinetics up to a good accuracy, which can be useful in the design of the low gradient magnetic separation in various industrial applications.

## TABLE OF CONTENTS

<b>DECLARATION</b>	<b>iii</b>
<b>APPROVAL FOR SUBMISSION</b>	<b>iv</b>
<b>ACKNOWLEDGEMENTS</b>	<b>vii</b>
<b>ABSTRACT</b>	<b>viii</b>
<b>TABLE OF CONTENTS</b>	<b>x</b>
<b>LIST OF TABLES</b>	<b>xiii</b>
<b>LIST OF FIGURES</b>	<b>xiv</b>
<b>LIST OF APPENDICES</b>	<b>xxiv</b>

### CHAPTER

<b>1</b>	<b>INTRODUCTION</b>	<b>1</b>
	1.1 Magnetic Nanoparticles (MNPs)	1
	1.2 Magnetophoresis of Magnetic Nanoparticles	2
	1.3 Mathematical Modelling on Magnetophoresis of MNPs	5
	1.4 Problem Statement	8
	1.5 Objectives	10
<b>2</b>	<b>LITERATURE REVIEW</b>	<b>11</b>
	2.1 Magnetic Nanoparticles (MNPs)	11
	2.1.1 Application of MNPs	19
	2.1.2 Advantages and Disadvantages of MNPs	22
	2.2 Magnetophoresis of MNPs	23
	2.2.1 Cooperative Effect	23
	2.3 Deviation from Classical Magnetophoresis Theory	29
	2.3.1 Cooperative Effect of Magnetophoresis	29
	2.2.2 Hydrodynamic Effect	35

	2.2.3	Unified View of Magnetophoresis	42
2.4		Modelling of Magnetophoresis Kinetics	45
	2.4.1	Classical Magnetophoresis Model	45
	2.4.2	Cooperative Magnetophoresis Model	49
	2.4.3	Hydrodynamic Magnetophoresis Model	52
2.5		Research Gap	55
<b>3</b>		<b>METHODOLOGY</b>	<b>57</b>
	3.1	Flowchart	57
	3.2	Material and Equipment	58
	3.3	Functionalization of MNPs	59
	3.4	Dynamic Light Scattering (DLS)	60
	3.5	Experimental Methods	60
<b>4</b>		<b>RESULT AND DISCUSSION</b>	<b>62</b>
	4.1	Functionalization of Magnetic Nanoparticles (MNPs)	62
	4.2	Magnetophoresis Kinetics of MNP Solution under Cooperative and Hydrodynamic Regimes: An Experimental Approach	68
	4.2.1	Calibration of Customized UV-Vis Spectrophotometer	68
	4.2.2	Time-Lapse Images of MNP Solution During Magnetophoresis	70
	4.2.3	Separation Kinetics Profile of MNP Solutions under Cooperative and Hydrodynamically Driven Magnetophoresis	75
	4.3	Modelling the Kinetics of Magnetophoresis in the Presence of Cooperative and Hydrodynamic Effects	77
	4.3.1	Aggregation Kinetics	78
	4.3.2	Magnetophoresis Kinetics	86
	4.3.3	Analysis on the Simulation Results from the Mathematical Model	88
<b>5</b>		<b>CONCLUSION</b>	<b>95</b>

		xii
5.1	Conclusion	95
5.2	Recommendations and Improvements	97
<b>REFERENCES</b>		<b>98</b>
<b>APPENDIX</b>		<b>104</b>

**LIST OF TABLES**

<b>TABLES</b>	<b>TITLE</b>	<b>PAGE</b>
3.1	Materials Used in the Experiment	58
3.2	Equipment Used in the Experiment	58
3.3	MNPs to PSS Mass Ratio Used in the Experiment	60
4.1	Average Hydrodynamic Size of MNP System Functionalized Under Different MNP:PSS ratio	64
4.2	Image J Analysis on Time-Lapse Image of MNP Solution During Magnetophoresis	73

## LIST OF FIGURES

<b>FIGURES</b>	<b>TITLE</b>	<b>PAGE</b>
1.1	TEM Image of Iron Oxide Magnetic Nanoparticles	2
2.1	Structure of a Regular MNP	12
2.2	Concept of Domains, Domain Walls, Magnetons; Magnetisation Degree of Ferromagnetic and Superparamagnetic Materials Under Magnetic Field and Without Magnetic Field	13
2.3	Hysteresis Loops of Superparamagnetic and Ferromagnetic Materials. X-axis Represents the Direction of an External Applied Magnetic Field; Y-axis Represents the Degree of Magnetization	15
2.4	Hysteresis Loops of Superparamagnetic, Ferromagnetic, and Paramagnetic Materials	16
2.5	Magnetic behaviour of different sized particles	17
2.6	Magnetism Reversal Spin Modes (a) Coherent Rotation, (b) Eddy Mode	18
2.7	Relationship between Coercivity and MNPs Size	18

2.8	Magnetic Separation Technique	20
2.9	Magnetic Resonance Images (A) without MRI agent (B) with MRI Agent	21
2.10	High Gradient Magnetic Separation and Low Gradient Magnetic Separation	28
2.11	Experiment Setup of LGMS	30
2.12	Motion of MNPs under an external applied magnetic field (a) 0 s, (b) 120 s, (c) 240 s, (d) 360 s	30
2.13	Cooperative Magnetophoresis and Non-cooperative Magnetophoresis	31
2.14	DLVO Interaction Curve	32
2.15	DLVO Interaction Curve with an External Applied Magnetic Field	33
2.16	Separation Kinetic Profiles with (a) Different MNPs Concentrations and (b) Different Measurement Positions	37
2.17	Time Lapse Image of Experiment Result	37
2.18	(a) Simulation Result without MNPs/Fluid Interaction. (b) Comparison of Separation Kinetic Profile between Simulation Result (Solid Lines) and Experiment Result (Markers)	38

2.19	Time Lapse Image with Different MNPs concentrations	39
2.20	Differences between Magnetophoresis and Natural Convection	40
2.21	Hydrodynamic Effect at Different Conditions	42
2.22	Aggregation Parameter against Magnetic Grashof Number	43
2.23	Concentration of MNPs against Magnetic Field Gradient	44
2.24	Concentration of MNPs against Magnetic Field Gradient, The MNPs Concentration and Magnetic Field Gradient in the Black-frame are given by 10-10000 mg/L and 1-100 T/m, respectively	45
2.25	Comparison between the Experiment Result (Markers Represent $\gamma$ -Fe <sub>2</sub> O <sub>3</sub> Nanocrystals with hydrodynamic diameter of 12 nm) and the Predicted Result (Solid Lines)	48
2.26	Comparison between the Experiment Result (Circles correspond to Sample S2 Core ( $\gamma$ -Fe <sub>2</sub> O <sub>3</sub> )/Shell (SiO <sub>2</sub> ) with hydrodynamic diameter of 82 nm, Circles correspond to Sample S3 Core ( $\gamma$ -Fe <sub>2</sub> O <sub>3</sub> )/Shell (SiO <sub>2</sub> ) with hydrodynamic diameter of 157 nm) and the Predicted Result (Solid Lines) at Magnetic Field of 60 T/m	49



2.27	The Scaled Bjerrum Length against the Diameter of MNPs	50
2.28	Separation Time Against Scaled Average Distance	52
2.29	Comparison between the Predicted Result with MNPs/Fluid Interaction Model to the Experimental Result	55
3.1	Flow Chart of the Project	57
3.2	Experimental Setup	61
4.1	The Sedimentation Time Lapse Images of MNP Solution with Different MNP to PSS Ratio	63
4.2	Average Hydrodynamic Size of MNP System Functionalized Under Different MNP:PSS Ratio	65
4.3	Hydrodynamic Size Distribution	67
4.4	Calibration Curve of MNP Solutions (1:1 Ratio)	69
4.5	Time Lapse Images of MNP Solutions (with Concentration of 50 mg/L, 75 mg/L, 125 mg/L, 175 mg/L, and 300 mg/L) for 10 Minutes After Being Subjected to Magnetophoresis	71
4.6	Mean Versus Time of MNP Solution During Magnetophoresis	74

4.7	Standard Deviation Versus Time of MNP Solution During Magnetophoresis	74
4.8	Magnetophoresis Kinetic Profile (with Concentration 50 mg/L, 75 mg/L, 125 mg/L, 175 mg/L, 300 mg/L,) During Magnetophoresis	76
4.9	Time to Achieve 80 % Separation	76
4.10	Free Volume Swept Through by the Elongated Aggregate (Magnetic Species A)	82
4.11	The Relationship Between the Number of Magnetic Species and Time	85
4.12	Magnetophoresis Kinetics Profile with Concentrations (a) 50 mg/L, (b) 75 mg/L, (c) 125 mg/L, (d) 175 mg/L, and (e) 300 mg/L. The Solid Lines Denote the Magnetophoresis Kinetic Predicted by the Mathematical Model while Markers Denote the Experimental Result	90
4.13	Magnetophoresis Kinetic Profile (Normalised Concentration Against Time Graph) of MNP Solution (with Concentration 50 mg/L, 75 mg/L, 125 mg/L, 175 mg/L, 300 mg/L) Subjected to an External Magnetic Field Created by NDFeB Magnet. The Solid Lines are the Magnetophoresis Kinetic Predicted by the Mathematical Model while Markers are the Experiment Result	91
4.14	Average MNP Clusters in a Magnetic Species	94

## LIST OF SYMBOLS / ABBREVIATIONS

$\nabla B$	Magnetic Flux Density Gradient, $T\ m^{-1}$
$B$	Magnetic Flux Density, T
$N^*$	Dimensionless Aggregation Parameter
$T_C$	Curie Temperature, K
$T_N$	Neel Temperature, K
$M_S$	Magnetization Saturation, $A\ m^2\ kg^{-1}$
$H_C$	Coercivity, $A\ m^{-1}$
$D_{cr}$	Critical Diameter for the Particle Transition from the Multidomain to Single Domain, m
$D_{sp}$	Critical Diameter for Superparamagnetic State, m
$\chi$	Magnetic Susceptibility, $m^3\ kg^{-1}$
$F_M$	Magnetophoretic Force, N
$\mu$	Magnetic Moment Possessed by the MNP, $A\ m^2\ kg^{-1}$
$b$	Required Magnetic Field Intensity to Reach the Magnetization Saturation
$M_{S(m)}$	Saturation Magnetization of the MNP (per Mass Basis), $A\ m^2\ kg^{-1}$
$M_{(m)}$	Magnetization of the MNP (per Mass Basis), $A\ m^2\ kg^{-1}$
$M_{S(v)}$	Magnetization Saturation per Unit Volume, $A\ m^{-1}$

$M_{(v)}$	Magnetization per Unit Volume, $A\ m^{-1}$
$F_D$	Viscous Drag Force, N
$\eta$	Viscosity of the Fluid, $Pa\ s^{-1}$
$D_h$	Hydrodynamic Diameter, m
$v$	Velocity of the MNP, $m\ s^{-1}$
$v_s$	Velocity of MNPs at Magnetization Saturation, $m\ s^{-1}$
$D_f$	Diffusivity of MNPs, $m^2\ s^{-1}$
$sk_B$	Boltzmann Constant, $J\ K^{-1}$
$T$	Absolute Temperature, K
$m_p$	Mass of the MNP, kg
$g$	Gravitational Acceleration Vector, $m\ s^{-2}$
$D$	Diameter of a MNP, m
$F_B$	Buoyancy Force, N
$\rho_f$	Fluid Density, $kg\ m^{-3}$
$F_{MB}$	Magnetic Buoyancy Force, N
$r$	Radius of a MNP, m
$H_o$	Magnetic Strength at the centre of the MNP, T
$\lambda_B$	Magnetic Bjerrum Length, m
$c$	MNPs Concentration, $kg\ m^{-3}$
$c_s$	MNPs Concentration of the Surface in the Vicinity of the Magnet Source, $kg\ m^{-3}$
$c_\infty$	MNPs Concentration in Bulk Solution, $kg\ m^{-3}$
$L_c$	Characteristic Length, m

$r_s$	Distance from the Centre to A Radius of the SEGMAP System, m
$L$	Distance from the Centre to the Wall Surface of the SEGMAP system, m
$t$	Time, s
$r_o$	A Distance with No Magnetic Field, m
$d_p$	Interparticle Distance, m
$t_s$	Separation Time, s
$v_f$	Velocity of the MNPs Solution, m s <sup>-1</sup>
$p_{abs}$	Absolute Pressure, Pa
$f_m$	Magnetophoretic Force per Unit Volume, N m <sup>-3</sup>
$B_r$	Remnant Magnetic Flux Density, T
$y$	Vertical Distance from the Pole Face of the Cylindrical Magnet, m
$h_{mag}$	Height of the Cylindrical Magnet, m
$r_{mag}$	Radius of the Cylindrical Magnet, m
$e^y$	Unit Vector Pointing to the Positive y-direction
$e^x$	Unit Vector Pointing to the Positive x-direction
$e^z$	Unit Vector Pointing to the Positive z-direction
$H$	Magnetic Flux Intensity, T
$\mu_o$	Permeability of Free Space in Water, H m <sup>-1</sup>
$m_o$	Magnetic Dipole Moment of a MNP Cluster, A m <sup>2</sup>
$\bar{v}$	Average Velocity of Magnetic Species in the Solution, m s <sup>-1</sup>

$V$	Volume of the Solution, $\text{m}^3$
$d_{H,0}$	Hydrodynamic Diameter of a Spherical MNP, m
$v_z _{z=0}$	Velocity of MNPs at the Collection Plane, $\text{m s}^{-1}$
$F_{mag} _{z=0}$	Magnetophoretic Force at the Collection Plane, N
$F_d _{z=0}$	Viscous Drag Force at the Collection Plane, N
$A_S$	Surface Area of the Collection Plane, $\text{m}^2$
$N^*$	Dimensionless Aggregation Parameter
$b$	Required Magnetic Field Intensity to Reach the Magnetization Saturation
$E_D$	Magnetic Energy of Two Particles at a Certain Distance
$\lambda$	Dipole Coupling Constant
$\lambda_{B(scaled)}$	Scaled Bjerrum Length
$\Gamma$	Magnetic Coupling Constant
$\phi_o$	Volume Fraction of Particles
$Gr_m$	Dimensionless Magnetic Grashof Number
$\beta$	A Dimensionless Parameter
$f$	Fraction of Particles Inside the Magnetic Separator
$t_0$	Fitting Experiment Data
$\alpha$	Fitting Experiment Data
$n_o$	Initial Number of Individual MNP Clusters
$n$	Number of Magnetic Species
$\bar{s}$	Average Number of MNP Clusters in a MNP Aggregate

$Z$	Fraction of Successful Aggregation
$f_a$	Total Aggregation Frequency
$\alpha$	Separation Factor
TEM	Transmission Electron Microscopy
MNPs	Magnetic Nanoparticles
PSS	Poly(sodium 4-styrenesulfonate)
AC	Alternating Current
DNA	Deoxyribonucleic Acid
MRI	Magnetic Resonance Imaging
HGMS	High Gradient Magnetic Separation
LGMS	Low Gradient Magnetic Separation
DLVO	Derjaguin, Landau, Verwey and Overbeek
DLS	Dynamic Light Scattering
SD	Standard Deviation
MB	Methylene Blue
RF	Radio Frequency

**LIST OF APPENDICES**

<b>APPENDIX</b>	<b>TITLE</b>	<b>PAGE</b>
A	Calculation of Aggregation Parameter and Magnetic Grashof Number	104
B	Magnetophoresis Kinetic Profile Calculation	109



## CHAPTER 1

### INTRODUCTION

#### 1.1 Magnetic Nanoparticles (MNPs)

Magnetic nanoparticles (MNPs) are considered as a subclass of nanomaterials that have paramagnetic, ferromagnetic, or superparamagnetic properties made of metals like cobalt, nickel, and iron (Yang et al., 2019). Commonly, the size of the MNPs ranges between 1 nm to 100 nm (Horikoshi and Serpone, 2013). MNPs have attracted the attention and interest of scientists, in which a tremendous amount of research has been conducted on MNPs due to their unique physicochemical properties and size. There is a wide spectrum of applications that can be contributed by MNPs, in particular, the iron oxide MNPs are found to be useful in therapeutic and clinical diagnosis (Gul et al., 2019). Supermagnetism and biocompatibility features of MNPs allow their applications in biomedical science, biotechnology, and environmental areas (Akbarzadeh, Samiei and Davaran, 2012). More specifically, MNPs are suitable for targeted drug delivery, hypothermia, magnetomechanical actuation of cell surface receptors, biomedical imaging, and triggered drug release (Savliwala et al., 2020).

The nanoscale size of MNPs has brought excellent features in various fields. Firstly, MNPs can be tailored into different sizes and functionalized with coating for targeted applications (Taira et al., 2009). At nanorange, domain walls will gradually diminish and form a single domain that provides superparamagnetic properties with no coercivity which allow MNPs to be manipulated through magnetic fields easily (Akbarzadeh, Samiei and Davaran, 2012). Furthermore, the surface area is closely related to the size of an object, thus, MNPs exhibit high- surface-to-volume ratio. As

a case in point is increased sorption capacities of MNPs for drug delivery, heavy metal removals, and adsorption separation (Lim et al., 2013). The transmission electron micrograph (TEM) image of the pure magnetite is illustrated in Figure 1.1.

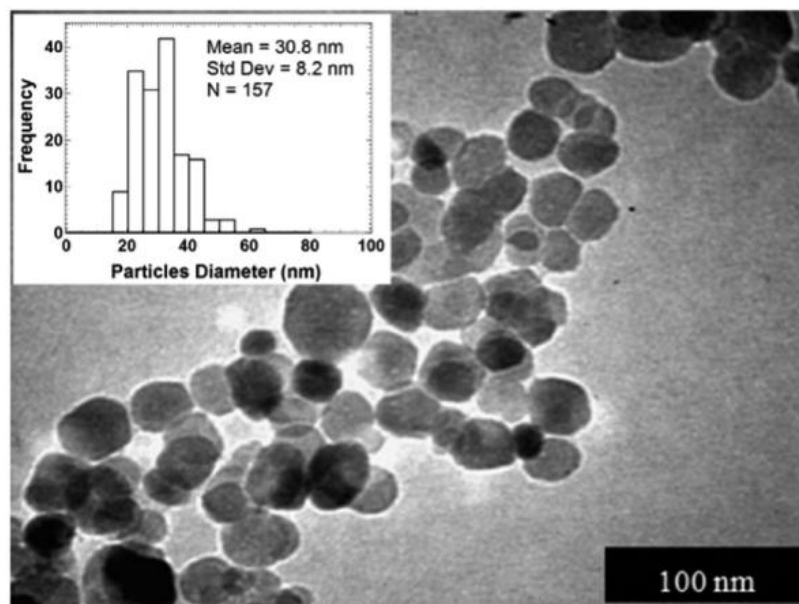


**Figure 1.1: TEM Image of Iron Oxide Magnetic Nanoparticles (Yeap et al., 2014).**

## 1.2 Magnetophoresis of Magnetic Nanoparticles

Migration of MNPs in relative to the surrounding fluid under the action of an external magnetic field is known as magnetophoresis (Lim et al., 2010). According to the moving direction of the MNPs towards or away from the magnetic source, this phenomenon can be further classified into positive magnetophoresis and negative magnetophoresis. The movement of magnetic particles in a diamagnetic medium is known as positive magnetophoresis, as the MNPs are migrated toward the magnetic source under this scenario. On the other hand, the movement of diamagnetic particles in a magnetic media is known as negative magnetophoresis because the MNPs are being driven away from the magnetic source due to the magnetic buoyancy effect (Munaz, Shiddiky and Nguyen, 2018). A gradient of magnetic field, a gradient of magnetisation of the surrounding medium or the presence of both gradients

simultaneously are required to impose magnetophoretic force towards MNPs and induce the occurrence of magnetophoresis.

Magnetophoresis is favourable amongst other active particles manipulation techniques such as thermophores, dielectrophoresis, optical trapping, acoustophoresis, and electrophoresis. Firstly, the properties of sample solution such as pH value, ion concentration, temperature, surface charge will not be affected by magnetophoresis because magnetophoresis is a contactless active particle manipulation technique. In addition, the particle manipulated by magnetophoresis also offers other advantages including low cost, simple design, and easy to operate (Gómez-Pastora et al., 2022).

From the classical point of view, magnetophoresis involves only MNPs that migrate individually through a quiescent fluid under the action of an external magnetic field. However, such a classical picture on magnetophoresis breaks down under real time experiments, as demonstrated by the experiments conducted by Yavuz et al. (2006) which successfully removed arsenic using  $\text{Fe}_3\text{O}_4$  nanocrystals (with size range of 12 to 20 nm) under low gradient magnetic field ( $\nabla B < 100 \text{ T/m}$ ) within relatively short duration (24 hours). By doing estimation using the well-known magnetostatics theory, Yavuz and his co-workers could not describe the separation of such  $\text{Fe}_3\text{O}_4$  nanocrystals under low gradient magnetic field if the nanocrystals are penetrating individually within a stagnant solution. Thus, such a contradiction between experimental results and theoretical calculation has made researchers to believe the microscopic picture of real time magnetophoresis has been deviated from the classical point of view, which can be initiated by certain possible interactions that occur within the magnetophoresis system (and being ignored in the classical magnetophoresis theory).

The first interaction is the particle-particle interaction that might occur during the magnetophoresis of MNPs, due to the magnetic dipole moment possessed by them. As MNPs can be magnetised under magnetic fields and acquire magnetic dipole moments, they behave like ‘tiny magnets’ that can be attracted among each other when they are sufficiently close. Such a phenomenon will lead to the formation of larger MNP aggregate that can be driven more rapidly towards the magnetic source (De Las Cuevas, Faraudo and Camacho 2008). This phenomenon is known as cooperative effect of magnetophoresis and it is the underlying reason that explains the much faster

separation of MNPs observed in the experiments as compared to the classical magnetophoresis theory calculation, as reported by Yavuz et al. (2006). In addition, such an enhancement in the separation rate is also being reported by De Las Cuevas, Faraudo and Camacho (2008). By looking at the occurrence of particle-particle interaction, magnetophoresis can be classified into cooperative magnetophoresis and noncooperative magnetophoresis (Andreu *et al.*, 2011). The former is a swift process involving particle-particles interaction amongst the MNPs; whereas the latter only involves the movement of individual particles in a stagnant fluid (as assumed by the classical point of view).

Later, it has been discovered that the interaction between MNP and the surrounding fluid also can alter the dynamical behaviour of magnetophoresis significantly. Such an interaction originates from the viscous effect of the fluid, and it involves the momentum transfer between MNPs and the surrounding fluid when the MNPs are moving during magnetophoresis. As a result of the momentum transfer, the surrounding fluid gains momentum and starts flowing convectively, which is contradictory with the stagnant fluid condition as assumed by the classical magnetophoresis point of view. Due to the presence of magnetophoresis, the result is deviated significantly from the prediction by classical magnetophoresis theory. Such a particle-fluid interaction is denoted as hydrodynamic effect magnetophoresis. In addition, it also has been proven that the separation rate of MNPs can be improved remarkably by the hydrodynamic effect, through both experimental and theoretical approaches (Leong et al., 2015).

Due to the co-exist of both cooperative and hydrodynamic effects in a magnetophoresis system, the dynamical behaviour of the magnetophoresis process can be very distinctive as compared to the prediction of classical magnetophoresis theory. Furthermore, it has been proven that cooperative and hydrodynamic effects can be dominating in almost all real time applications of magnetophoresis (Leong et al., 2020). Therefore, it is crucial to elucidate the dynamical behaviour of the magnetophoresis process in which both cooperative and hydrodynamic effects occur simultaneously.

### 1.3 Mathematical Modelling on Magnetophoresis of MNPs

One of the best methods to understand a phenomenon is to build a mathematical model to describe it. With an appropriate and well-developed mathematical model, the phenomenon can be predicted and described precisely. Scientists are always striving to figure out a mathematical model to predict the kinetics of magnetophoresis.

According to classical magnetophoresis theory assumptions, kinetics of non-cooperative magnetophoresis can be predicted by a relatively simple analytical model. As a pioneer in this field, Andreu *et al.* (2011) have developed a model to describe the concentration profile of MNPs solution subjected to a uniform magnetic gradient by assuming there are no particle-particle interactions in the magnetophoresis process. The particles are moving individually within a stagnant fluid under an external applied magnetic field. Besides, the MNPs are assumed to be of a perfect sphere, and the magnetisation curve is described by a Langevin function. In addition, the sedimentation of MNPs due to gravitational force is neglected in the modelling, as the sedimentation velocity is much smaller than the magnetophoresis velocity. Due to the symmetrical geometry of the experimental setup (the MNPs are moving out in the radial direction toward the wall of a cylindrical container), the separation efficiency of MNPs can be described by an analytical formula under this configuration. The prediction of the model is revealed to be well-aligned with the experimental results, which have validated the accuracy of the model.

However, the modelling according to the classical magnetophoresis theory assumption is not always valid for all magnetophoresis cases, especially for highly concentrated MNP solution (cooperative effect is non-negligible) and subjected to non-uniform magnetic field (hydrodynamic effect is dominant). The cooperative effect and hydrodynamic effects, as well as the polydispersity of MNPs have a huge impact on the transport behaviour magnetophoresis process, which brings about the failure of classical magnetophoresis assumption in predicting the separation kinetics. De Las Cuevas, Faraudo and Camacho (2008) showed that for the cases in which the cooperative effect is crucial, the separation kinetics of the magnetophoresis process strongly rely on the concentration of MNPs. Under the higher MNP concentration, the particle-particle interaction can be more intensive, which is leading to the formation

of larger aggregates that are able to be captured by the magnets more rapidly. This phenomenon has been mathematically captured by using a physical quantity known as magnetic Bjerrum length. The magnetic Bjerrum length is a characteristic length at which the magnetic attraction energy is equal to the thermal energy. De Las Cuevas and his co-workers have successfully predicted the formation of aggregations through the magnetic Bjerrum length.

In addition, the dispersion of MNPs in the liquid medium might induce the formation of MNPs clusters of different sizes, which are acted upon by magnetophoretic forces of different intensity (the intensity of the forces exerted on particles depend on the sizes). Thus, the polydispersity of the MNPs should be taken into account during the development of mathematical models to describe the magnetophoresis of the polydisperse MNPs system. Such an attempt has been initiated by Helseth and Skodvin (2009). In order to simplify the analytical solutions, several assumptions have been made throughout the model development. Even electrostatic, magnetostatic and hydrodynamic interactions are likely to occur when the distance between particles is relatively close. These interactions are neglected due to the difficulty to evaluate analytically. (Helseth and Skodvin, 2009). The computed result is highly matched with the experimental results.

Hydrodynamic effect (MNPs/fluid interactions or momentum transfer between MNPs and fluid) during the magnetophoresis has been ignored in the modelling of this process all over the time and the first attempt to include this effect into the magnetophoresis modelling is conducted by Leong, Ahmad and Lim (2015). In this work, they have developed two mathematical models to describe the dynamical behaviour of a non-cooperative magnetophoresis system, one with the consideration of hydrodynamic effect and one without it. The consideration of hydrodynamic effect is addressed by the incorporation of the Navier-Stoke equation in the modelling and simulation of the magnetophoresis process. The simulation results of both models were compared with the experiment observation and it was found that the model with consideration of hydrodynamic effect is able to ensemble the experimental results up to good accuracy: (i) the MNPs are dispersed uniformly throughout the medium all over the magnetophoresis process, (ii) there is an induced convective flow observed within the MNP solution and (iii) the separation rate of MNPs has been accelerated by

the hydrodynamic effect and it is similar to the experimental observation. Thus, it can be proven that hydrodynamic effect is crucial and should be included in the mathematical modelling even for the MNPs system in which the particle-particle interaction is not significant. In fact, it has been proven that the hydrodynamic effect is crucial for the magnetophoresis of MNPs within the magnetic field that does not distribute evenly (non-uniform magnetic field gradient).

Moreover, the magnetic dipoles of the particles are expected to point in the direction of the external applied magnetic field, forming elongate aggregates. The direction of the magnetophoretic force  $F_M$  is totally opposite to the direction of viscous drag  $F_d$ , the magnetophoretic force is directed to the magnetic gradient and balanced by the viscous drag. Besides, van der Waals and electrostatic forces are ignored in the analytical solutions due to the presence of a surfactant layer, and Derjaguin-Landau-Verwey-Overbeek (DLVO) theory was applied to predict the dipolar magnetophoretic forces and the stability of the system. The dispersion of MNPs in the medium affects the size of the particles, the intensity of the forces exerted on particles depend on their sizes. Thus, the polydispersity of the MNPs should be taken into account during the development of mathematical models. In order to keep the simplicity of the analytical solutions, several assumptions have been made. Electrostatic, magnetostatic and hydrodynamic interactions are likely to occur when the distance between particles is relatively close. But these interactions are difficult to evaluate analytically, thus, these interactions are neglected. Besides, it is reasonable to ignore the inertia of small single particles and assume the aggregation of particles is insignificant at the beginning of the experiment (Helseth and Skodvin, 2009). Hydrodynamic effect proposes that there is a MNPs/fluid interaction during the; the fluid can be disturbed by the movement of the MNPs, hydrodynamic effect is one of the governing effects in magnetophoresis. Leong, Ahmad and Lim (2015) have developed two mathematical models for the hydrodynamic effect, the first model is a non MNPs/fluid interacting magnetophoresis model, another is a hydrodynamically interacting magnetophoresis model. Leong, Ahmad and Lim (2015) claimed that the MNPs are dispersed uniformly throughout the medium at the beginning of the experiment, and interactions between MNPs are trivial owing to their non-interactive nature. Moreover, the MNPs are perfect spheres coated with a layer of non-magnetic polyethylene glycol (PEG). The migration of MNPs by an external applied magnetic field is creeping motion that complies with

Stoke's Law. In addition, the magnetic flux density gradient that points vertically is far more dictating than its horizontal counterpart. Lastly, the magnetic field does not distribute evenly resulting in the presence of a magnetic field gradient.

#### 1.4 Problem Statement

The ability to predict the kinetics of magnetophoresis is pivotal in designing or optimising a magnetic separator. With a proper mathematical model, the motion of the MNPs can be described and predicted precisely by the calculation or simulation with a computer software. Therefore, the optimum condition for magnetophoresis can be determined without conducting an experiment, thus, saving a lot of time and cost. However, the simple classical magnetophoresis theory fails in predicting the real life magnetophoresis experiments due to the interruption of cooperative and hydrodynamic effects.

In the existing literature, there are some attempts to incorporate the cooperative effect (particle-particle interaction) into the modelling of magnetophoresis. For example, De Las Cuevas, Faraudo and Camacho (2008) have tried to relate the significance of particle-particle interaction to the concentration of MNPs in a solution, which is then related to the MNP separation time by using an empirical fitting. Even though the empirical fitting is showing a positive outcome, the relationship between the fitting constants and the properties of the magnetophoresis system is still unclear, and such an empirical model is only applicable to specific MNP systems that have been studied by using the same procedure. Here, they claimed that the cooperative effect is the key factor for a successful magnetic separation process within a reasonable timescale, hence, the precise capture of this phenomenon by using a mathematical tool is essential. In addition, Andreu et al. (2011) have established a dimensionless parameter to characterise the intensity of cooperative effect during magnetophoresis, which is known as aggregation parameter  $N^*$ . This parameter is able to estimate the occurrence of cooperative effect (it is significant  $N^* > 1$ ) and capture the number of MNPs per aggregate under aggregation equilibrium. However, it is also essential to relate it to the kinetics of MNP separation so that the transport behaviour and



separation time of cooperative magnetophoresis can be captured by a mathematical model. By the incorporation of the cooperative effect, the transport process of magnetophoresis has been greatly complicated. Yet, apart from the cooperative effect, there are still more factors that govern the dynamical behaviour of magnetophoresis and should be considered in the modelling of it.

The second factor that also has been taken into consideration in the modelling of magnetophoresis process is hydrodynamic effect. Leong, Ahmad and Lim (2015) have conducted a study on hydrodynamic effect and successfully built a mathematical model that considering this factor in describing the transport behaviour of the magnetophoresis of non-cooperative MNP system ( $N^* < 1$ ). The simulation results are in good agreement with the experimental observation, in which the MNPs are distributed in the medium uniformly throughout the entire time scale of magnetophoresis. However, this mathematical model is only valid under relatively low MNPs concentration (without cooperative effect), because the cooperative effect is being ignored. Therefore, the result obtained from this mathematical model will only be accurate under the restriction that the particle-particle interaction is not significant.

The mathematical models described above have certain restrictions to depict the dynamic behaviour of magnetophoresis, as the cooperative and hydrodynamic effects were studied independently. Yet, it has been proven that both cooperative and hydrodynamic effects can take place simultaneously in many engineering applications involving magnetophoresis, as the co-existence of the two unique physical phenomena that accelerate the magnetophoresis kinetics (Leong et al., 2020). However, up to the current stage, there is no attempt to incorporate both cooperative and hydrodynamic effects simultaneously into the model to predict the magnetophoresis kinetics. Therefore, in order to complement the entire theoretical set of magnetophoresis kinetics prediction, the cooperative and hydrodynamic effects should be taken into consideration in the modelling to depict its kinetics. The successful establishment of such a model that can describe the magnetophoresis process in which both cooperative and hydrodynamic effects are important, which is always the case for engineering applications of magnetophoresis.

In this project, the magnetophoresis experiment will be conducted under different concentrations, which correspond to different intensity of cooperative effect. The experiment will be conducted under a setup similar to those reported by Leong et al. (2015) so that the hydrodynamic effect also occurs simultaneously during the magnetophoresis experiment. Then, a mathematical model to describe the magnetophoresis kinetics is developed by taking both cooperative and hydrodynamic effects into consideration. The model is simulated, and the simulation results are then compared with the experimental results. The ultimate goal of this project is to understand the fundamental behaviour of cooperative magnetophoresis in hydrodynamic interacting regime and produce a mathematical model that is able to predict this process up to great accuracy.

## **1.5 Objectives**

- To functionalize magnetic nanoparticles with poly(sodium 4-styrenesulfonate) to obtain a colloidally stable magnetic nanoparticle system.
- To measure the magnetophoresis kinetics under different concentrations of magnetic nanoparticles experimentally.
- To build a mathematical model to predict magnetophoresis kinetics of magnetic nanoparticles under the cooperative and hydrodynamic regimes.

## CHAPTER 2

### LITERATURE REVIEW

#### 2.1 Magnetic Nanoparticles (MNPs)

Magnetic nanoparticles (MNPs) belong to a class of nanoparticles that could be controlled by an external applied magnetic field and have at least 1 nm dimension. MNPs also can be categorised as quasi-zero-dimensional (0 D) nano-objects known which have linear characteristics and with the dimension not more than 100 nm. Fascinatingly, the physical and chemical properties of the are influenced by the dimension of the MNPs, causing them to demonstrate different features from their bulk materials (Horikoshi and Serpone, 2013). For instance, the MNPs possess a much stronger magnetisation, magnetic anisotropy than their bulk material. In addition, there are remarkable differences in other physical properties such as Curie ( $T_C$ ) or Neel ( $T_N$ ) temperature. Moreover, MNPs exhibit some unique behaviours like high magnetocaloric effect, giant magnetoresistance, etc. The change in the physicochemical properties is contributed by the change in the particles' size, since the chemical potential of the particles can be significantly increased by the reduction in particle size (Gubin, Koksharov, Khomutov and Yurkov, 2005). The structure of a regular magnetic particle is illustrated in Figure 2.1.

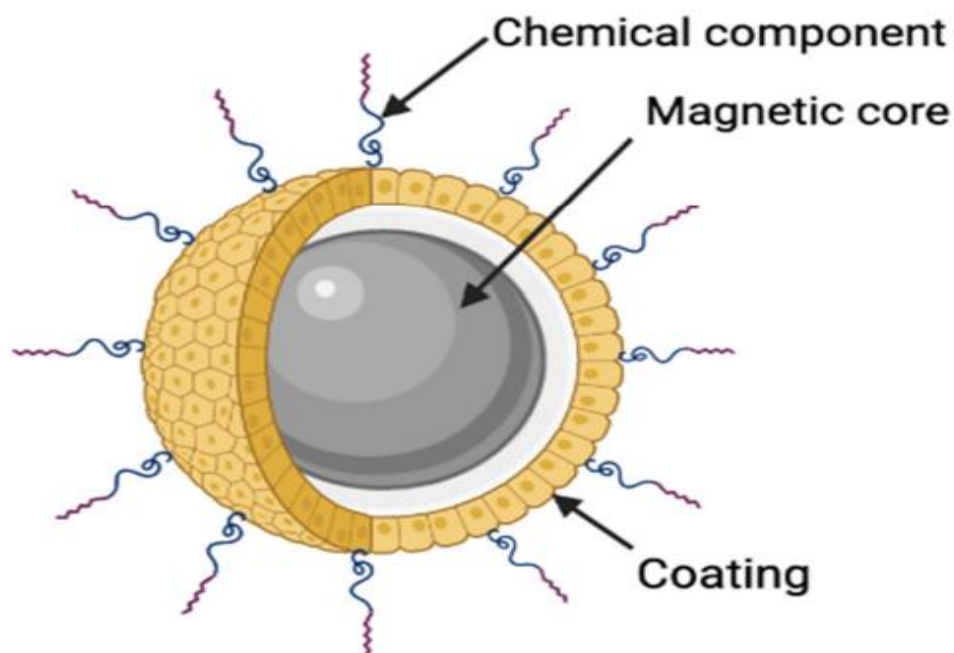


**Figure 2.1: Structure of a Regular MNP (Dasari, Xue and Deb, 2022).**

Due to the tiny size of MNPs, the total surface area contributed by a MNP suspension system is extremely large, which causes the particle suspension system to have a high surface energy and is prone to aggregate (Chong et al., 2020). This scenario is not favourable as the specific surface area of the MNPs (which is a good platform for certain functionalities such as reaction or adsorption) is reduced upon the particle aggregation, incurring loss of their efficiency in a particular application. Therefore, the colloidal stability of the MNPs play a vital role to ensure the MNPs can be dispersed uniformly, so that the high specific surface area can be retained. Conventionally, the MNPs are functionalized with different polyelectrolytes to boost their colloidal stability, by imposing electrostatics and steric repulsion between the particles in suspension. Different polyelectrolytes also have different functional groups, with distinctive functionalization, which is another factor to be considered when coating MNPs to meet the specific requirements in different applications (Yeap, Lim, Ooi and Ahmad, 2017).

As mentioned earlier, the MNPs can be classified into ferromagnetic, paramagnetic, and superparamagnetic materials according to their magnetic susceptibility. The magnetic characteristic of these materials can be described through

hysteresis loops. According to Mody, Singh and Wesley (2013) magnetism of a MNP is induced by the motion of an electron, a proton, a hole, a positive or a negative ion within its constituent atoms. The movement of an electron in atoms generates a magnetic dipole moment, this is also known as magneton. In this case, it is reasonable to imagine that every atom is a tiny magnet. A ferromagnetic material is composed of a lot of tiny atoms, which can be imagined as tiny magnets that point in random directions. However, there are groups of magnetons that are neighbouring each other pointing at the same directions, which subsequently form the domains in the ferromagnetic material. Here, each magnetic domain is separated by domain walls. These domain walls should be viewed as zones of transition of limited thickness, the magnetization progressively changes the direction from one domain to another. The concept of domains, domain walls, magnetons, and the magnetisation of ferromagnetic materials are depicted in Figure 2.2.

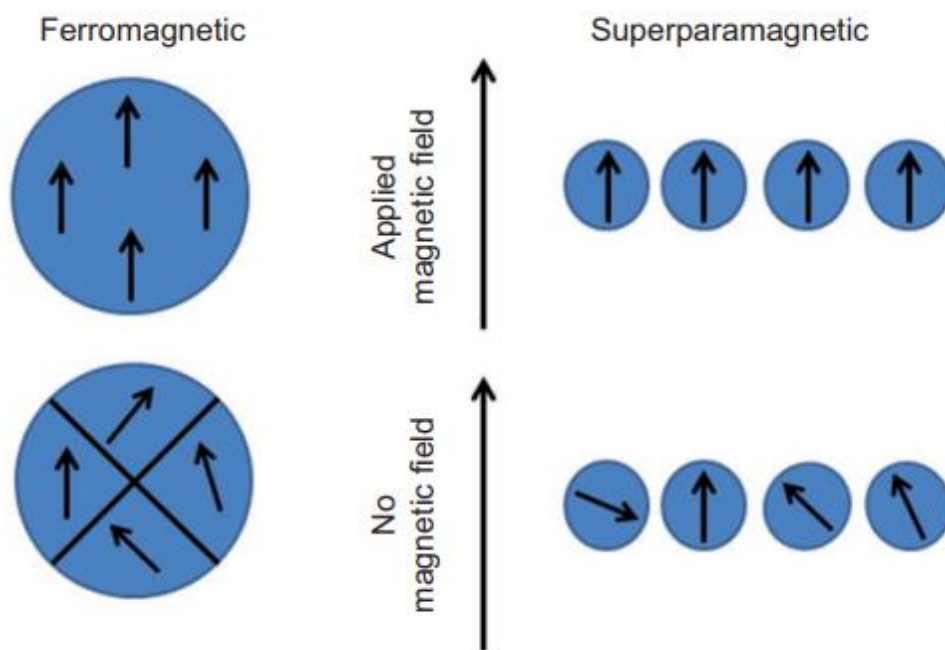


**Figure 2.2: Concept of Domains, Domain Walls, Magnetons; Magnetisation Degree of Ferromagnetic and Superparamagnetic Materials Under Magnetic Field and Without Magnetic Field (Mody, Singh and Wesley, 2013).**

The hysteresis loops of ferromagnetic materials are illustrated in Figure 2.3. When these materials are exposed to an external applied magnetic field, the magnetons tend to align in the direction of the external applied magnetic field. For the ferromagnetic material, the domain walls are eliminated gradually because the magnetic moments are getting aligned in the same direction, which increases the magnetization in that particular direction. The degree of magnetization is kept increasing until reaching magnetization saturation ( $M_S$ ). At this point, all the magnetons are pointed in the direction of the external applied magnetic field, further increasing the external magnetic field strength will not affect the degree of magnetisation. However, after removing the external applied magnetic field, the degree of magnetisation does not return to the original value due to the intrinsic retention characteristic of ferromagnetic materials. This scenario indicates that part of the magnetic moments flips randomly and forms new domains, while most part of the magnetic moments stay aligned. The retention of the memory or magnetization (Figure 2.3 point A) after the removal of the external applied magnetic field is known as remanence. In order to completely demagnetise the ferromagnetic materials to zero (Figure 2.3 point B), an external magnetic field with opposite direction needs to be applied. At that point, half of the domains align in the initial direction, and another half of the domains align in the opposite direction, causing the magnetic field of the ferromagnetic materials to be approximately zero. Continuous increase of the external magnetic field strength forces more magnetons to align in another direction until reaching saturation magnetization. The resistance of a ferromagnetic material to change in magnetization is determined by coercivity ( $H_C$ ), a broader gap implies that a larger coercive force is required for demagnetization or change of its magnetization direction. Thus, ferromagnets can be classified into hard and soft magnetic materials according to their coercivity. Hard magnetic materials have high coercivity and low permeability, therefore, an intense magnetic field is required to change its magnetization status and the external magnetic field is harder to penetrate into ferromagnetic materials due to their low permeability. On the other hand, soft magnetic materials have the inverse properties as compared to that of hard magnetic materials. Furthermore, the area under the curve of the hysteresis loop can be viewed as energy loss (in the form of heat energy) during magnetization or demagnetization (Mody, Singh and Wesley, 2013).

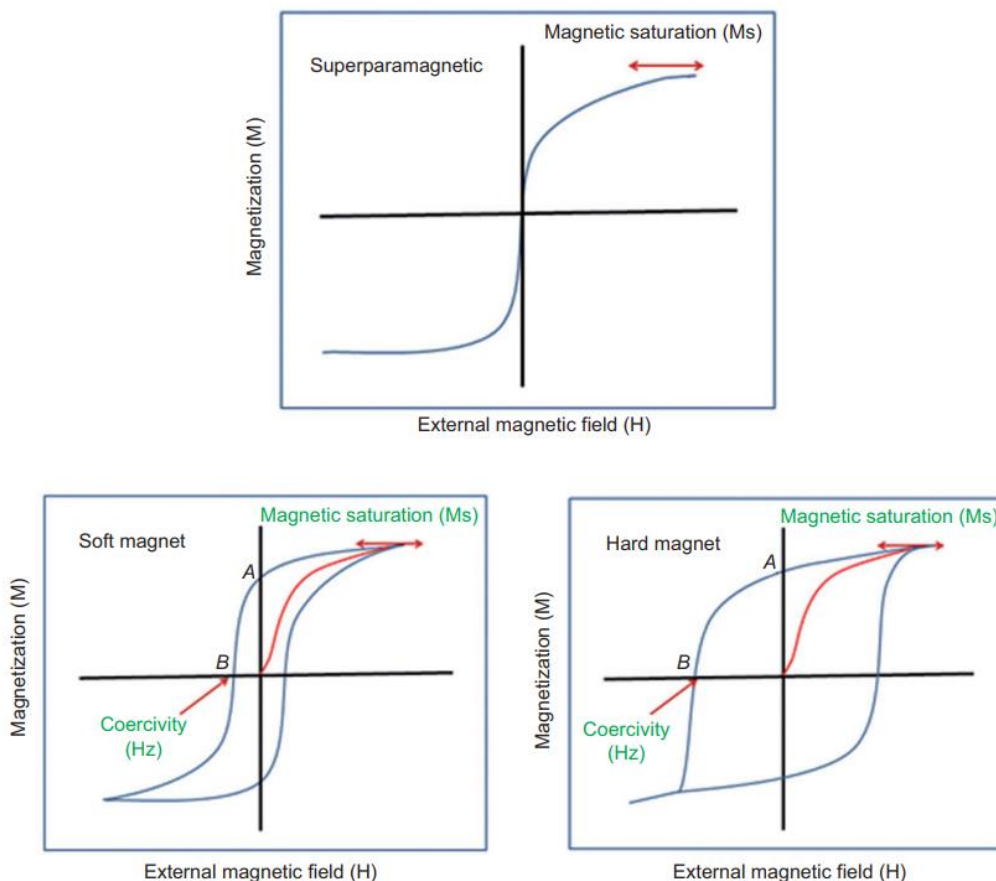


**Figure 2.3: Hysteresis Loops of Superparamagnetic and Ferromagnetic Materials. X-axis Represents the Direction of an External Applied Magnetic Field; Y-axis Represents the Degree of Magnetization (Mody, Singh and Wesley, 2013).**

In contrast, there is a significant difference between ferromagnetic and superparamagnetic materials in terms of their magnetism behaviour. Like ferromagnetic material the magnetic moments orient in the direction of the external magnetic field until magnetic saturation when a superparamagnetic material is being magnetised. However, the superparamagnetic material retracted its original trail on the magnetization curve upon the removal of the external magnetic field. This phenomenon manifests that superparamagnetic materials have no magnetic memory, low retentivity, low coercivity, and high permeability (Mody, Singh and Wesley, 2013). The paramagnetic and superparamagnetic materials have similar responses on external applied magnetic fields; however, the latter materials have a much higher saturation magnetization and can only be observed on the nanomaterials that are sufficiently small. Comparison of hysteresis loops of ferromagnetic, paramagnetic,

superparamagnetic materials are shown in Figure 2.4.

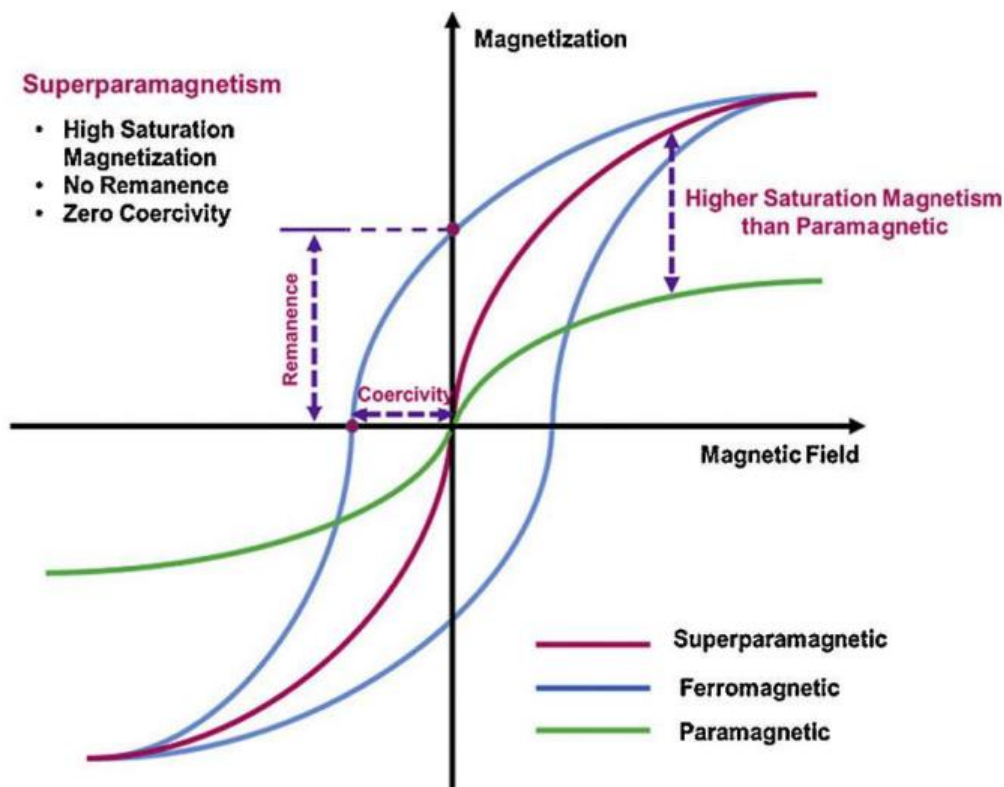


**Figure 2.4: Hysteresis Loops of Superparamagnetic, Ferromagnetic, and Paramagnetic Materials (Mohammed, Goma, Ragab and Zhu, 2017).**

Figure 2.5 portrays the effect of particle size on the magnetic behaviour of MNPs. In this figure,  $D_{cr}$  represents the critical diameter for the particle transition from the multidomain to single domain, and the  $D_{sp}$  represents the critical diameter for superparamagnetic state (Leong et al., 2020). In addition, the magnetic moments in a single domain are not always homogeneous (magnetons are not pointing in the same direction), the single domain just denotes there are no domain walls in the bulk particle (Gubin, Koksharov, Khomutov, and Yurkoy, 2005).



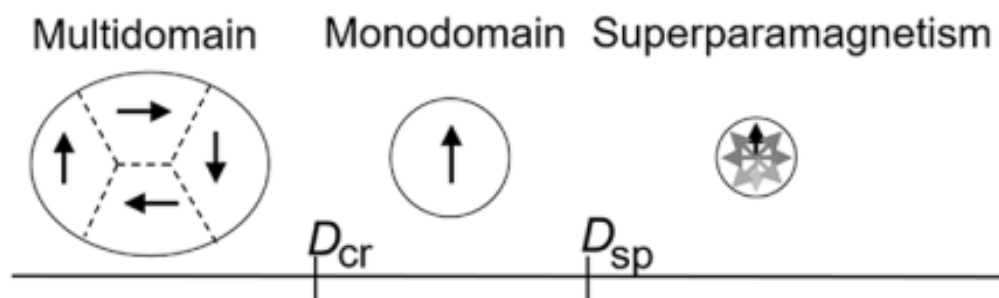


**Figure 2.5: Magnetic behaviour of different sized particles (Leong et al., 2020).**

As described earlier, a ferromagnetic material consists of multidomain that are separated by domain walls, and each domain is homogeneous magnetised. The domains are formed due to nature's tendency of the ferromagnetic material to attain a low energy state, and the magnetostatic energy of the bulk single domain is higher than those appearing in multidomain states (see Figure 2.7). However, as the reduction in particle size gets smaller, the surface energy of the domain walls increases more rapidly than the reduction of magnetostatic energy due to the formation of multiple magnetic domains. In this context, the formation of multiple domains will be naturally more energetically unfavourable and the number of magnetic domains in the particle can be getting smaller when the particle size is decreased. Ultimately, when the particle size is reduced until a threshold value, a single domain is formed and the coercivity of the particle reaches a peak value and this threshold size is known as the critical diameter ( $D_{cr}$ ) of the particle (Mody, Singh and Wesley, 2013). The two types of magnetism reversal spin modes are shown in Figure 2.6. At the regime where the particle size is smaller than the critical diameter ( $D_{cr}$ ), the coercivity of the particle gradually reduces to zero if the particle size is further reduced. This is because when the particle size gets smaller, the size of the only magnetic domain in the particle also decreases as well, and the impact of displacements of the domain walls on the magnetism reversal is getting insignificant. To switch the magnetization direction of a single domain particle, the particle needs to be rotated wholly. When the particle size is small enough, it experiences remarkable thermal fluctuation which causes it to rotate randomly and rapidly under the absence of a magnetic field. Consequently, the magnetic dipole of the particle undergoes thermal flipping continuously, which renders it to exhibit zero magnetization if it is observed under timescale much larger than the

flipping time. With the presence of magnetic fields, the particles can align with the magnetic fields and gain the net magnetization overall. The zero magnetization of the particle upon the removal of the magnetic field causes the particle to possess no magnetic memory, which indicates that the particle has gained superparamagnetic state (Leong et al., 2020).

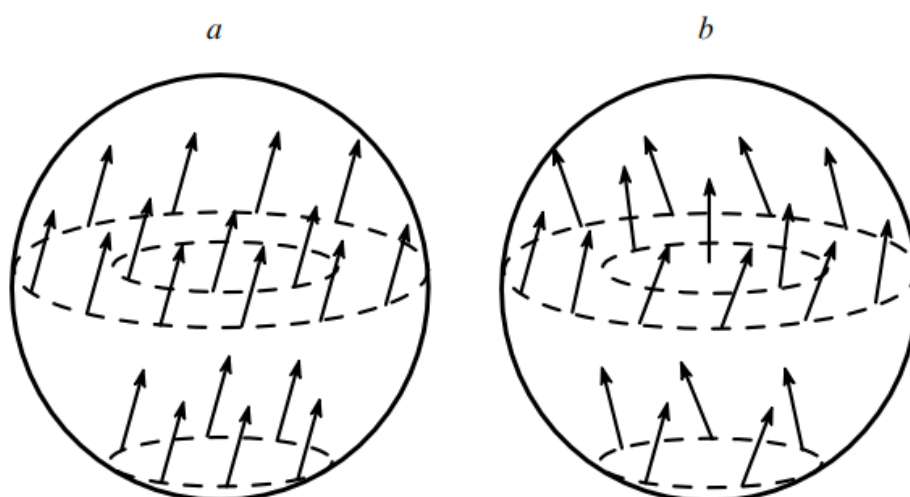


**Figure 2.6: Magnetism Reversal Spin Modes (a) Coherent Rotation, (b) Eddy Mode (Gubin, Koksharov, Khomutov and Yurkov, 2005).**

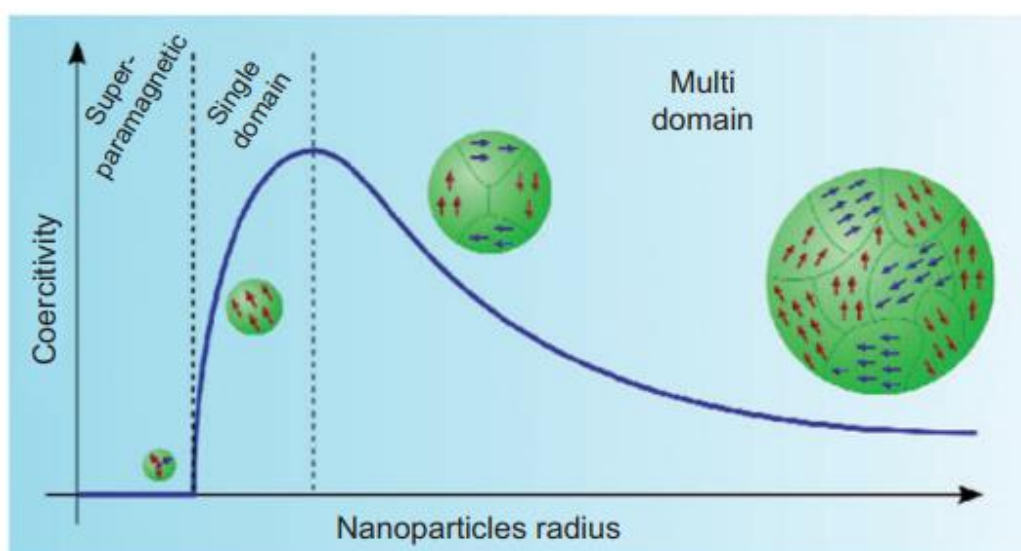


**Figure 2.7: Relationship between Coercivity and MNPs Size (Akbarzadeh, Samiei and Davaran, 2012).**

### 2.1.1 Application of MNPs

MNPs have attracted a remarkable interest of scientists due to their intrinsic biocompatible features, non-toxic properties, nanoscale size, tunable ability, and the ability to interact with external magnetic fields. Furthermore, the physicochemical properties of MNPs can be easily designed and tailored through coating with various surface materials (Yang et al., 2019). In addition, functionalized MNPs offer high selectivity and high affinity to targeted materials due to the distinctive functional groups on the coating. The magnetic behaviours owned by the MNPs also allows them to be manipulated by a magnetic source, which subsequently enables the MNPs to be fixed or delivered to the specific area precisely. Despite their nano-size, properly functionalized MNPs can possess excellent colloidal stability, high volume to surface area, and outstanding dispersibility which offers high efficiency for particular reaction and adsorption applications. Due to these unique features of MNPs as described above, they are very versatile and can be applied in various engineering fields, such as biomedical technology and environmental treatment (Taira et al., 2009).

The applications of MNPs in the biomedical field can be categorised into *in vivo* (inside body) and *in vitro* (outside body) applications. One of the *in vivo* applications of MNPs is hyperthermia, in which this therapeutic application utilises superparamagnetic iron oxide to generate heat energy in the human body through interactions with external alternating current (AC) magnetic fields. Here, the AC magnetic fields force the MNPs to flip between parallel and antiparallel directions, which cause the magnetic energy transformed into heat energy. Since the tumour cells are more heat sensitive than healthy cells, this process has enabled *in situ* heating to destroy the pathological cells. Additionally, drug delivery to a specific site in a body can also be performed by using MNPs. With the aid of a localised magnetic field to manipulate the trajectory of MNPs, the drug can be delivered to the targeted cells precisely, and the medication can be released to the designated area. Drug delivery by MNPs requires lesser dosage and has lesser side effects (Akbarzadeh, Samiei and Davaran, 2012). Besides, repeated treatments are allowable owing to the positive charged MNPs that can form a stable deposit onto the tumour cells (Chung, Leon, and Rinaldi, 2020).

MNPs possess the capability to effectively separate and select biomaterials, making them highly useful in *in vitro* applications like bioseparation. Bioseparation involves isolating and concentrating targeted materials from a larger sample, using MNPs as adsorbents to bind to the targeted materials. The MNPs and targeted materials are then separated using a magnetic separator. This technique can separate biological substances such as proteins, cells, and DNA from their matrix using superparamagnetic nanoparticles. Additionally, MNPs are well-suited for heterogeneous catalysis, as a catalyst supported by MNPs can be easily recovered compared to traditional methods like centrifugation and filtration. MNPs also have significant potential for environmental applications, such as wastewater treatment, where functionalized MNPs can remove organic and inorganic pollutants (Akbarzadeh, Samiei and Davaran, 2012). The magnetic separation technique is shown in Figure 2.8.

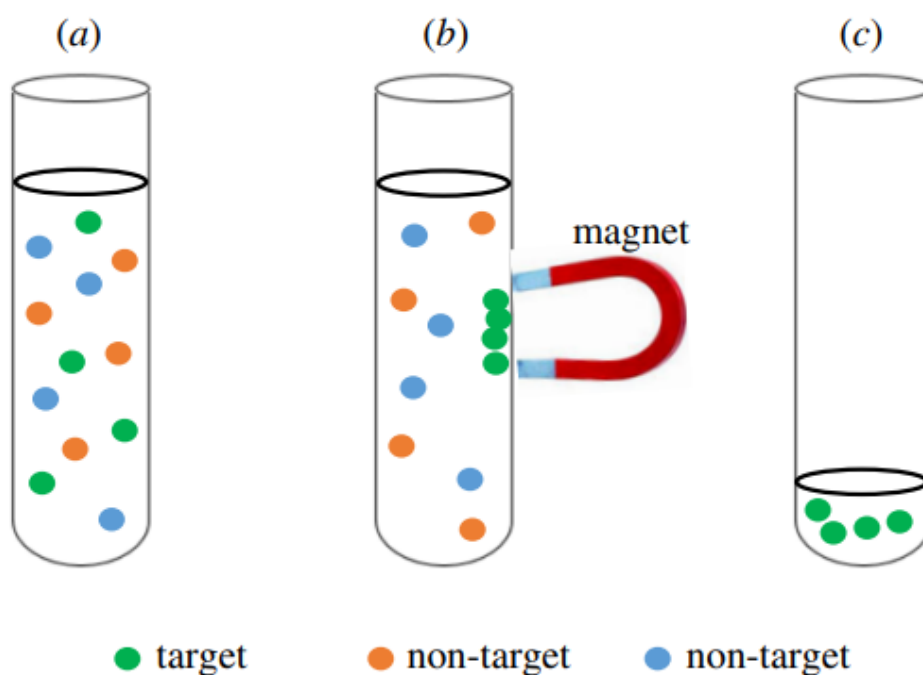


**Figure 2.8: Magnetic Separation Technique (Leong, Yeap and Lim, 2016).**

The development of magnetic resonance imaging (MRI) for diagnosis has urged the need of a magneto-pharmaceutical. MRI is a technique that generates anatomical images by observing the magnetic response of proton dipoles from water molecules. Upon exposure to an external magnetic field, the magnetic moments of the

protons are arranged in a particular manner. When radio frequency (RF) pulses are introduced, the protons will be disarranged. However, the proton will be rearranged once the radio waves stop radiating. The time difference of disarrangement and rearrangement of hydrogen atoms (varies by organs) is processed by a computer to produce an image. Throughout this process, MRI contrast agents are required to improve the clarity of the image, which are usually made of MNPs. This is because MNPs accumulate on healthy cells and create a dark signal which enhances the image contrast between the healthy cells and pathological cells. A contrast image is shown in Figure 2.9 (Chung, Leon and Rinaldi, 2020).

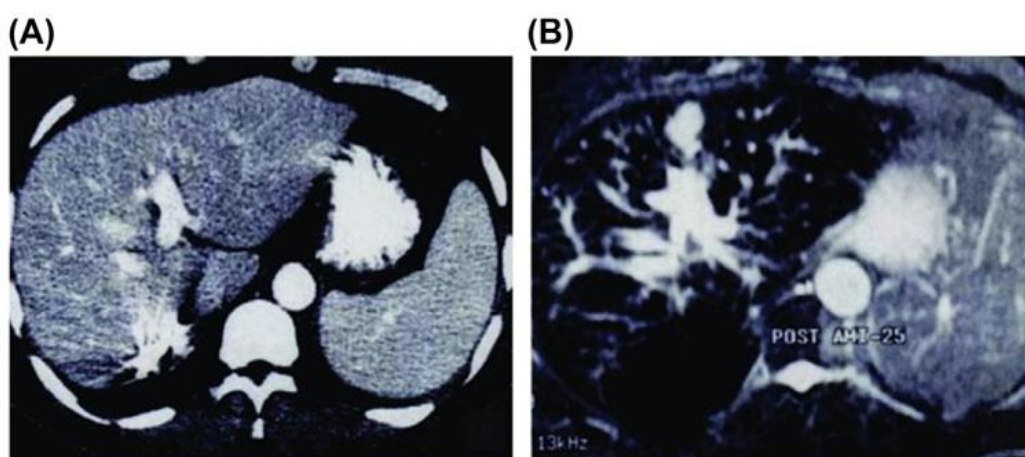


**Figure 2.9: Magnetic Resonance Images (A) without MRI agent (B) with MRI Agent (Chung, Leon and Rinaldi, 2020).**

MNPs can be utilised for grafting with heterogeneous catalysts to overcome the limitations of traditional heterogeneous catalysts, which are difficult to regenerate and separate. The catalyst supported by MNPs can be easily recovered compared to conventional separation methods, like crossflow filtration and centrifugation. Moreover, MNPs, being nanoscale, provide benefits such as high reactivity and dispersion when supported on the catalyst. The catalysts that have been functionalized can be utilised in a range of chemical reactions, such as carboxylate resolution using enzymes, ester hydrolysis using amino acids, and carbon-carbon cross-coupling reactions (Akbarzadeh, Samiei and Davaran, 2012).

In addition, MNPs have potential for waste removal applications, including the selective removal of organic and inorganic pollutants from complex matrices containing numerous other substances such as removal of dyes and hazardous metal ions. Due to their nanoscale size, MNPs have a high surface-to-volume ratio, which enables them to effectively remove pollutants when coated appropriately. MNPs offer a promising alternative to conventional, less efficient absorbents, as they are highly efficient and reusable (Akbarzadeh, Samiei and Davaran, 2012).

### **2.1.2 Advantages and Disadvantages of MNPs**

These characteristics make MNPs suitable for a wide span of applications. The magnetic behaviours owned by the MNPs allows them to be manipulated by a magnetic source. Because the MNPs are magnetizable, this feature enables the MNPs to be fixed or delivered to the specific area precisely. The nanoscale MNPs possess excellent colloidal stability, high volume to surface area, and outstanding dispersibility offers high efficiency. For justification, drug delivery by MNPs requires lesser dosage and has lesser side effects (Akbarzadeh, Samiei and Davaran, 2012). Besides, repeated treatments are allowable owing to the positive charged MNPs that can form a stable deposit onto the tumour cells (Chung, Leon and Rinaldi, 2020).

Although MNPs offer numerous advantages, they also have some drawbacks that must be addressed. In diagnostic applications, the high polydispersity of MNPs can lead to uneven heating during hyperthermia, which is unfavourable. Additionally, MNPs cannot be utilised for treating disseminated tumours and are only suitable for localised, invasive therapy (Chung, Leon, & Rinaldi, 2020). Due to their extremely small size, MNPs have limited loading capacity for drugs or targeted materials, as only a small amount of material can be carried by each MNP (Wilczewska, Niemirowicz, Markiewicz, & Car, 2012).

## 2.2 Magnetophoresis of MNPs

The properties of the particles and surrounding medium are determined by their magnetic susceptibility. Magnetic susceptibility is a vital parameter for magnetophoresis and denoted as symbol  $\chi$ . The values of magnetic susceptibility categorise the materials into diamagnetic ( $\chi < 0$ ), paramagnetic ( $\chi > 0$ ), and ferromagnetic ( $\chi \gg 0$ ), and superparamagnetic materials are belong to another category of paramagnetic materials. Diamagnetic materials prone to repel from the magnetic field; Paramagnetic, superparamagnetic, and ferromagnetic materials prone to attract toward the magnetic field. Interestingly, paramagnetic, superparamagnetic, and diamagnetic materials can be magnetised with the presence of magnetic field and lose the magnetism once the magnetic field is removed. For positive magnetophoresis, the paramagnetic particles move toward the source of the magnetic field. For the negative magnetophoresis, diamagnetic particles serve as magnetic holes, due to the difference in magnetic susceptibility between the diamagnetic particles and paramagnetic medium, the diamagnetic particles move away from the magnetic field by a negative magnetophoresis force. Separation, spreading, trapping, and mixing can be done by using either positive magnetophoresis or negative magnetophoresis. The efficiency of negative magnetophoresis is higher than positive iontophoresis owing to the paramagnetic medium having higher magnetic susceptibility than paramagnetic particles. However, paramagnetic medium offers less opacity and labelling of targeted materials is essential for tracking and visualisation. Intriguingly, negative magnetophoresis and positive magnetophoresis can occur simultaneously in a system. Paramagnetic particles can exhibit diamagnetic behaviour when the surrounding medium is adjusted to a stronger paramagnetic medium; this scenario can be achieved by altering the concentration of MNPs in a paramagnetic medium (Munaz, Shiddiky and Nguyen, 2018).

### 2.2.1 Cooperative Effect

This section focuses on describing the mechanism of positive magnetophoresis, which is an essential phenomenon in the application of MNPs in magnetic separation in

various technology and engineering fields.

Upon exposure to an external magnetic field, MNPs in fluid suspension are magnetised and aligned in the direction of the magnetic field, which are then driven toward the magnetic source by magnetophoretic force. The motion of MNPs relative to the surrounding fluid is known as magnetophoresis.

There are several factors that dominate the kinetics of magnetophoresis, which are magnetophoretic force, viscous drag, gravitational force, and Brownian force (Leong, Ahmad and Lim, 2015). Magnetophoretic force is the force that acts on the MNPs due to the response of their intrinsic magnetic dipole moments toward the externally applied magnetic field.

The external magnetic field exerts magnetophoretic force to drive a MNP toward the magnetic source along the magnetic gradient, which can be formulated as:

$$F_M = \mu \nabla B \quad (2.1)$$

where  $F_M$  denotes the magnetophoretic force,  $\mu$  denotes the magnetic moment possessed by the MNP and  $\nabla B$  denotes the magnetic field gradient (Leong, Ahmad and Lim 2015). According to Equation (2.1), magnetophoretic force is steering the MNP to move towards the region with greater  $B$  value (which is also known as magnetic flux density) and its magnitude is greater if the field strength is higher. The magnetic moment possessed by a MNP can be calculated as follow:

$$\mu = m_p M_{(m)} \quad (2.2)$$

where  $m_p$  is the mass of the MNP and  $M_{(m)}$  is the magnetization of the MNP (per mass basis). In fact, the magnetization of a MNP depends on its state of magnetization, which is a function of the magnetic flux density experienced by it:

$$M_{(m)} = M_{(s)} \mathcal{L}(b\mu_o H), \mathcal{L}(x) = \coth x - \frac{1}{x} \quad (2.3)$$

where,  $x = b\mu_o H \frac{\partial H}{\partial r}$  and  $B = b\mu_o H$



where  $b$  denotes the required magnetic field intensity to reach the magnetization saturation and  $M_{S(m)}$  stands for saturation magnetization of the MNP (per mass basis) that is dependent on the type of material. Equation (2.3) is known as the Langevin function which indicates that the value of  $M_{(m)}$  will be increasing with the value of  $x$  (or  $B$ ) and approaches  $M_{S(m)}$  under very high value of  $x$  (or  $B$ ), demonstrating superparamagnetic property as shown in Figure 2.4.

Interaction of MNPs with medium creates a viscous drag, which is a resistance that inhibits the motion of MNPs in fluid and it is mainly contributed by the viscosity of the medium. The movement of MNPs under low gradient magnetophoresis can be classified as laminar flow due to its tiny size and low Reynolds number. Thus, the viscous drag exerted on the MNPs can be formulated by Stoke's Law as given by:

$$F_D = 3\pi\eta D_h v \quad (2.4)$$

where  $F_D$  is the viscous drag force,  $\eta$  represents the viscosity of the fluid,  $D_h$  represents the hydrodynamic diameter of the MNP, and the symbol  $v$  represents the velocity of the MNP in relative to the surrounding fluid (Leong, Ahmad, and Lim, 2015). It should be emphasised that the MNP is assumed to be in spherical shape if Equation (2.4) is used to calculate the viscous drag force encountered by it during magnetophoresis.

In addition, from the microscopic point of view, there is random collision of MNPs with the surrounding medium particles if the MNPs are suspended in the medium, which causes the MNP to move at random direction even under the absence of external magnetic field. This kind of motion is known as Brownian motion, which can be defined as the arbitrary movement of particles due to collisions with the surrounding particles. The Brownian motion results in the diffusion of MNPs in the suspension medium, which causes the net MNP flux that directs the MNPs to move from the region with high concentration to the region of lower concentration (Floyd, Eberly and Hadjifrangiskou, 2017). Leong, Ahmad and Lim (2015) stated that the significance of the Brownian motion can be reflected by the diffusivity of MNPs ( $D_f$ ) which can be computed by the Einstein-Stokes equation as formulated by:

$$D_f = \frac{k_B T}{3\pi\eta D_h} \quad (2.5)$$

where  $k_B$  is the Boltzmann constant ( $1.3806 \times 10^{-23} \text{ m}^2 \text{ kg s}^{-2} \text{ K}^{-1}$ ), and the symbol  $T$  is the absolute temperature (Miller, 1924). The equation (2.4) and (2.5) are only suitable for spherical particles.

In addition, MNPs under magnetophoresis can also be subjected to gravitational attraction which can be described as:

$$F_g = m_p g \quad (2.6)$$

where  $m_p$  is the mass of the MNP and  $g$  is the gravitational acceleration vector that points toward the centre of earth. Also, the MNPs are dispersed in a medium, hence, the MNPs also experience an upward force that is opposing the gravitational force, which is known as the buoyancy force. Buoyancy force is the result of the difference of hydrostatic pressure between the bottom and the top of an object (Teague, Allen and Scott, 2018). Intriguingly, the buoyancy force does not depend on the immersed depth of the object because the hydrostatic pressure at the top and the bottom of the object increases simultaneously. The buoyancy force acting on a MNP with diameter of  $D$  can be formulated as:

$$F_B = \frac{1}{6} \pi D^3 \rho_f g \quad (2.7)$$

where  $F_B$  is the buoyancy force, and the  $\rho_f$  is the density of the surrounding fluid. It should be emphasised that the gravitational force acting on a MNP and its corresponding buoyancy force is negligible as compared to the magnetophoretic force during the magnetophoresis process.

For additional information, there is also a magnetic buoyancy force present in the magnetophoresis process, especially when the surrounding fluid possesses some degree of magnetization. However, the impact of the magnetic buoyancy force is typically trivial, and it is reasonable to be neglected because most engineering applications related to magnetophoresis of MNP involve the suspension of MNPs in

a non-magnetic fluid (such as aqueous medium). This force is acting in the opposite direction of the magnetophoretic force, which causes the particle to move away from the region with higher magnetic flux density. The magnetic buoyancy force is insignificant in a diamagnetic medium and has a stronger effect in a paramagnetic medium. The magnetic buoyancy force is given as follow:

$$F_{MB} = \frac{4}{3}\pi r^3(\chi_{MNP} - \chi_L)H_o\left(\frac{dH}{dx}\right) \quad (2.8)$$

where  $F_{MB}$  is the magnetic buoyancy force,  $r$  is radius of a MNP, and the  $H_o$  is the magnetic strength at the centre of the MNP (Wakayama, 1997).

According to the magnitude of magnetic field gradient employed, magnetophoresis of MNPs can be categorised into high gradient magnetic separation (HGMS) and low gradient magnetic separation (LGMS), as shown in Figure 2.10. The separation of MNPs is a tough process because the motion control of MNPs by magnetophoretic force is significantly disturbed by thermal energy and viscous drag due to their tiny size. In order to control the motion of MNPs effectively and separate them out of their suspension in a reasonable time, a high gradient magnetic field is required to overcome such random thermal energy and opposing drag force. In this regard, HGMS is introduced to impose a high magnetic field gradient (and hence strong magnetophoretic force) with magnitude greater than 100 T/m to manipulate the motion of MNPs effectively so that they can be separated from the solution rapidly. In HGMS, the high magnetic gradient is generated by inserting a randomly entangled magnetizable wire into a column where the MNP solution is flowing through. The magnetic field in the column is not homogenised due to the presence of the wires, thus generating ‘spots’ with a very high magnetic field gradient in the vicinity to the wires. Then the MNP solution flows through the column, MNPs can be trapped onto the wires by the enormous magnetophoretic force exerting on them, leaving the clear solution flowing out of the column. Yet, there are several drawbacks associated with the application of HGMS in engineering applications. Firstly, the HGMS column has a highly randomised inhomogeneous distribution of the magnetic field, which imposes difficulty in obtaining the analytical solutions to describe the kinetic of HGMS. Furthermore, the HGMS column suffers from high purchase, installation and operating

cost because the magnetic field is typically generated by an electromagnet for HGMS applications. Additionally, a strong magnetic source increases the propensity for MNPs to deposit on the wires in the HGMS column, which reduces separation effectiveness or even results in MNPs being permanently retained in the column. Lastly, during the HGMS process, energy is lost as a result of the Joule effect (a portion of electrical energy is dissipated as heat energy when a current passes through the electromagnet).

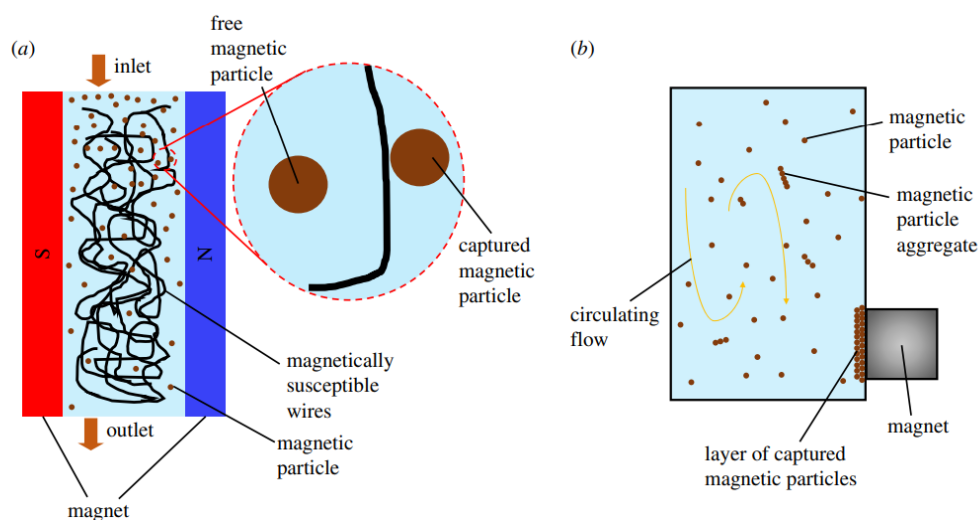


**Figure 2.10: High Gradient Magnetic Separation and Low Gradient Magnetic Separation (Leong, Yeap and Lim, 2016).**

Due to this scenario, LGMS strategy has deserved much attention from research worldwide. LGMS involves only a container with a magnet placed outside it to induce the magnetophoresis of MNP solution filled in the container. However, as magnetic flux density decays very rapidly as one moves away from the magnet, the magnetic field gradient in the container is typically low at the magnitude of  $\nabla B < 100 \text{ T m}^{-1}$  in most regions. Thus, the magnetophoretic force exerted on a MNPs under LGMS is generally low even though LGMS technology is low-cost and simple (Leong, Ahmad and Lim, 2015). However, many research works have shown that LGMS also can result in outstanding separation efficiency and MNPs can be separated out of the solution within reasonable timescale. This is because there are two effects that have greatly accelerated the magnetophoresis of MNPs subjected to LGMS and caused the

dynamics of it to deviate greatly from the prediction by classical magnetophoresis theory. These two effects will be discussed thoroughly in the next section.

## **2.3 Deviation from Classical Magnetophoresis Theory**

### **2.3.1 Cooperative Effect of Magnetophoresis**

Yavuz and his colleagues had successfully demonstrated the possibility of rapid magnetic separation of MNPs under low gradient magnetic fields (Yavuz et al., 2006). De Las Cuevas, Faraudo and Camacho (2008) had further conducted an experiment to study the feasibility of LGMS in separating MNPs effectively, in which the experiment setup and expected MNPs' motion are shown in Figure 2.11. Surprisingly, these results have suggested that the experimentally observed magnetophoresis kinetics is much faster than those predicted by the classical magnetophoresis theory. The classical model predicts a separation time of 1250 s, whereas experimental results have shown that the separation time can be as rapid as 25 s, which is approximately 50 times quicker than the classical prediction (Leong et al., 2020). These unexpected results have revealed that there should be another mechanism that has been neglected in the classical picture of magnetophoresis, and this mechanism is so significant that it is able to accelerate the magnetophoresis up to a great extent. The researchers have denoted this mechanism as cooperative effect, which is the self-aggregation and collective motion of MNPs owing to the attraction between magnetic dipole moments possessed by MNPs. After the aggregation, MNPs are moving in larger particle clusters which gain larger magnetophoretic velocity and can be separated more rapidly. Evidently, the optical micrograph of MNP solution subjected to LGMS has shown the MNPs are moving in long chain aggregates toward the magnet, as displayed in Figure 2.12. Here, MNPs are aligned in the direction of the external applied magnetic field, forming elongated aggregation while moving toward the magnetic source.

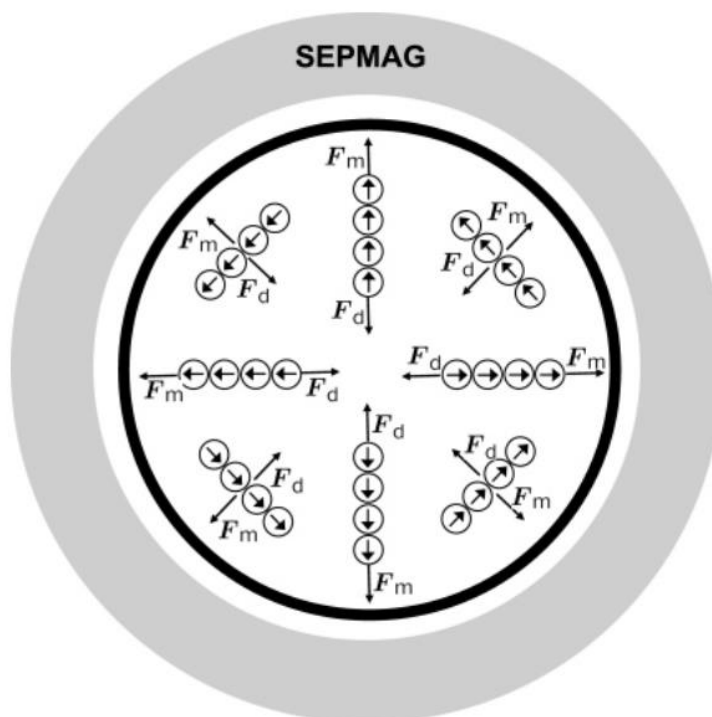


**Figure 2.11: Experiment Setup of LGMS (De Las Cuevas, Faraudo and Camacho 2008).**

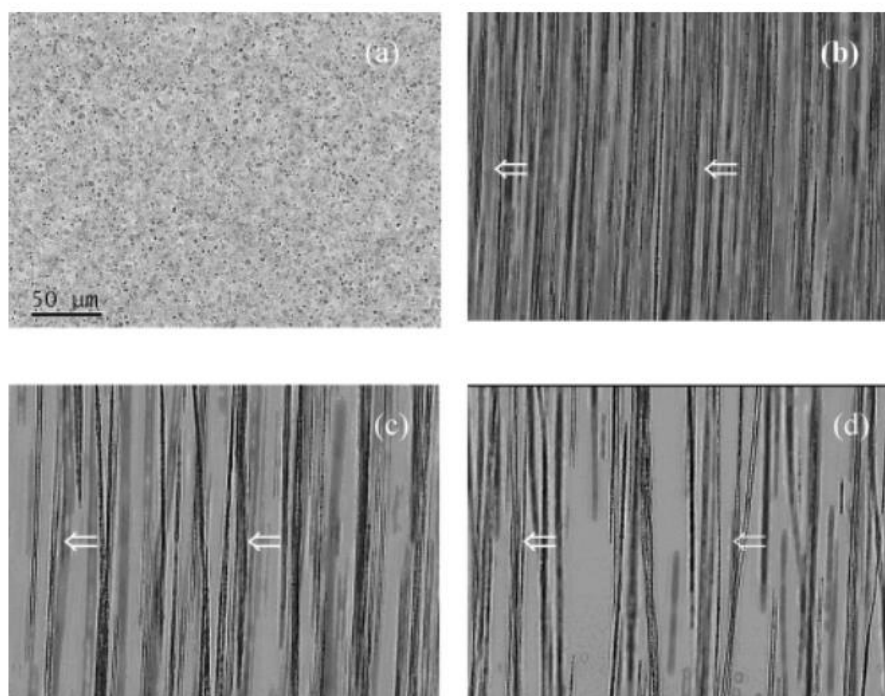


**Figure 2.12: Motion of MNPs under an external applied magnetic field (a) 0 s, (b) 120 s, (c) 240 s, (d) 360 s (De Las Cuevas, Faraudo and Camacho 2008).**

The cooperative effect leads to the formation of MNP clusters that are being separated collectively upon exposure to external magnetic fields. This type of magnetophoresis is known as cooperative magnetophoresis, which is different from non-cooperative magnetophoresis that involves the individual motion of MNPs under the magnetic field (see Figure 2.13). The aggregation of MNPs under external magnetic fields can be explained quantitatively by the DLVO theory, which discusses the surface interaction energy related to electrostatic, Van der Waals and magnetostatic forces.

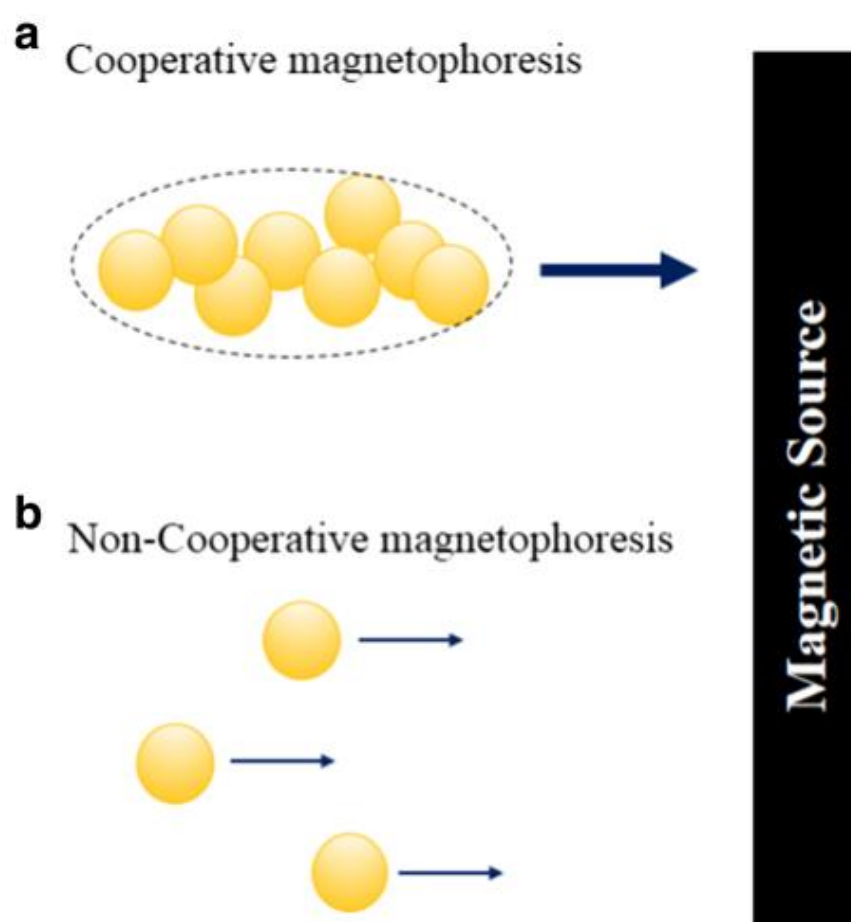


**Figure 2.13: Cooperative Magnetophoresis and Non-cooperative Magnetophoresis (Yeap, Lim, Ooi and Ahmad, 2017).**

Figure 2.14 illustrates the DLVO curve of MNPs without an externally applied magnetic field. Within a 5 nm surface separation, the DLVO curve has an excellent prediction about the surface forces. There are two dominating forces here: (i)

electrostatics repulsion due to the charges carried by the particles and (ii) Van der Waals attraction due to the instantaneous dipole moment of the particles. Both interaction forces decrease very rapidly with the distance between particles. The curve in the middle is the total interaction energy, which is the summation of Van der Waals attraction and electrostatic potential. At high ionic strength (a lot of ions in the medium), the Van der Waals force is governing because the surface of a particle is covered by layers of charged ions, which can effectively screen and reduce the electrostatic repulsion. At close and intermediate distance between the particles, the repulsion force generated by the charged ions is dominated, the peak of the curve is the potential barrier that impedes the formation of aggregates. In this case, the particle system is said to exhibit good colloidal stability. If the thermal energy of the particles is large enough to overcome the potential barrier and the separation distance between particles is very small, the surface energy will eventually reach a minimum energy and cause irreversible aggregation. When the distance between particles is far enough, the Van der Waals forces are slightly larger than the electrostatic repulsion and the particles tend to attract each other (Adair, Suvaci and Sindel, 2001). The Van der Waals forces are prevailed at the secondary minimum well, a reversible aggregation is formed when the particles approach each other (Piacenza, Presentato and Turner, 2018).

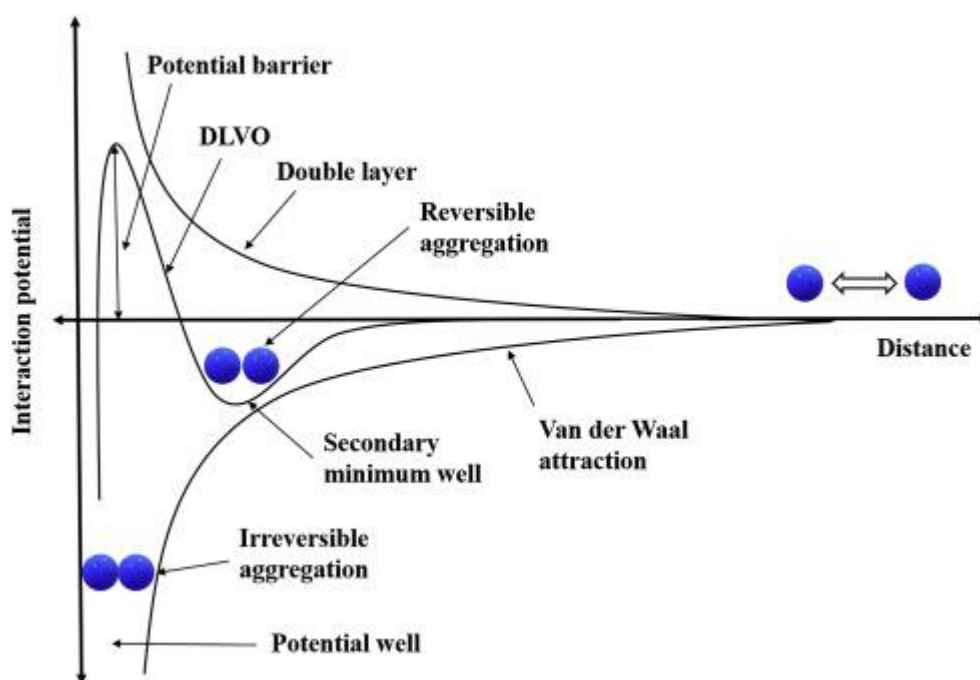


**Figure 2.14: DLVO Interaction Curve (Langford, Bruchsaler and Gupta, 2022).**



Under the presence of an external magnetic field, there is an additional interaction energy between MNPs, namely magnetic energy. Magnetic energy arises from the interaction between magnetic dipole moments possessed by MNPs, which is attractive in nature. By observing Figure 2.15, the presence of an external magnetic field induces the creation of magnetic energy between MNPs that is much longer-range than the Van der Waals attraction, and this is leading to the formation of supraparticles even if the distance between particles is wider than  $5\ \mu\text{m}$  (Al Harraq, Lee and Bharti, 2020).

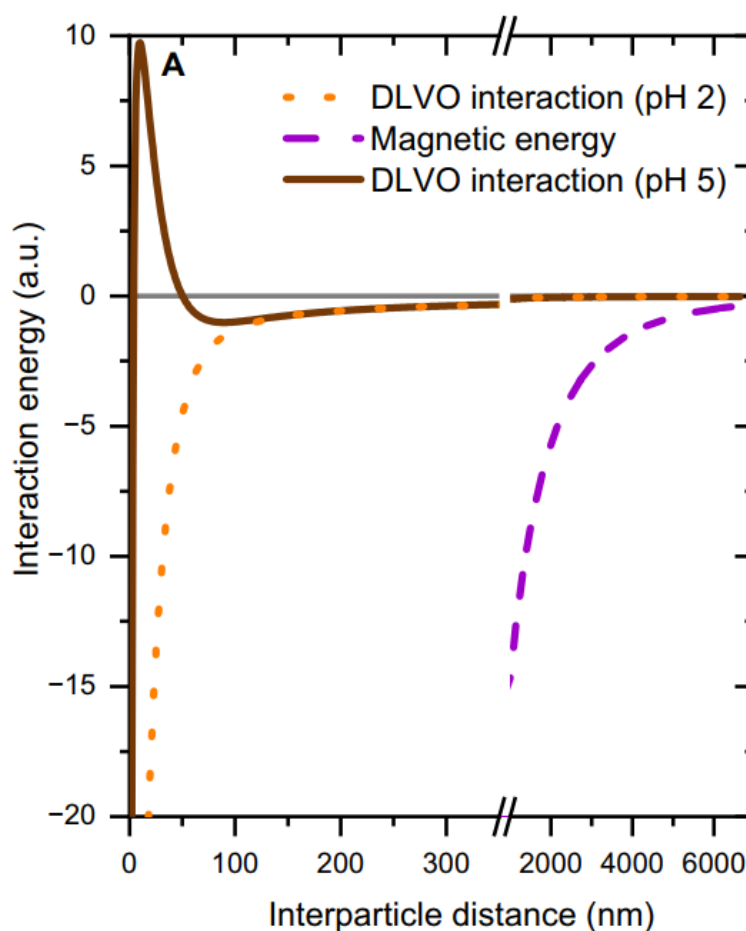


**Figure 2.15: DLVO Interaction Curve with an External Applied Magnetic Field (Al Harraq, Lee and Bharti, 2020).**

The external magnetic field magnetises the MNPs and accelerates the formation of supraparticles. This phenomenon results in the formation of MNP aggregates and occurrence of cooperative magnetophoresis. De Las Cuevas, Faraudo

and Camacho (2008) claimed that the dipole coupling constant ( $\lambda$ ) can be applied to predict the significance of MNP aggregation:

$$\lambda = \frac{E_D}{k_B T} \quad (2.9)$$

$$\lambda = \frac{\pi \mu_0 D^3 \chi^2 H^2}{72 k_B T} \quad (2.10)$$

where  $E_D$  is the magnetic energy of two particles at a certain distance. The equation (2.10) describes the ratio between the magnetic energy ( $E_D$ ) and the thermal energy ( $k_B T$ ) in a MNP system. When the value of  $\lambda$  is larger than one, the formation of aggregates is feasible as the magnetic energy being greater than the thermal energy. At saturation magnetization, the magnetic moment can be calculated by the following equation:

$$\mu = \frac{1}{6} \pi D^3 M_{s(v)} \quad (2.11)$$

where  $M_{s(v)}$  denotes the magnetization saturation per unit volume ( $A \text{ m}^{-1}$ ), therefore, the magnetic dipole-constant become:

$$\lambda = \frac{\pi \mu_0 D^3 M_{s(v)}^2}{72 k_B T} = \left[ \frac{\lambda_B}{D} \right]^3 \quad (2.12)$$

By incorporating equation (2.11) to equation (2.12):

$$\lambda_B = \left[ \frac{\pi \mu_0 D^3 M_{s(v)}^2}{72 k_B T} \right]^{\frac{1}{3}} D^2 \quad (2.13)$$

where  $\lambda_B$  is the magnetic Bjerrum length, which is analogous to conventional Bjerrum length that depicts the significance of electrostatics interaction energy over the thermal energy for electrostatic pairing between electrolytes in a medium. Here, the magnetic Bjerrum length is defined as the distance between parallel dipoles where the magnitude of the magnetic energy is equal to the thermal energy. Therefore, the formation of aggregate is feasible if the  $\lambda_B > D$ , and no aggregate formation when  $\lambda_B < D$ .

In addition, Andreu et al. (2011) have suggested a new parameter to predict the significance of cooperative effect in a MNP system subjected to magnetophoresis. Here, the magnetic coupling constant  $\Gamma$  is needed in the calculation and it is defined as:

$$\Gamma = \frac{\pi M_s(m)}{2\pi D^3 k_B T} \quad (2.14)$$

Aggregation parameter  $N^*$  is related to  $\Gamma$  and it can be formulated as:

$$N^* = \sqrt{\phi_o e^{\Gamma-1}} \quad (2.15)$$

where  $\phi_o$  is the volume fraction of particles in the MNP system. The criteria for the onset of particle aggregation and cooperative magnetophoresis is  $N^* > 1$ . Under this scenario, the value of  $N^*$  can be used to denote the average number of particles per aggregate in the MNP system in which the cooperative effect is dominant:

$$\bar{n} \approx N^* \quad (2.16)$$

where  $\bar{n}$  is the average number of particles per aggregate.

### 2.2.2 Hydrodynamic Effect

Besides the cooperative effect that involves the interaction between MNPs, the interaction between MNPs and the surrounding is also inevitable during magnetophoresis because the MNPs are fully immersed in a medium. Such a MNPs/fluid interaction that occurs during magnetophoresis is known as hydrodynamic effect and plays a vital role in governing the dynamical behaviour of magnetophoresis. The interactions between the MNPs and the medium typically involves momentum transfer between them through the particle collision. Owing to the momentum transfer between MNPs and fluid, the non-magnetic surrounding fluid also can gain momentum and move convectively, which induces the mixing effect during the magnetophoresis.

The hydrodynamic effects eventually enhance separation rates by approximately 30 times when compared to situations with no induced convection (Leong et al., 2017). As a consequence, the MNP solution appears to be uniformly distributed (homogeneous in concentration) throughout the entire timescale of magnetophoresis. This phenomenon has been observed in the work reported by Leong, Ahmad, and Lim (2005) that involves the magnetophoresis of non-cooperative MNP system ( $N^* < 1$ ) under a low gradient magnetic field. As shown in Figure 2.16, the separation kinetic profiles (or concentration profiles) recorded at different points of the MNP solution collapse into one exponential curve decay with time (all data curves in Figure 2.16 (a) and Figure 2.16 (b)). This observation indicates the concentration is uniform throughout the solution and has indirectly implied the existence of convective flow in the solution that induces the mixing and solution homogenising. The time-lapsed photos of the magnetophoresis have proven the uniform distribution of particles within MNP solution subjected to magnetophoresis at all times (Figure 2.17).

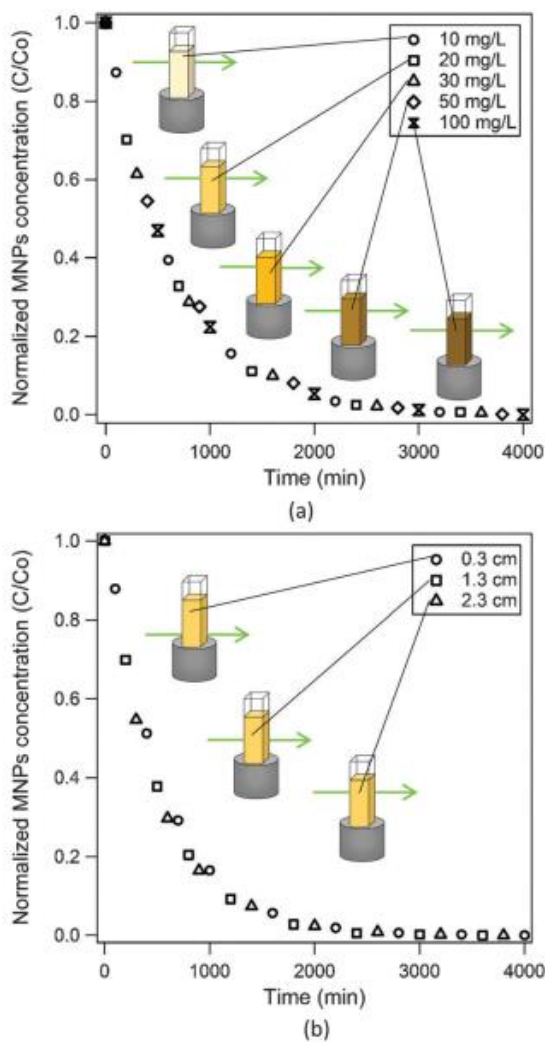


**Figure 2.16: Separation Kinetic Profiles with (a) Different MNPs Concentrations and (b) Different Measurement Positions (Leong, Ahmad and Lim, 2005).**

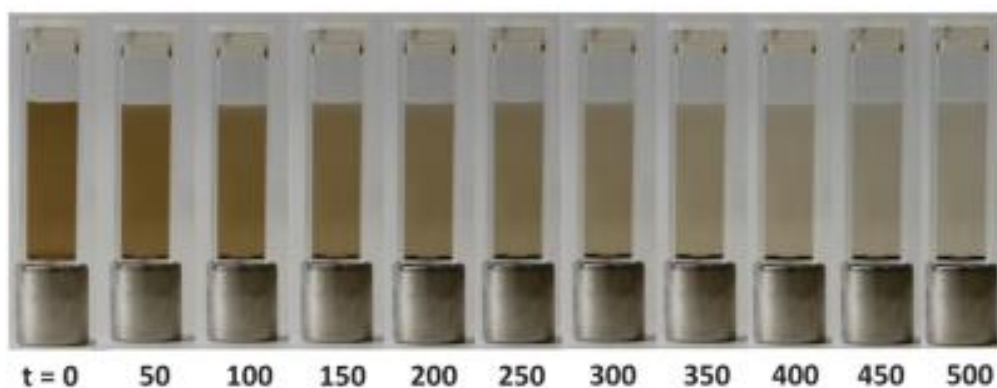


**Figure 2.17: Time Lapse Image of Experiment Result (Leong, Ahmad and Lim, 2005).**

Figure 2.18 shows the results of the simulation of the magnetophoresis model without incorporating the hydrodynamic effect, in which all MNPs are assumed to penetrate individually across the stagnant fluid toward the magnet. These simulation results show progressive clearance of the MNPs at the bottom (the region near to the magnet) and obvious inhomogeneity of MNP concentration throughout the solution after being subjected to magnetophoresis. If there are no hydrodynamic effects and induced convection in the MNP solution, the MNPs near the magnetic source should experience a stronger magnetophoretic force due to the magnetic field decaying along the distance from the magnetic source. The MNPs close to the magnetic sources should be collected more quickly and create a concentration gradient. However, in real life circumstances, the concentration of MNPs is homogeneous during the experiment. The contradictory result has proven the presence of hydrodynamic effect and induced convection is essential in governing the dynamical behaviour of magnetophoresis kinetics in real time experiment.

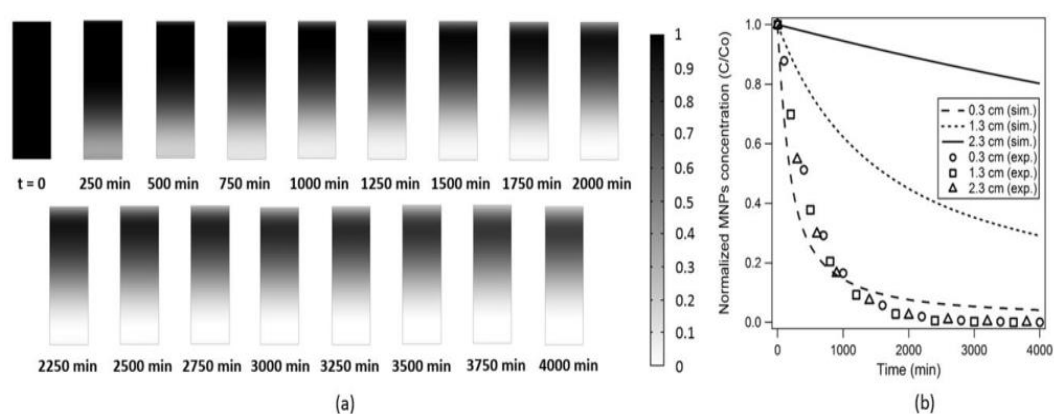


**Figure 2.18: (a) Simulation Result without MNPs/Fluid Interaction. (b) Comparison of Separation Kinetic Profile between Simulation Result (Line) and Experiment Result (Shape) (Leong, Ahmad and Lim, 2005).**

In addition, it also has been revealed that the intensity of the induced convection arising from hydrodynamic effect is concentration dependent. This statement has been proven by conducting experiments in which  $3000 \text{ mg L}^{-1}$  of methylene blue (MB) was added in the MNP solution with different concentrations (before applying a magnetic field) and the flow profile of the MNP was then observed by the aid of MB dye (Leong, Ahmad and Lim, 2005). The result is illustrated in Figure

2.19, which indicates the existence of convective flow induced by hydrodynamics in all cases (except the controlled experiment carried by using blank solution in which only diffusion can be observed). Interestingly, the intensity of this hydrodynamic effect is affected by the concentration of the MNPs, as the dye can be homogenised more rapidly in the MNP solution with the higher concentration. This is because there are more MNPs in the MNP solution of higher concentration that gain momentum from their response toward the external magnetic field, which causes more abundant amounts of momentum to be transferred to the surrounding fluid and generate more intense convective flow. Therefore, the induced convection flow is more vigorous and swifter if the magnetophoresis is performed by MNP solution of higher concentration.

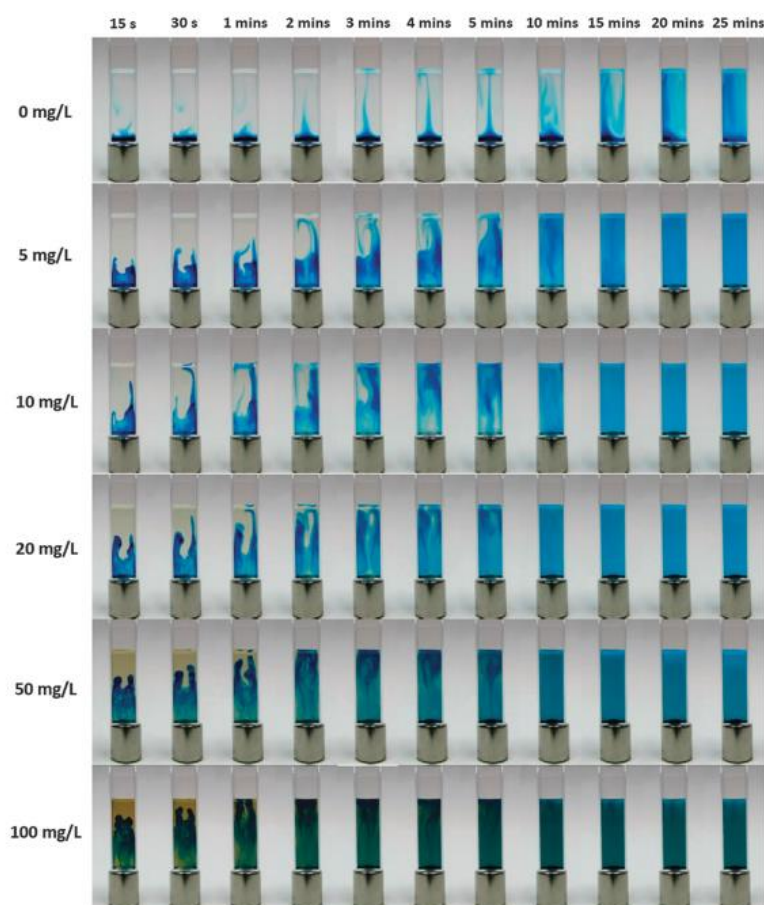


**Figure 2.19: Time Lapse Image with Different MNPs concentrations (Leong, Ahmad and Lim, 2005).**

The occurrence of induced convection flow under an external field also can be explained macroscopically by taking analogous to the natural convection that involves heat transfer (Figure 2.20). In the magnetophoresis configuration as shown in Figure 2.20 (a magnet placed at the bottom of the MNP solution), stronger magnetophoretic force is exerted on the MNPs located at the bottom as compared to those located at the top (further away from the magnet), which causes this portion of MNPs to be captured on the cuvette wall adjacent to the magnet in a split second, resulting in a concentration gradient. Consequently, the magnetization per unit volume at the bottom part of the MNP solution is diminished whereas there are still a lot of MNPs at the top part of the MNP solution which causes this portion of MNP solution to have high magnetization per unit volume. Since, the magnetophoretic force is proportional to the magnetization of the MNP solution, the MNP solution at top region can experience a larger magnetophoretic force as compared to that of the lower region that are pointing at the downward direction, which generates mechanical instability throughout the MNP solution. This mechanical instability is naturally relaxed by generating a convective flow that induces the circulation of MNP solution to flow so that the MNPs are being dispersed throughout the medium uniformly and the MNP concentration exhibits homogeneity during magnetophoresis. This phenomenon is indeed analogous to the natural convection observed in a fluid being heated at the bottom (Figure 2.20), in which the mechanical instability created by the density difference (and hence the difference in the gravitational force exerted on the solution per unit volume) of the fluid at the top and bottom portions is relaxed by the generation of circulating flow in the fluid.

Process	Illustration	'Substance' to be transferred	Type of field	Driving force	Fluid property which induces convection
Natural convection		Heat energy	Gravitational field	Temperature gradient	Volume per unit mass
Magnetophoresis		MNPs	Magnetic field	Concentration gradient	Magnetization per unit mass

**Figure 2.20: Differences between Magnetophoresis and Natural Convection (Leong, Ahmad and Lim, 2005).**



Due to the analogous similarity of natural convection and magnetophoresis, Leong, Ahmad and Lim (2015) have proposed a new dimensionless number, namely magnetic Grashof number ( $Gr_m$ ), to depicts the intensity of magnetophoresis induced convection in a MNP system subjected to magnetophoresis. The magnetic Grashof number is derived, in analogous manner, from the Grashof number ( $Gr$ ) that describes the intensity of natural convection in a heating system (ratio of buoyancy force to viscous drag). Magnetic Grashof number describes the ratio of magnetic buoyancy force to viscous drag, which can be mathematically formulated as:

$$Gr_m = \frac{\nabla B(\partial M_{(m)}/\partial c)_H(c_s - c_\infty)L_c^3}{\rho_f \eta_k^2} \quad (2.17)$$

where  $c_s$  denotes the MNPs concentration of the surface in the vicinity of the magnet source,  $c_\infty$  denotes the MNPs concentration in bulk solution,  $\eta_k$  denotes the kinematic viscosity of the medium and the  $L_c$  denotes the characteristic length. The criteria for the onset hydrodynamic effect are dependent on the magnitude of magnetic Grashof number of a particular MNP system. For instance, the hydrodynamic effect is significant when  $Gr_m > 1$ ; the hydrodynamic effect is not significant and there are no noticeable induced convective currents during magnetophoresis when  $Gr_m < 1$ .

The validity of magnetic Grashof number in estimating the significance of magnetophoresis induced convection can be justified by the velocity contour plots of MNP solution subjected to magnetophoresis under different conditions (and hence the magnitude of magnetic Grashof number) such as different concentration of MNPs, degree of confinement, and magnetic flux density (Leong et al., 2020), as shown in Figure 2.21. According to this figure, the hydrodynamic effect is notable when the magnetic Grashof number is larger than unity while it is less significant for the cases with the magnetic Grashof number less than unity.

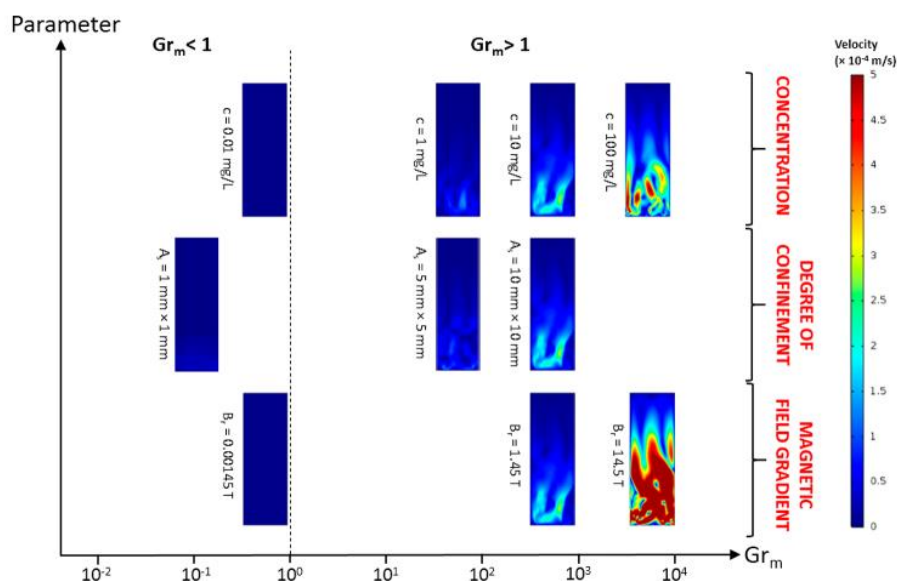
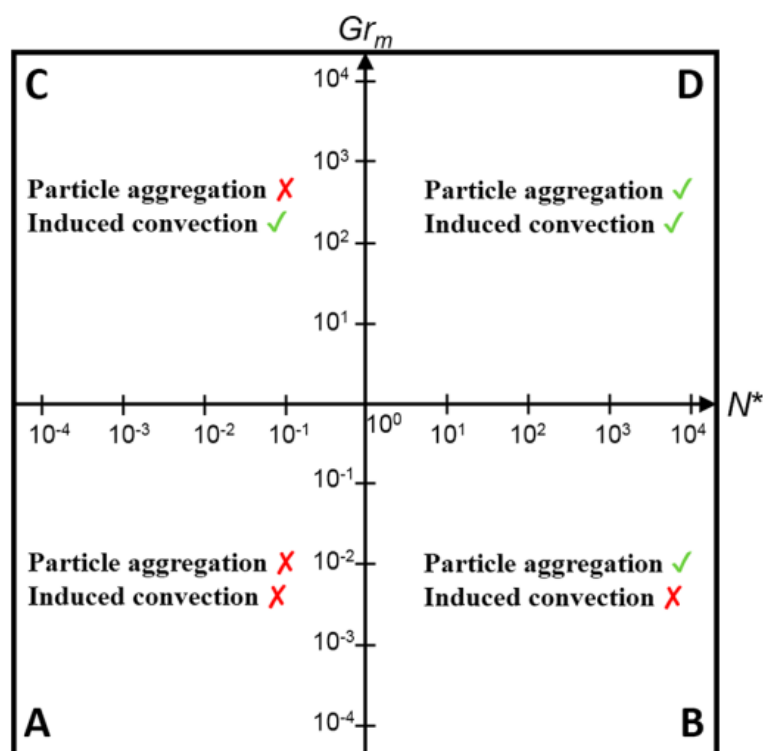


Figure 2.21: Hydrodynamic Effect at Different Conditions (Leong et al., 2020).

### 2.2.3 Unified View of Magnetophoresis

As mentioned earlier, the following two dimensionless parameters: aggregation parameter  $N^*$  and the magnetic Grashof number  $Gr_m$  can determine the presence or absence of cooperative and hydrodynamic effects, respectively. By taking these two effects into consideration, the mechanism of magnetophoresis process can be categorised into four parts, each part has its own peculiar mechanisms and mathematical models to describe its magnetophoresis kinetics (Leong et al., 2020). The four regions are depicted in Figure 2.22, and different values of the aggregation parameter  $N^*$  and the magnetic Grashof number  $Gr_m$  resulting in different magnetophoresis mechanisms. In region A, the hydrodynamic and cooperative effect is insignificant. Therefore, the classical magnetophoresis theory can safely be used to predict the kinetic profile of MNPs. In region B, only the cooperative effect occurs during the magnetophoresis process; a cooperative model can be applied to predict the kinetic of MNPs. In region C, only the hydrodynamic effect occurs during the magnetophoresis process; a hydrodynamic model can be applied to predict the kinetic of MNPs. However, in region D, both the cooperative and hydrodynamic effects occur simultaneously. Most industry and commercial applications fall within the region D;

therefore, it is essential to derive a mathematical model to study the kinetic profile of MNPs in the region D.



**Figure 2.22: Aggregation Parameter against Magnetic Grashof Number (Leong et al., 2020).**

For regions A, B, and C, there are readily derived mathematical models to predict their magnetophoresis kinetics. Andreu et al. (2011) have established a model for region A (without the cooperative and hydrodynamic effects), De Las Cuevas, Faraudo and Camacho (2008) establish a mathematical model for region B (with the cooperative effect), and Leong et al., (2015) establish a mathematical model for region C (with the hydrodynamic effect). However, in the existing literature, there is no mathematical model available for the prediction of magnetophoresis kinetics in region D, where both cooperative and hydrodynamic effects are dominating the overall process. From a practical perspective, it is also convenient to transform the universal diagram shown in Figure 2.22 to the diagram with some useful physical quantities (such as concentration and magnetic field gradient) as the axis variables (see Figure 2.23).

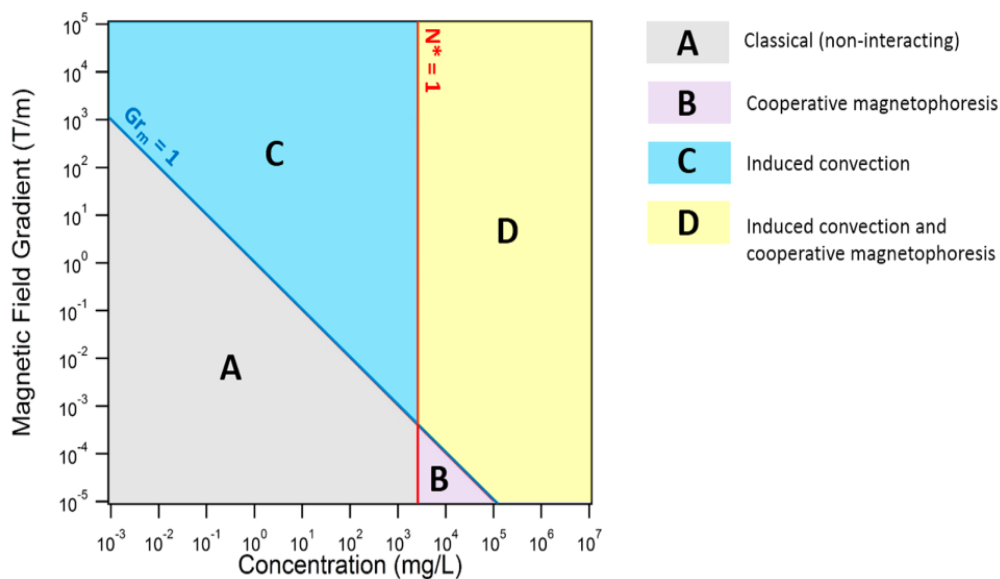


**Figure 2.23: Concentration of MNPs against Magnetic Field Gradient (Leong et al., 2020).**

Figure 2.24 suggests that in most real-life applications, the mechanism taking place in Region D is a common phenomenon (Leong et al., 2020). To better understand this mechanism and its impact on the system, there is a need to develop a mathematical model that can capture the kinetics of magnetophoresis in this region. This model can help researchers and scientists to better predict and analyse the behaviour of magnetic particles under the influence of magnetic fields and other relevant parameters in Region D. Such understanding and modelling can be useful in a variety of fields, such as drug delivery, biomedical research, and environmental engineering, among others.

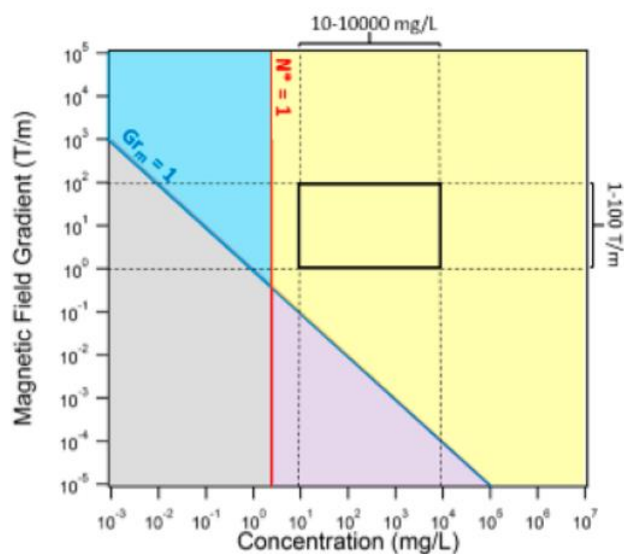


**Figure 2.24: Concentration of MNPs against Magnetic Field Gradient, The MNPs Concentration and Magnetic Field Gradient in the Black-frame are given by 10-10 000 mg/L and 1-100 T/m, respectively (Leong et al., 2020).**

## 2.4 Modelling of Magnetophoresis Kinetics

This section describes the previous attempts of researchers to develop mathematical models to predict the kinetics of the magnetophoresis of MNPs.

### 2.4.1 Classical Magnetophoresis Model

Firstly, the mathematical model derived according to the classical magnetophoresis theory to depict the LGMS of MNP solution under a uniform magnetic field created by SEPMAG was introduced (Andreu et al., 2011), as shown in Figure 2.11. While deriving this LGMS model, MNPs were assumed to be distributed uniformly in a diamagnetic medium and surrounded by a cylindrical magnet (radius of the cylindrical magnet is  $L$ ) with homogeneous magnetic gradient, forcing the MNPs move toward the cylindrical wall. The magnetophoretic force, velocity, and saturation velocity of

MNPs can be computed through equation (2.18), equation (2.19), and equation (2.20), which is given as the following equations:

$$F_M = \frac{1}{6}\pi D^3 \rho_p M_{(m)} \mu_o \left(\frac{\partial H}{\partial r}\right) \quad (2.18)$$

$$v = \frac{D^3}{18\eta D_h} \rho_p M_{(m)} \mu_o \left(\frac{\partial H}{\partial r}\right) \quad (2.19)$$

$$v_s = \frac{1}{18\eta} D^2 \rho_p M_{s(m)} \mu_o \left(\frac{\partial H}{\partial r}\right) \quad (2.20)$$

where  $v_s$  is the velocity of MNPs at magnetization saturation, the ratio of the magnetic field intensity at the wall of the magnet to those required to enable the MNPs to reach the magnetization saturation can be determined by a dimensionless parameter ( $\beta$ ), which can be defined as:

$$\beta = b \mu_o \left(\frac{\partial H}{\partial r_s}\right) L \quad (2.21)$$

where  $L$  is the distance from the centre to the wall surface of the SEGMAP system. Since the magnetic field is uniform throughout the system, the change of the magnetic intensity with respect to the radius ( $\frac{\partial H}{\partial r_s}$ ) is constant which causes the  $\beta$  value in Equation (2.21) to be a constant for a particular LGMS experiment. With the value of,  $\beta$ , the velocity of MNPs located at a distance  $r_s$  from the centre of the SEGMAP system can be calculated by:

$$v(r_s) = \frac{dr}{dt} = v_s \mathcal{L}\left[\frac{\beta r}{L}\right] \quad (2.22)$$

By rearranging and integrating the equation (2.22), which is an ordinary differential equation, the separation time of a particle can be calculated as:

$$\int_0^t v_s dt = \int_{r_0}^r \frac{dr}{\coth(\beta r/L) - (L/\beta r)}$$

$$t = \frac{L}{\beta v_s} \ln\left[\frac{\beta \cosh(\beta) - \sinh(\beta)}{(\beta r_0/L) \cosh((\beta r_0/L) - \sinh(\beta r_0/L))}\right] \quad (2.23)$$

where  $r_o$  is the initial distance of the particle from the centre (at time  $t = 0$ ), and  $r$  is the distance of the particle from the centre at time  $t$ . As this LGMS system is induced by SEPMAG, which is a system that exhibits cylindrical symmetry and the magnetic field is directed in the radial direction, the magnetic flux density is zero at the centre of the system (as the magnetic field is cancelling each other at this point). When the MNPs approaches magnetization saturation, the  $\beta r_o/L \gg 1$  and the  $\mathcal{A}[\beta r/L] \approx 1$ . Under these circumstances, the equation (2.23) can be simplified to:

$$t = \frac{L - r_o}{v_s} \quad (2.24)$$

Then, the fraction of particles dispersed in the medium at time  $t$ ,  $f$ , can be derived analytically by the following concept: The number of particles remaining dispersed in the medium is proportional to the surface area of the dispersed MNPs, and all the MNPs are distributed homogeneously in the medium initially. At a particular time  $t$ , only particles with initial radial coordinates smaller than  $r_o$  (A distance with no magnetic field) retain in the medium and the fraction of particles inside the magnetic separator  $f$  can be mathematically written as:

$$f = \frac{N(t)}{N(0)} = \left(\frac{r_o}{L}\right)^2 \quad (2.25)$$

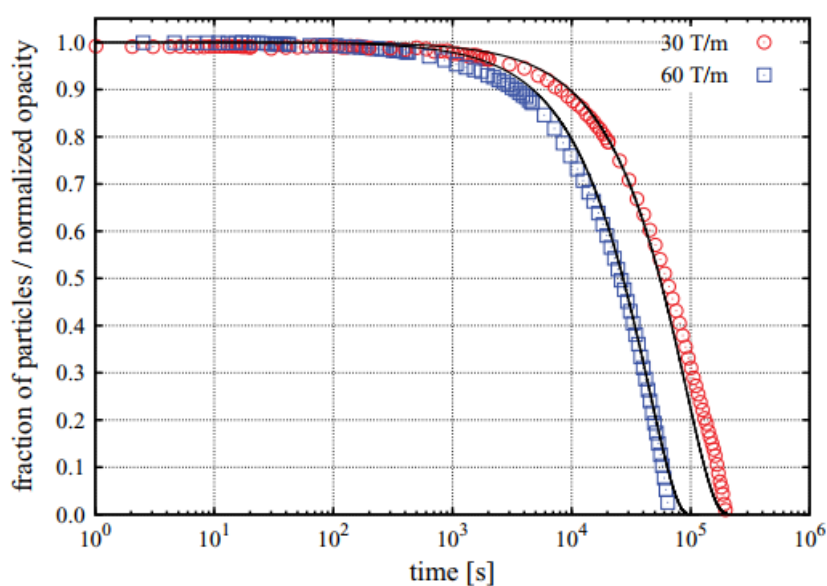
where  $N(t)$  is the remaining MNPs in the medium at time  $t$ , and the  $N(0)$  is the initial amount of particles dispersed in the medium. By substituting the mathematical expression of  $f$  and  $\beta$  into the equation (2.23), the following equation is resulted:

$$t = \frac{L}{\beta v_s} \ln \left[ \frac{\beta \cosh(\beta) - \sinh(\beta)}{(\beta \sqrt{f}) \cosh((\beta \sqrt{f}) - \sinh(\beta \sqrt{f}))} \right] \quad (2.26)$$

Under certain conditions (when  $\beta \gg 1$  and the  $\beta \sqrt{f} \gg 1$ ), the equation can be further simplified to:

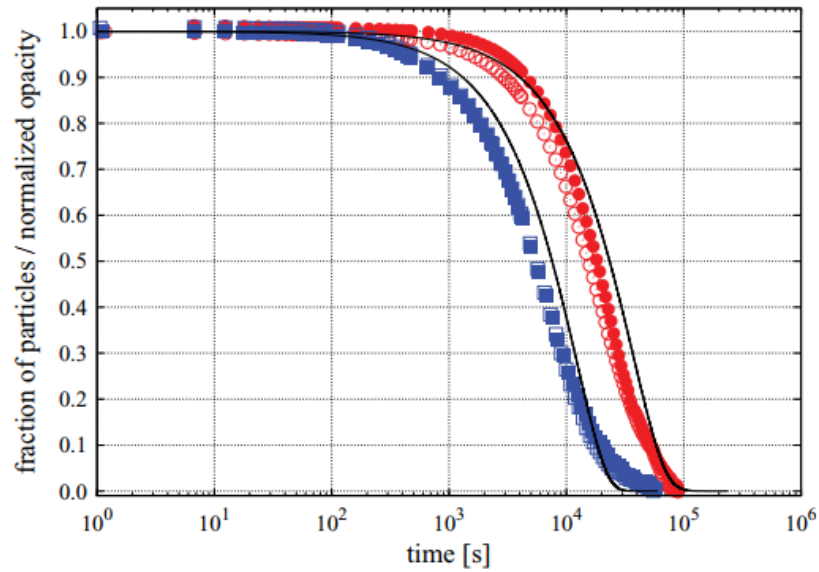
$$f \approx \left(1 - \frac{v_s}{L} t\right)^2 \quad (2.27)$$

Figure 2.25 and figure 2.26 display the comparison of the experimental results and theoretical prediction by using equation (2.24), for LGMS conducted with MNP solution of different size and magnetic field gradient (generated by SEPMAG). The experiment result has a good fit to the predicted result, despite having minor deviations. The slight deviations from the model prediction are caused by real life perturbations such as polydispersity (dispersed MNPs may not entirely uniform which may have different sizes and shapes), spurious effects (viscosity of the medium varies with temperature), and the magnetic properties of particles. Despite that, the model developed is sufficiently accurate to predict the kinetics of the LGMS process induced by a uniform magnetic field (Andreu et al., 2011).



**Figure 2.25: Comparison between the Experiment Result (Markers Represent  $\gamma$ - $\text{Fe}_2\text{O}_3$  Nanocrystals with hydrodynamic diameter of 12 nm) and the Predicted Result (Solid Lines) (Andreu et al., 2011).**





**Figure 2.26: Comparison between the Experiment Result (Circles correspond to Sample S2 Core ( $\gamma\text{-Fe}_2\text{O}_3$ )/Shell ( $\text{SiO}_2$ ) with hydrodynamic diameter of 82 nm, Circles correspond to Sample S3 Core ( $\gamma\text{-Fe}_2\text{O}_3$ )/Shell ( $\text{SiO}_2$ ) with hydrodynamic diameter of 157 nm) and the Predicted Result (Solid Lines) at Magnetic Field of 60 T/m (Andreu et al., 2011).**

#### 2.4.2 Cooperative Magnetophoresis Model

The cooperative effect greatly affects the kinetics of MNPs, the LGMS separation time is much faster with the presence of the cooperative effect. As the significance of cooperative effect is heavily dependent on the concentration of the MNP solution, thus, the extent in which the cooperative effect can accelerate the cooperative magnetophoresis is related to the concentration of MNP solution employed. De Las Cuevas, Faraudo and Camacho (2008) have established an empirical model to relate the separation time induced by a LGMS on a cooperative MNP solution to the concentration of the MNP solution. In this regard, a parameter that is used to estimate the intensity of cooperative effect is introduced, namely scaled Bjerrum length  $\lambda_{B(\text{scaled})}$  which is defined as:

$$\lambda_{B(\text{Scaled})} = \frac{\lambda_B}{D} \quad (2.28)$$

The magnetic Bjerrum length is the separation distance of two MNPs in which the magnetic attraction is well-balanced by the thermal randomization energy. If the separation distance between the MNPs is lower than  $\lambda_B$ , the magnetic attraction energy is overwhelming over the thermal energy. On the other hand, if the separation distance between MNPs is larger than the magnetic Bjerrum length, then the thermal randomization energy is more dominant. Figure 2.27 shows several samples extracted from various literatures with the calculated reciprocal of scaled Bjerrum length. The grey region (without the cooperative effect) and the white region (with the cooperative effect) are separated by a horizontal line ( $\lambda_B/D = 1$ ). This figure shows that the sample from the work by Miller et al. is the only MNP system in which the cooperative effect is trivial, which has been supported by the experimental results from the given work. On the other hand, the other three samples are cooperative in nature according to the theory calculation, and this argument has been proven experimental because the separation time of these MNP solutions were found to be concentration dependent.

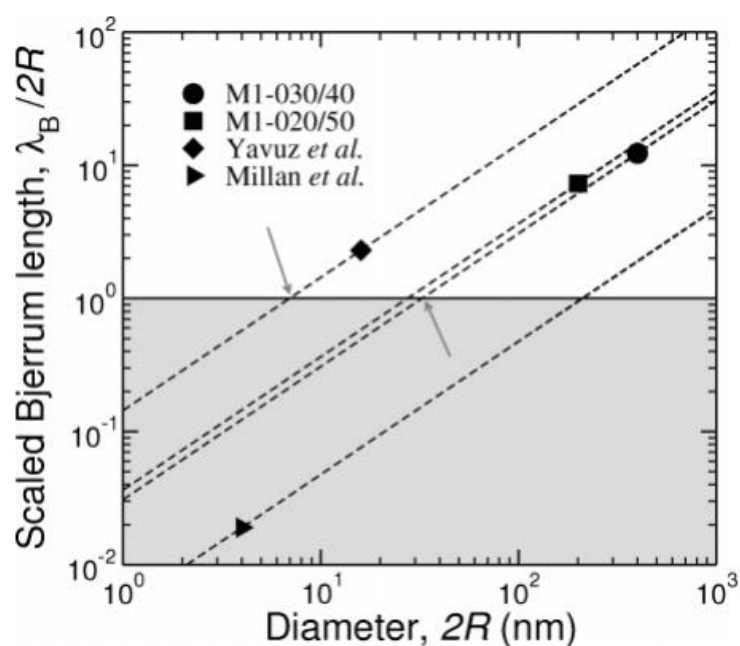


**Figure 2.27: The Scaled Bjerrum Length against the Diameter of MNPs (De Las Cuevas, Faraudo and Camacho, 2008).**

By comparing the magnetic Bjerrum length of MNPs with their diameter, it is possible to deduce the significance of cooperative effect of the MNP system upon

being subjected to LGMS. The cooperative effect is more effective if the magnetic Bjerrum length is higher and the interparticle distance  $d_p$  is lower (as there is more space for the magnetic attraction between MNPs to dominate). This implies that the MNP solution with the lower  $\frac{d_p}{\lambda_B}$  ratio has the greater intensity of cooperative effect which is leading to the more rapid magnetophoretic separation and the shorter separation time. The expression of the  $\frac{d_p}{\lambda_B}$  ratio can be expressed as follows:

$$\frac{d_p}{\lambda_B} = \left[ \frac{3k_B T \rho_p}{2\mu_o M(m)^2 c} \right]^{(1/3)} \left( \frac{1}{R} \right) \quad (2.29)$$

Since  $\frac{d_p}{\lambda_B}$  value can be correlated to the separation time (the smaller the  $\frac{d_p}{\lambda_B}$  value, the greater the intensity of cooperative effect and, hence, the shorter the separation time), the following empirical model can be deduced:

$$t_s = t_0 \left[ \frac{d_p}{\lambda_B} \right]^\alpha \quad (2.30)$$

where  $t_s$  denotes the LGMS separation time while  $t_0$  and  $\alpha$  are constants that are unique for different MNP system and LGMS configuration. In the work reported by De Las Cuevas, Faraudo and Camacho (2008), they attempted to plot the separation time  $t_s$  against scaled average distance  $\frac{d_p}{\lambda_B}$  for LGMS experiments conducted with MNP solution of different concentration, which can be fitted into Equation (2.30) up to great accuracy with  $t_0 = 0.73 \pm 0.10$  and  $\alpha = 66 \pm 6$  s, as shown in Figure 2.28 (De Las Cuevas, Faraudo and Camacho, 2008). This result indicates the validity of Equation (2.30) to predict the separation time of a particular LGMS system with a specified MNP system empirically, provided the  $t_0$  and  $\alpha$  values of it are known.

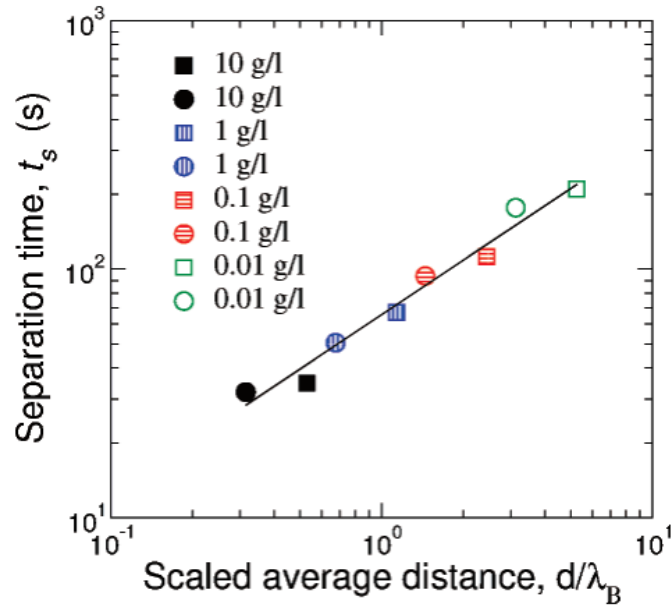


**Figure 2.28: Separation Time Against Scaled Average Distance (De Las Cuevas, Faraudo and Camacho, 2008).**

### 2.4.3 Hydrodynamic Magnetophoresis Model

As magnetophoresis induced convection (hydrodynamic effect) was observed in the LGMS of MNP solution, Leong, Ahmad and Lim (2015) have attempted to develop a theoretical model to depict the magnetophoresis kinetics of it by incorporating the hydrodynamic effect. The simulation results of this model were then compared with the real time experimental observation and simulation result from the classical model (without considering the hydrodynamic effect or MNPs/fluid interaction). The MNP system used in their study is non-cooperative in nature (with  $N^* < 1$ ) so that the cooperative effect can be safely excluded from the analysis. The forces that are taken into consideration in the modelling of this magnetophoresis process are the magnetophoretic force, the gravitational force, and the Brownian force action on the MNP solution. All these forces are included in the Navier-Stokes equation as shown in Equation (2.31):

$$\rho_f \left( \frac{\partial v_s}{\partial t} + v_f \cdot \nabla v_f \right) = -\nabla p_{abs} + \eta \nabla^2 v_f + \rho_f g + f_m \quad (2.31)$$

where  $v_f$  is a vector that denotes the velocity of the MNPs solution,  $p_{abs}$  is the absolute pressure of the system, and  $f_m$  is the magnetophoretic force per unit volume that is exerted on the MNPs solution. Equation (2.31) is solved by coupling with continuity equation (Equation (2.32)) and drift-diffusion equation (Equation (2.33)) to obtain the velocity and concentration profile of the MNP solution throughout the magnetophoresis process:

$$\nabla \cdot v_f = 0 \quad (2.32)$$

$$\frac{\partial c}{\partial t} = D\nabla^2 c - \nabla \cdot v_f c = 0 \quad (2.33)$$

The volumetric magnetophoretic force can be mathematically written as:

$$f_m = M_{(v)} \nabla \cdot B \quad (2.34)$$

where the magnetization of MNPs per unit volume,  $M_{(v)}$  is related to the concentration of the MNPs,  $c_{(m)}$  and the magnetization of MNPs per unit mass,  $M_{(m)}$  as follow:

$$M = c_{(m)} M_{(m)} \quad (2.35)$$

For the experimental model is illustrated in Figure 1.1, a cuvette was placed on the top of a cylindrical magnet, in which the magnetic flux density generated by the magnet along the axis of the magnet can be defined as:

$$B = \frac{B_r}{2} \left[ \frac{y + h_{mag}}{\sqrt{(y + h_{mag})^2 + r_{mag}^2}} - \frac{y}{\sqrt{y^2 + r_{mag}^2}} \right] \quad (2.36)$$

where the symbol  $B_r$  represents the remnant magnetic flux density, the symbol  $y$  represents the vertical distance from the pole face of the cylindrical magnet, the symbol  $h_{mag}$  and the symbol  $r_{mag}$  represents the height and radius of the cylindrical magnet respectively. It can be assumed that the intensity of the magnetic flux pointed to the axial direction is much stronger than the radial direction in the MNP solution under

this magnetophoresis setup, thus, the magnetic flux density gradient can be formulated as follow:

$$\nabla B = \frac{B_r r_{mag}^2}{2} \left[ \frac{1}{[\sqrt{(y + h_{mag})^2 + r_{mag}^2}]^{\frac{3}{2}}} - \frac{y}{[\sqrt{y^2 + r_{mag}^2}]^{\frac{3}{2}}} \right] e^y \quad (2.37)$$

where  $e^y$  denotes the unit vector pointing to the positive y-direction (pointing upward see Figure 3.2). By using this magnetic field profile, the magnetization of MNP per unit mass can be predicted by the Langevin function, which is given as follow:

$$M_{(m)} = M_{s(m)} \mathcal{L}\left(\frac{mH}{k_B T}\right) \quad (2.38)$$

and the magnetic flux density  $B$  is related to the magnetic flux intensity  $H$ , which can be formulated as:

$$B = \mu_o H \quad (2.39)$$

In this model, the momentum obtained by the MNPs due to an external applied magnetic field is being transferred to the surrounding medium through MNPs/fluid interactions, which has been accounted for in the Navier-Stokes equation (Equation (2.31)). In addition, the MNPs and the surrounding fluid are viewed as an integrated system which cannot be compressed, and the momentum is conserved within the MNP system. The equations (2.31) and (2.32) are the main equations that incorporate the hydrodynamic effect into the model, and these equations related the spatial fluid flow profile of MNPs solution to its viscosity and external forces exerted on it.

The predicted result by using this model has a good agreement with the experimental result illustrated in Figure 2.29 (Leong, Ahmad and Lim, 2015). For instance, the MNP solution appears to be uniform throughout the entire magnetophoresis process. In addition, the concentration profile resulting from the model simulation agrees with the experimental results up to very good accuracy.

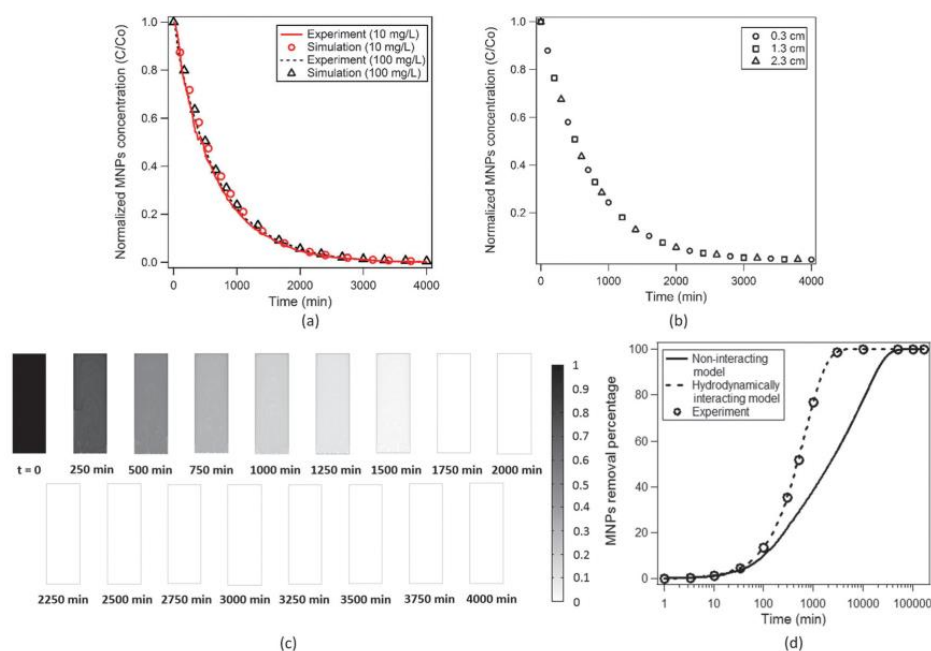


**Figure 2.29: Comparison between the Predicted Result with MNPs/Fluid Interaction Model to the Experimental Result (Leong, Ahmad and Lim, 2015).**

## 2.5 Research Gap

In most real-life applications of LGMS in the engineering field, the cooperative and hydrodynamic effects occur simultaneously. In order to exclude these effects from the LGMS system, very low concentration of MNPs must be employed to ensure that either the aggregation parameter or the Grashof number to be less than unity. Under this scenario, the magnetophoresis kinetics can be predicted by using classical magnetophoresis theory that has been well-established, which is possible to yield a specific analytical solution if the geometry is simple enough. However, the low MNP concentration leads to poor efficiency, which makes the LGMS process impractical for engineering applications. In addition, both effects accelerate the LGMS process by a few orders of magnitudes, which can be utilised to enhance the performance of the LGMS technology. As mentioned earlier, to the best of knowledge, the analytical solutions that incorporate the cooperative and cooperative effects are not available at present. This article is focused on establishing a mathematical model that accounts for the cooperative effect and the hydrodynamic effect simultaneously.

The analytical solutions available for the cooperative effect have neglected the interaction between magnetic nanoparticles and fluid, while the solutions for the hydrodynamic effect have disregarded the interactions between magnetic nanoparticles. To address this limitation, a new mathematical model can be developed by integrating the characteristics of both cooperative and hydrodynamic models. The cooperative effect alters the size of magnetic nanoparticles, leading to different magnetic susceptibilities, velocities, and saturation velocities. The conservation of momentum in the system can be described by the continuity and Navier-Stokes equations, which can also be used to account for the interaction between magnetic nanoparticles and fluid. By deriving a formula that can predict changes in particle size and incorporating it with the continuity and Navier-Stokes equations for the hydrodynamic effect, a comprehensive mathematical model that captures both effects can be established.



## CHAPTER 3

### METHODOLOGY

#### 3.1 Flowchart

The flowchart of this project is illustrated in Figure 3.1.

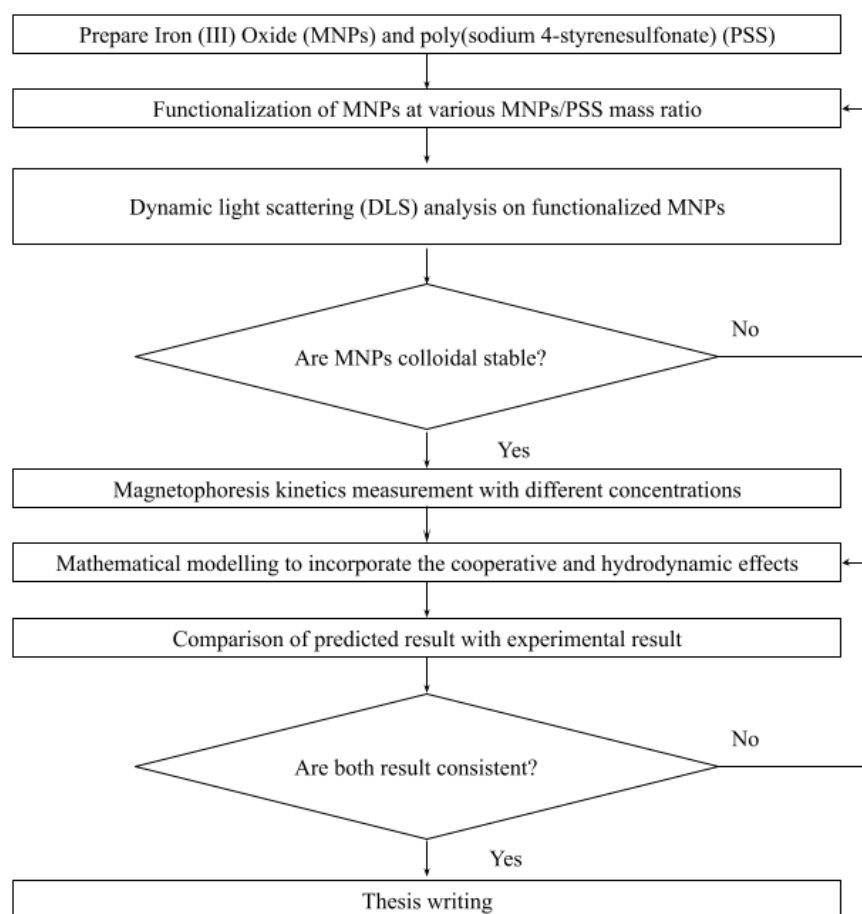


**Figure 3.1: Flow Chart of the Project.**

### 3.2 Material and Equipment

**Table 3.1: Materials Used in the Experiment.**

Materials	Supplier
Iron oxide (III) nanoparticles, Fe <sub>3</sub> O <sub>4</sub> *	Sigma Aldrich
Poly(sodium 4-styrenesulfonate), PSS	Sigma Aldrich
Sulphuric acid, H <sub>2</sub> SO <sub>4</sub>	Chemiz
Deionized water	-

**Table 3.2: Equipment Used in the Experiment.**

Equipment	Brand	Model Number
Magnet	-	-
Sonicator bath	Elmasonic	S 180H
End-to-end rotator	SLA Advanced Technology	MX-RL-E
pH meter	EUtech Instrument	PC2700
Centrifugation machine	Eppendorf	Centrifuge 5430
Dynamic light scattering machine (DLS)	Malvern Panalytical	Zetasizer lab
Scanning electron microscope (SEM)	Joel microscope	JSM-7610F
Beaker	-	-
Measuring Cylinder	-	-
Pipette	-	-
Spatula	-	-
Weighing boat	-	-
Electrical digital weight balance	-	-

### 3.3 Functionalization of MNPs

PSS was determined for the functionalised process system as the MNPs coated with PSS have the highest colloidal stability and excellent regeneration capacity reported by Chong et al. (2020). Initially, 0.0625 g of iron oxide (III) nanoparticles ( $\text{Fe}_3\text{O}_4$ ) and 0.0625 g of PSS were measured with an electrical digital weight balance and put into different centrifuge tubes. Afterward, the MNPs and the PSS were mixed with 25 mL of deionized water. In order to disperse the particles in the deionized water uniformly, both solutions were subjected to sonication in a sonicator bath for 60 minutes. Then, the solutions were adjusted to around pH of 3 by using 1 M of sulphuric acid. The isoelectric point of the iron oxide (III) nanoparticles is approximately pH 6.8 (Alfredo Reyes Villegas et al., 2020) with the net charge on a particle is zero at this particular pH (Novák and Havlíček, 2016) and it is positively charged at pH lower than 6.8. The PSS is slightly negatively charged at all pH values due to the presence of  $\text{SO}_3^-$  functional groups. Hence, under pH 3, the PSS and MNPs tend to attract each other due to electrostatic force, which improves the effectiveness of the functionalization process. Then, the MNP and PSS solutions were mingled together and sonicated for 20 minutes to facilitate the dissolution of the PSS and the dispersion of MNPs. The coating process on oppositely charged particles is a swift, irreversible process with a short relaxation time, because of the electrostatic attraction forces (Yeap, Ahmad, Ooi and Lim, 2012). After sonication, the mixture was placed on an end-to-end rotator for 24 hours (suffice for physisorption) to promote the coating process. To obtain high quality coated MNPs, the mixture was centrifuged in a centrifugal machine under 4000 rpm for one hour. After centrifugation, the functionalized MNPs were captured at the bottom of the centrifuge tube due to the centrifugal force, and the PSS solution was removed from the centrifuge tube. Subsequently, the MNPs were resuspended in a 50 mL of deionised water and sonicated for 20 minutes to wash off the remaining PSS before conducting another centrifugation process. The washing process was repeated three times to ensure all the residue PSS were removed from the functionalized MNPs. The procedures were repeated to produce functionalized MNPs under different MNPs to PSS mass ratio that displayed in Table 3.3, with the purpose of determining the most optimal MNPs to PSS mass ratio during the functionalization process that results in the most colloidal stable MNP system.

**Table 3.3: MNPs to PSS Mass Ratio Used in the Experiment.**

<b>Sample</b>	<b>Mass of MNPs (g)</b>	<b>Mass of PSS (g)</b>	<b>MNPs/PSS mass ratio</b>
S1	0.0625	0.03125	1:0.5
S2	0.0625	0.06250	1:1
S3	0.0625	0.12500	1:2
S4	0.0625	0.25000	1:4

### **3.4 Determination of Hydrodynamic Size of Functionalized Magnetic Nanoparticles**

The hydrodynamic diameter of the functionalized MNPs are measured through dynamic light scattering (DLS) technique. The MNP solution was diluted to  $10 \text{ mg L}^{-1}$  to reduce the effect of multiple scattering and particle interaction prior to DLS analysis. An incident light was introduced, and the fluctuation of the scattered light was measured at an angle of  $173^\circ$  relative to the incident light. The resulting intensity fluctuation was fitted to an exponentially decaying correlation function, which decayed more quickly for smaller MNPs due to their higher diffusibility. The translational diffusivity is then obtained through the cumulants method, and eventually determined the hydrodynamic diameter of the MNPs by employing Einstein-Stokes equation (Ramos, 2017).

### **3.5 Experimental Methods**

MNP solutions with different concentrations (50 mg/L, 75 mg/L, 125 mg/L, 175 mg/L, and 300 mg/L) are prepared through diluting the functionalized MNPs with deionized

water. An arduino spectrometer was built to measure the concentrations of MNPs during the magnetophoresis process and the blank solution is deionized water. The blank solution is a reference point used to determine the complete magnetophoresis separation process. MNP solutions with different concentrations are extracted into cuvettes ( $1\text{ cm} \times 1\text{ cm} \times 4\text{ cm}$ ) by using a pipette, each cuvette is filled with 3 mL homogenous dispersed MNP solution with different concentrations. Afterward, a cuvette with homogenous dispersed MNP solution is placed on the top of a grade N50 NdFeB cylindrical permanent magnet (2 cm height, 1.5 cm diameter, 1.45 Tesla) and switched on the arduino system. A LED light source penetrates the MNP solution for every 3 s and the penetrated light intensity is detected by a LED detector. The data is collected to study the kinetic profile of MNPs during magnetophoresis by plotting a normalised concentration against time graph. The experiment setup is illustrated in Figure 3.2.

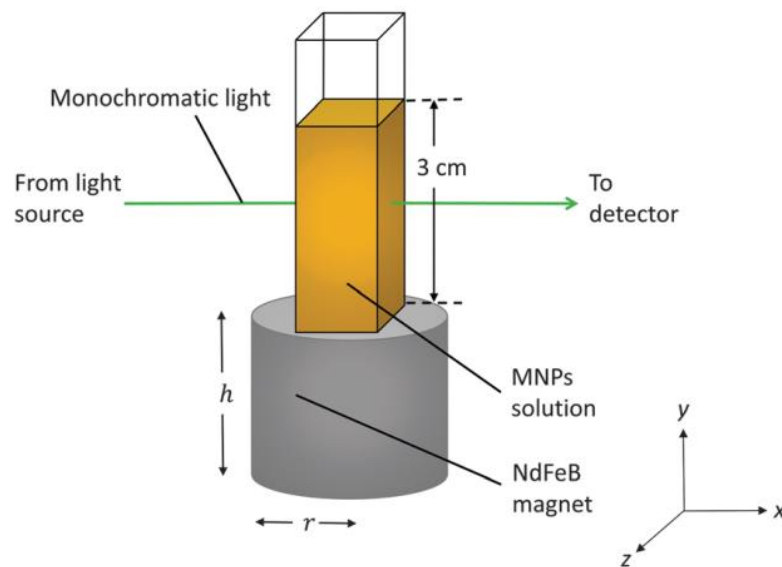


**Figure 3.2: Experimental Setup (Leong et. al., 2015).**

## CHAPTER 4

### RESULT AND DISCUSSION

#### 4.1 Functionalization of Magnetic Nanoparticles (MNPs)

In this section, the outcome of the functionalization of MNPs by using PSS is discussed. Before performing the magnetophoresis experiments to investigate the influence of concentration on the magnetophoresis kinetics of MNP solution (which is the major aim of this project), it is essential to obtain a relatively stable MNP system such that the magnetophoresis kinetics can be effectively captured in the experiment. As such, magnetite ( $\text{Fe}_3\text{O}_4$ ) nanopowder with average particle size of 30 nm are functionalized with poly(sodium 4-styrenesulfonate) (PSS) polyelectrolyte to acquire a colloiddally stable MNP solution and the relevant results are reported in this section. The functionalization process aims to modify the surface properties of the MNPs to enhance the colloidal stability of the MNP system. In this study, the functionalization of MNPs was performed by adsorbing polymer molecules directly onto the MNP surface as this approach is less time and material consuming. Here, the functionalization was carried out with different MNP/PSS mass ratios to evaluate the optimal ratio that will result in the MNP solution with greatest colloidal stability. In order to examine the successfulness of the functionalization process, the sedimentation behaviour of the functionalized MNP solution was being observed for five days and the results are presented in Figure 4.1.

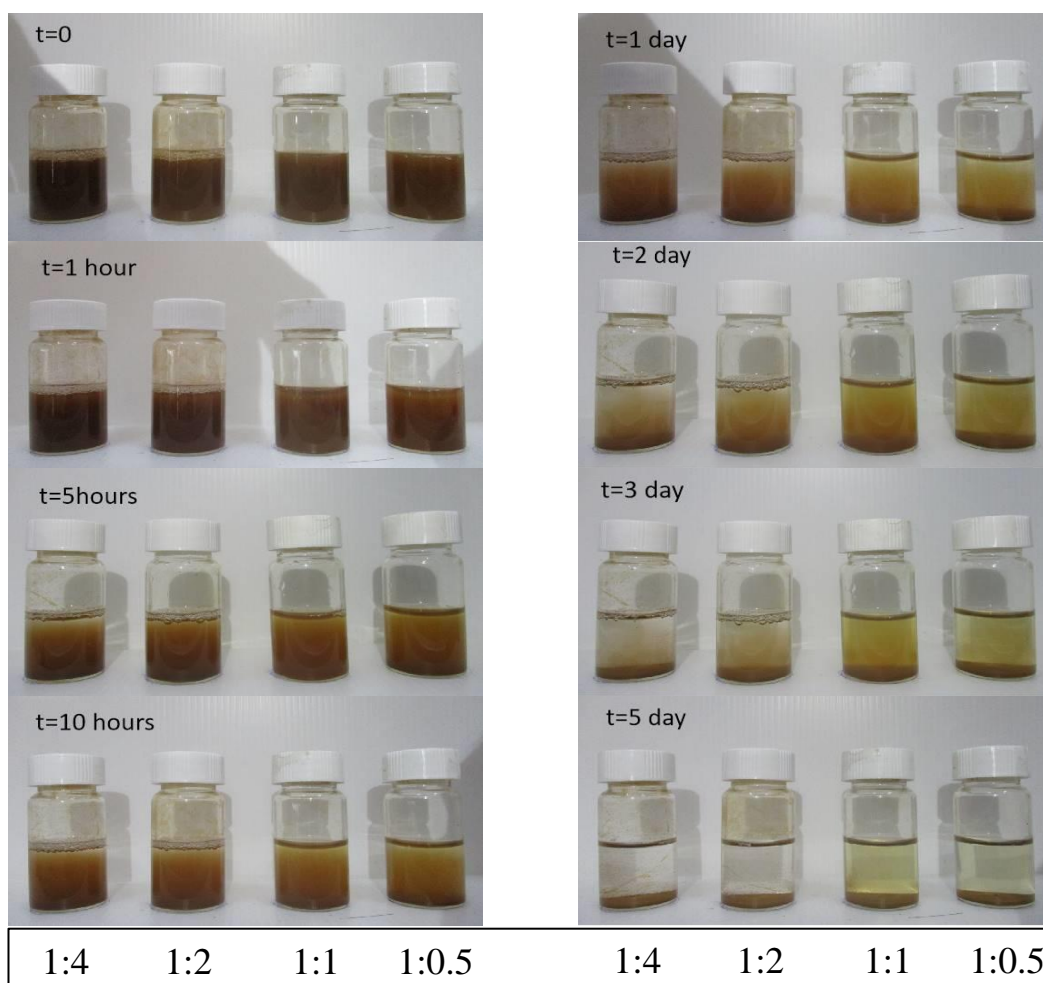


**Figure 4.1: The Sedimentation Time Lapse Images of MNP Solution with Different MNP to PSS Ratio (1:0.5, 1:1, 1:2, 1:4).**

The results show that the MNP to PSS ratio of 1:1 produced functionalized MNP system that exhibited the highest colloidal stability, as demonstrated by its ability to remain suspended in the solution for the longest time (Bolívar & Gonzalez, 2018). This is because this functionalized MNP solutions still have slightly brownish colour after 5 days of sedimentation (as compared to the other samples), which implies there are still some MNPs remain suspended in the solution. In addition, this observation also suggests that the functionalization of MNPs was successful, as the PSS coating on the MNPs' surface carried identical charges, generating a repulsive force that prevented the MNPs' aggregation (HEDDLE, 1971). Consequently, it can be deduced that the hydrodynamic size of the MNPs produced a 1:1 of MNP to PSS mass ratio was the smallest, allowing the MNPs to remain suspended for a longer period. Indeed,

this deduction is consistent with the hydrodynamic size measurement as shown in Figure 4.2 and Table 4.1. This reduced the possibility of disrupting experimental outcomes since the cooperative effect is related to the MNPs' aggregation (magnetic dipole-dipole interaction) under an external magnetic field. These individual MNPs tend to cluster together naturally to reduce their surface energy, leading to agglomeration and causing the MNPs less stable (Chong et al., 2020).

**Table 4.1: Average Hydrodynamic Size of MNP System Functionalized Under Different MNP:PSS ratio.**

Number of measurements	MNP:PSS Ratio			
	1:0.5	1:1	1:2	1:4
	<b>Hydrodynamic Diameter (nm)</b>			
<b>1</b>	412.2	264.8	400.5	347.0
<b>2</b>	376.6	276.0	383.0	354.6
<b>3</b>	356.4	264.7	390.0	353.6
<b>4</b>	306.3	223.6	320.1	305.3
<b>5</b>	322.0	230.4	330.4	318.8
<b>6</b>	297.2	234.0	326.6	313.6
<b>Average</b>	345.12	248.92	358.43	332.15



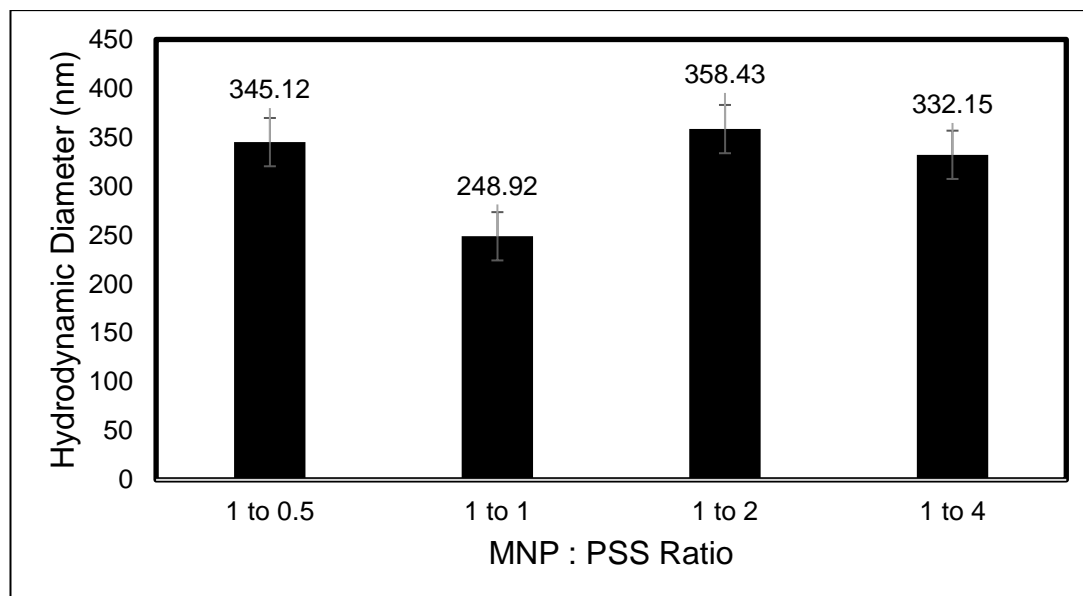


**Figure 4.2: Average Hydrodynamic Size of MNP System Functionalized Under Different MNP:PSS Ratio.**

PSS is a strong anionic polymer which exhibits negative surface charge at all pH condition. PSS completely dissociates in water forming an anionic polyelectrolyte and a positively charged sodium ion. At pH 3, the surface of MNPs will be dominated by the hydrogen ions ( $H^+$ ) and exhibit a net positive charge. Hence, at this pH value, both the MNPs and PSS have opposite charge which promotes electrostatic attraction, allowing the attachment of PSS onto the surface of the MNPs and leading to the successful functionalization (Chong et al., 2020). According to the Figure 4.1, the MNP to PSS ratio of 1:1 has the highest colloidal stability as its sedimentation time is the longest. The reason for this can be attributed to the appropriate ratio of PSS and MNPs, where there are enough PSS to cover the surface of MNPs while the electrostatic repulsion is not dominant.

Based on the DLS result, the hydrodynamic diameters of the MNPs were found to decrease in the following order: MNP to PSS ratio of 1:2, MNP to PSS ratio of 1:0.5, MNP to PSS ratio of 1:4, and MNP to PSS ratio of 1:1. The functionalized MNP produced under MNP/PSS ratio of 1:0.5 is showing a relatively higher hydrodynamic diameter (345.12 nm). This observation indicates that this functionalized MNP system is having the relatively lower colloidal stability and the PSS functionalization process might to be effectively, thus causing the functionalized PSS to form larger aggregates

during the measurement (Nikam et al., 2014). This is likely attributed to insufficient PSS to fully functionalize the surface of all the MNPs in the suspension. When the amount of PSS supplied is increased (the functionalization is carried under MNP/PSS ratio of 1:1), the hydrodynamic diameter of the resulted MNP system is 248.92 nm. The lower hydrodynamic diameter implies the less extent of aggregation within the MNP system, as the aggregation of MNPs is prohibited by the like charge (negative charge originated the PSS functionalized on the MNP surface). In the other word, the lower hydrodynamic diameter indicates the more effective functionalization process, due to the sufficient amount of PSS supplied to the system as compared to the functionalization process conducted under MNP/PSS ratio of 1:0.5. Conversely, when the amount of PSS during the functionalization is further increased (MNP/PSS ratio of 1:2 and 1:4), the effectiveness of the functionalization is declined as indicated by the larger average hydrodynamic sizes of the resulted MNP system functionalized under these conditions (358.43 nm and 332.15 nm, respectively) were the largest for the MNP to PSS ratio of 1:2 in both samples, which could be due to the electrostatic repulsion force among the PSS particles outweighing the attractive force between the MNPs and PSS. This is because when the PSS molecules are oversupplied, the amount of long chain PSS in MNP solution will increase which subsequently lead to the formation of larger flocs through the bridging effect (Mohammed et al., 2017). This situation causes the shorter-range attractive Van der Waals and magnetic dipole–dipole forces to dominate the interparticle interaction which will lead to the formation of large cluster with higher value of hydrodynamic diameter. Thus, the functionalized MNP system generated with high amount of PSS will exhibit faster sedimentation rate as indicated in Figures 4.1.

In addition, the size distribution of the MNPs functionalized under different MNP to PSS ratio is also tabulated in Figure 4.3. The MNP system functionalized under a MNP to PSS ratio of 1:0.5 shows a bell-shaped curve, indicating a normal distribution of particle sizes, with a peak at 300 nm. This suggests that the majority of MNPs in this sample are around this size. However, as the MNP to PSS ratios increase to 1:1, 1:2, and 1:4, the curves become skewed, indicating a wider spread of particle sizes due to more PSS coating on the surface of MNPs. When the ratio of PSS increases, more PSS can be coated on the surface of MNPs, which results in wider spread of particle size. At a ratio of 1:1, the peak shifts to the left (smaller size) at

around 250 nm, indicating that this is the size of most MNPs present in the sample. However, at ratios of 1:2 and 1:4, the peak shifts at the reverse direction (to the right) to 350 nm, suggesting that the increased PSS coating is producing larger functionalized MNP clusters in overall. However, it is important to note that the MNP system functionalized under MNP to PSS ratio of 1:0.5 (lower amount of PSS) as compared those functionalized under MNP to PSS ratio of 1:1. This might be due to some of the MNPs not being functionalized with PSS, resulting in the more apparent magnetic dipole-dipole interactions between MNPs and eventually causing aggregation of MNPs. According to the research conducted by Chong et al. (2020), magnetic nanoparticles (MNPs) that are not functionalized and are present in a solution tend to have low colloidal stability. This is because their hydrodynamic size increases rapidly, causing them to sediment quickly. The experimental finding is consistent with the result reported in this study.

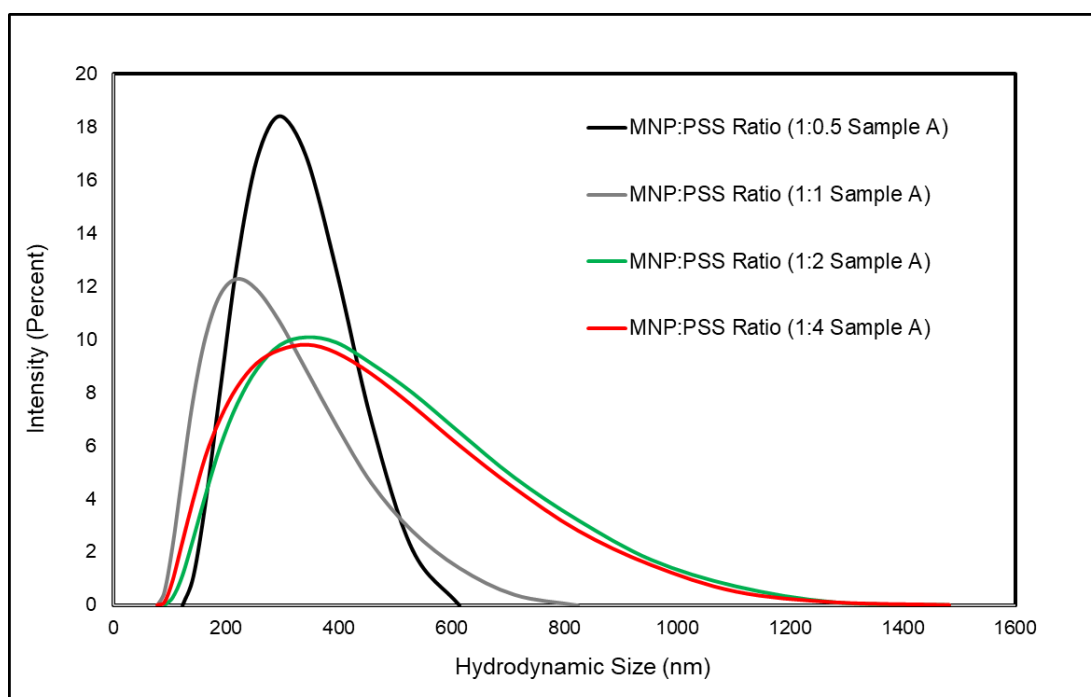


**Figure 4.3: Hydrodynamic Size Distribution.**

In overall, the optimum ratio of MNP/PSS to produce the most colloidally stable, smallest hydrodynamic sizes and consistent results is 1:1, and the functionalized MNP system produced under this MNP/PSS ratio will be used in the subsequent experiments to examine the effect of concentration on the magnetophoresis

kinetics of MNP solution.

## **4.2 Magnetophoresis Kinetics of MNP Solution under Cooperative and Hydrodynamic Regimes: An Experimental Approach**

In this section, the kinetics of magnetophoresis of MNP solutions with different initial concentration was recorded experimentally. The result obtained is crucial in evaluating the effect of MNP concentration on the rate of magnetophoresis of MNP under a low gradient magnetic field, in which the hydrodynamic effect is also dominating. In addition, it is also essential to compare with the prediction of the mathematical model that is established in the later part of this study.

### **4.2.1 Calibration of Customized UV-Vis Spectrophotometer**

In order to measure the magnetophoresis kinetics of MNP solution effectively, a ultraviolet–visible (UV-vis) spectrophotometer was built by using an arduino board prior to conducting the experiment. In this customized UV-vis setup, a LED light source emits a beam of light that will penetrate through the MNP solution, with a portion of the light being absorbed by the MNP solution while the remaining light will be detected by a light dependent resistor (LDR). To ensure the magnetophoresis kinetics is measured accurately, it is crucial to identify the working range of the customized UV-vis spectrophotometer (the range of MNP concentration that it can detect) by a calibration experiment. This calibration experiment involves the measurement of the intensity of the light passing through the MNP solution with different concentration (detected by the LDRs), with the aim to determine the correlation between the recorded light intensity and the concentration of MNP solution. Within the working range of the UV-vis spectrophotometer, the intensity of the light that penetrates the MNP solution will decrease linearly with the increasing concentration of MNP solution. In other word, the correlation between the intensity of the light passing through the MNP solution and the concentration of MNP solution is

obeying Beer-Lambert law in the working range of the UV-vis spectrophotometer (Yeap et al., 2014). Figure 4.4 shows the light intensity recorded by the UV-vis spectrophotometer when MNP solution with different concentrations (ranging from 0 to 300 mg/L) were employed.

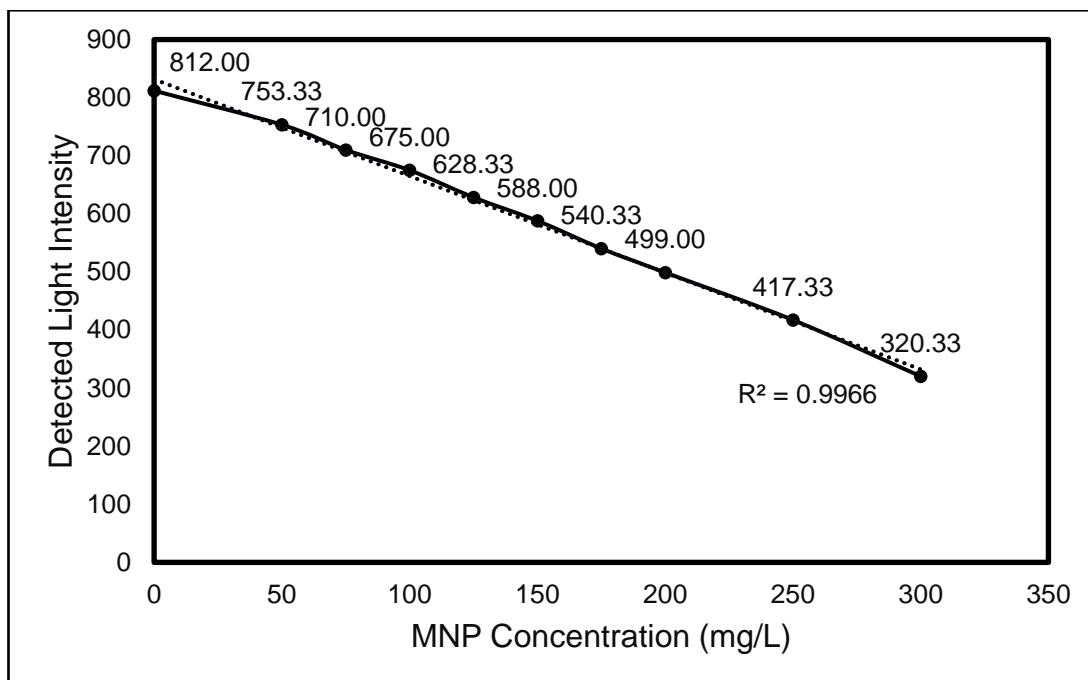


**Figure 4.4: Calibration Curve of MNP Solutions (1:1 Ratio).**

According to Figure 4.4, it was revealed that the light intensity values recorded decreased almost linearly from 812.00 to 320.33 as the MNP concentration was increased from 50 to 300 mg/L. Apart from that, by fitting the data points with a linear function, the  $R^2$  value obtained was given by 0.9966 which indicates that the measurement from the LDR of the UV-vis spectrophotometer is obeying with Beer-Lambert Law up to high accuracy, as the intensity of the light passing through the MNP solution varies almost linearly with the concentration of it. Thus, in this MNP concentration range, the customized UV-vis spectrophotometer is able to capture the MNP concentration effectively, since the flattening of the calibration curve upon reaching its threshold limit is not yet observed.

#### 4.2.2 Time-Lapse Images of MNP Solution During Magnetophoresis

Figure 4.5 displays time-lapse images of MNP solutions at different concentrations (50 mg/L, 75 mg/L, 125 mg/L, 175 mg/L, and 300 mg/L) after undergoing magnetophoresis for 10 minutes. The experimental result indicates that, after 240 seconds, most of the MNPs are effectively removed from the solution at all concentrations, as the solution has become clear after 5 minutes of magnetophoresis. Moreover, the mean values of all concentrations (50 mg/L, 75 mg/L, 125 mg/L, 175 mg/L, and 300 mg/L) displayed in Figure 4.6 eventually overlap with each other after 240 seconds. Even though there are higher number of MNPs in more concentrated MNP solution, all MNP solution is cleared within the similar duration, which implies that the separation rate is quicker for MNP solution with the higher concentrations as the fraction of MNPs removed from the initial solution is higher after undergoing the same duration of magnetophoresis. This observation has indicated the existence of cooperative effect which induces the concentration dependence of the rate of magnetophoresis (the detailed explanation of this phenomenon will be given in the next subsection). De Las Cuevas, Faraudo and Camacho (2008) discovered that when there is a cooperative effect among particles, the separation times are significantly shorter compared to non-interacting particles. This suggests that at higher concentrations, the rate of separation is faster, showing similar trend with the experimental result. Additionally, the result demonstrates that all MNP solution of different concentrations used in this study can be fully separated within 10 minutes.



**Figure 4.5: Time Lapse Images of MNP Solutions (with Concentration of 50 mg/L, 75 mg/L, 125 mg/L, 175 mg/L, and 300 mg/L) for 10 Minutes After Being Subjected to Magnetophoresis.**

In addition, the concentration of the MNP solution appears to be almost uniform throughout the entire duration of the magnetophoresis process. This observation is attributed to the occurrence of magnetophoresis induced convection within the MNP solution during the magnetophoresis process. In fact, this phenomenon is also denoted as hydrodynamic effect of magnetophoresis, which is resulted from the momentum transfer between the MNPs with the surrounding fluid during magnetophoresis and causes the fluid (which is non-magnetic) to gain momentum and flow convectively. By observing Figure 4.5, the flow pattern is similar to the flow pattern (see Figure 2.19) observed by Leong, Ahmad and Lim (2005), the consistent result proving the hydrodynamic effect exhibit in this experiment.

Furthermore, the time lapsed images are further analysed by using ImageJ software to verify the qualitative observation in a quantitative manner, which is tabulated in Table 4.2, Figure 4.6 and Figure 4.7. In fact, this quantitative analysis yields the consistent results as that of the discussion above. The mean denotes the average colour intensity of MNP solution, and the standard deviation (SD) measures the deviations from the mean value. Initially, as the concentration of MNP solution is higher increased, the colour of the solution appeared darker, resulting in lower values of light intensity as measured by the ImageJ software. As the experiment progressed and more MNPs were captured on the collection plane, fewer MNPs remained suspended in the solution, causing the colour of the solution to lighten, which resulted in higher values of light intensity as measured by the ImageJ software. Therefore, the light intensity values across the MNP solution became lighter as the magnetophoresis proceeded. According to the Table 4.2 and Figure 4.7, the standard deviations of all concentration (50 mg/L, 75 mg/L, 125 mg/L, 175 mg/L, and 300 mg/L) are relatively low (with highest value of 9.79 and lowest value of 1.80) as compared to the mean value, indicating that the MNP solution are homogenous at all times during magnetophoresis process due to the convective flow originated from the hydrodynamic effect of magnetophoresis. The experimental data is consistent with the theoretical framework proposed by Leong, Ahmad and Lim (2005).



**Table 4.2: Image J Analysis on Time-Lapse Image of MNP Solution During Magnetophoresis.**

<b>Concentration</b>	<b>50 mg/L</b>		<b>75 mg/L</b>		<b>125 mg/L</b>		<b>175 mg/L</b>		<b>300 mg/L</b>	
<b>Time (s)</b>	<b>Mean</b>	<b>SD</b>	<b>Mean</b>	<b>SD</b>	<b>Mean</b>	<b>SD</b>	<b>Mean</b>	<b>SD</b>	<b>Mean</b>	<b>SD</b>
<b>0</b>	137.39	3.99	117.83	3.06	100.07	4.82	91.49	4.53	66.60	7.92
<b>30</b>	144.42	7.09	132.94	8.19	121.58	9.79	119.02	5.06	98.66	8.81
<b>60</b>	152.20	8.58	144.00	6.61	138.19	6.04	140.39	4.30	128.87	6.92
<b>90</b>	155.58	6.94	149.36	5.08	148.51	4.51	152.61	5.18	145.01	3.99
<b>120</b>	157.82	5.90	155.00	4.08	153.16	4.17	155.66	2.95	152.81	4.73
<b>150</b>	161.58	5.80	157.22	2.74	157.19	2.73	158.88	3.70	156.30	4.06
<b>180</b>	161.89	3.44	159.30	2.34	159.34	3.42	160.91	4.05	158.01	3.54
<b>240</b>	164.80	5.13	164.98	2.33	161.64	1.95	163.17	4.49	161.67	2.92
<b>300</b>	166.24	2.33	164.86	1.80	161.98	2.75	166.38	4.05	164.34	3.13
<b>600</b>	166.33	3.64	164.91	2.37	162.52	4.49	166.33	4.08	164.15	3.37

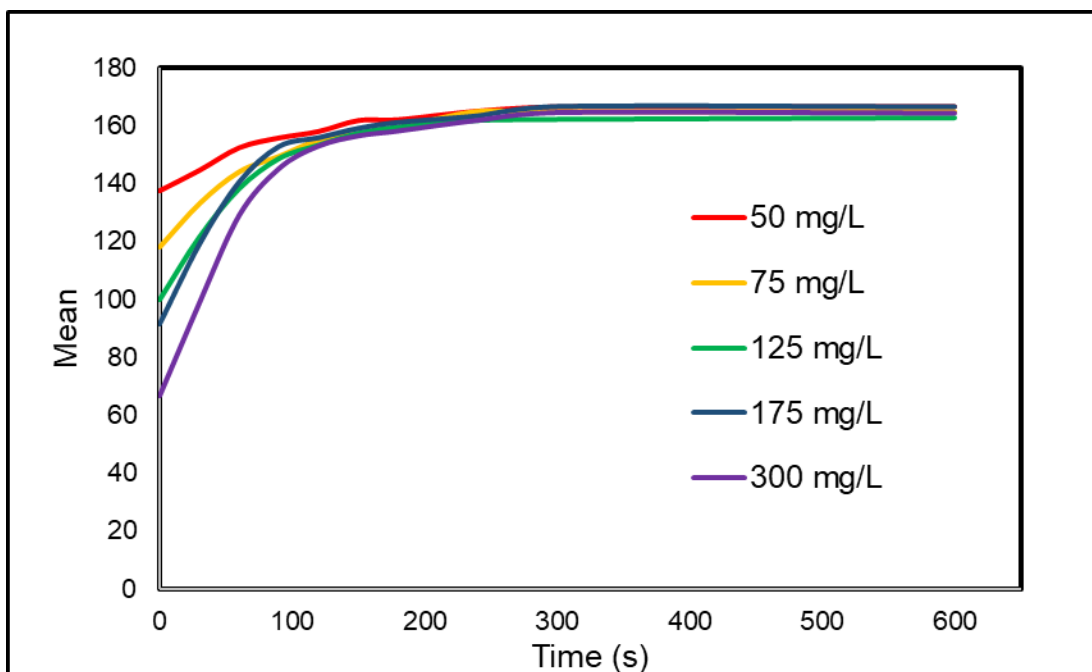


**Figure 4.6: Mean Versus Time of MNP Solution During Magnetophoresis.**

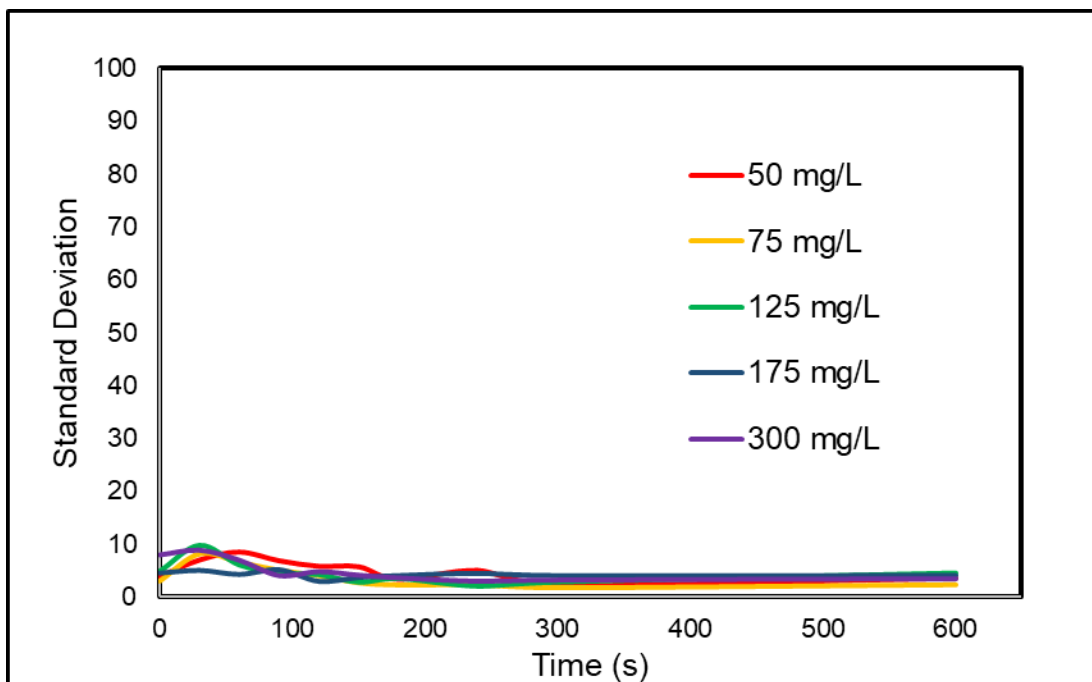


**Figure 4.7: Standard Deviation Versus Time of MNP Solution During Magnetophoresis.**

### 4.2.3 Separation Kinetics Profile of MNP Solutions under Cooperative and Hydrodynamically Driven Magnetophoresis

Figure 4.8 shows the magnetophoresis kinetics of MNP solution conducting with MNP solution of different initial concentration (50, 75, 125, 175 and 300 mg/L). As shown in this figure, with an increase in MNP concentration, the normalized concentration of MNP solution declines more rapidly and the separation time is shortened significantly. In addition, the time required to achieve 80% separation of MNP solution is also tabulated in Figure 4.9, which also implies that the MNP solution with higher concentration requires shorter separation time. For instance, 50 mg/L of MNP solution required 162 s to achieve 80% of MNP separation while 300 mg/L of MNP requires only 54 s to accomplish the same degree of separation (which is about 3 times faster). This dependence of separation time on the concentration of MNP solution is attributed to the cooperative effect of magnetophoresis. Under the higher concentration of MNP solution, MNPs are more densely placed, which causes collision frequency of the MNPs to be higher and the aggregation of MNPs is occurring at a higher rate. Due to the higher rate of aggregation process, the resulted aggregates are larger in size and subjected to the greater magnetophoretic force (De Las Cuevas, Faraudo and Camacho 2008). Therefore, the larger MNP aggregates will experience the greater magnetophoretic velocity and can be separated more easily from the suspension (Lim et al., 2014).

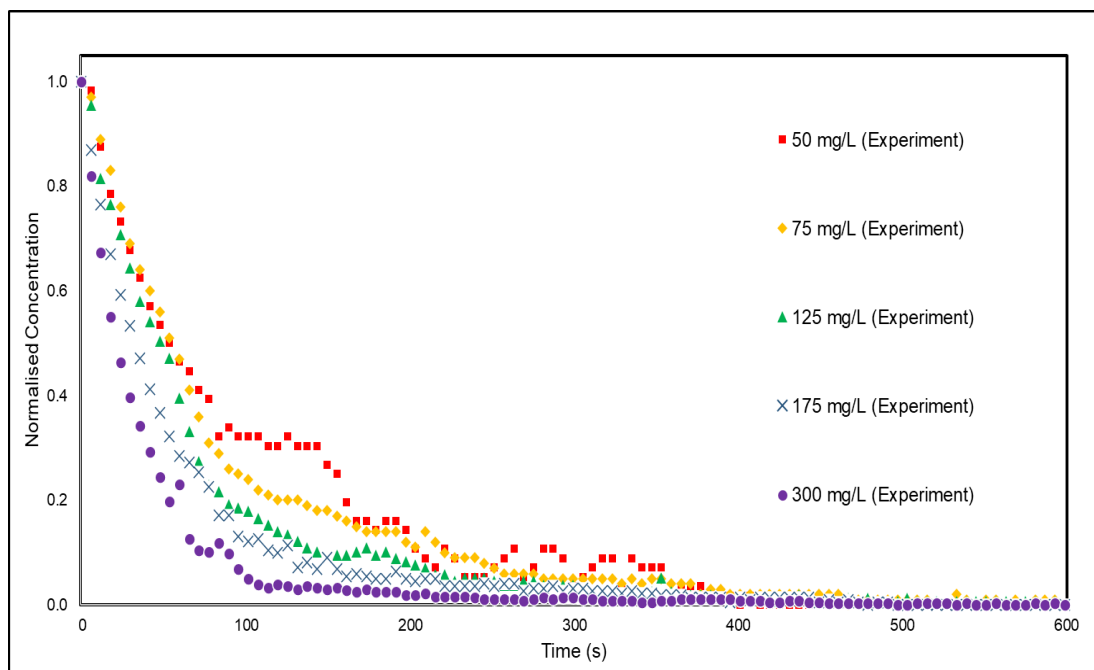


**Figure 4.8: Magnetophoresis Kinetic Profile (with Concentration 50 mg/L, 75 mg/L, 125 mg/L, 175 mg/L, 300 mg/L,) During Magnetophoresis.**

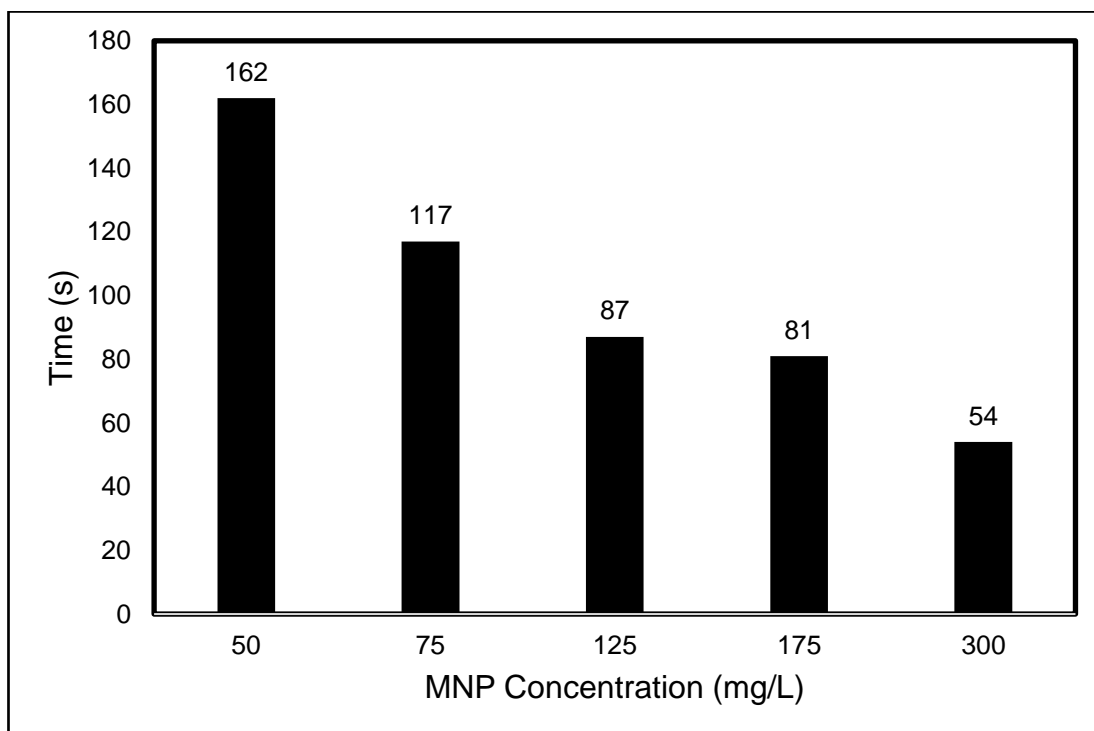


**Figure 4.9: Time to Achieve 80 % Separation.**

Additionally, the hydrodynamic effect of magnetophoresis is also found to be dependent on the concentration of MNP solution. The hydrodynamic effect is the phenomenon that induces a convective flow within the MNP solution upon subjected to magnetophoresis, due to the momentum transfer between the MNPs and the surrounding fluid. The occurrence of magnetophoresis induced convection tends to sweep the MNPs towards the magnet and being captured more rapidly, ultimately reducing the separation time (Leong et al., 2017). It has been revealed that the induced convection is more intensive within the MNP solution of higher concentration upon subjected to magnetophoresis, thus, it is reasonable to deduce that the hydrodynamic effect is also a factor that leads to the concentration-dependence of the magnetophoresis kinetics (Leong et al., 2020). These findings provide compelling evidence of the role played by the hydrodynamic and cooperative effects in magnetophoresis kinetics, which is consistent with previous reports in the literature.

### **4.3 Modelling the Kinetics of Magnetophoresis in the Presence of Cooperative and Hydrodynamic Effects**

In this section, the mathematical modelling of the magnetophoresis kinetics of MNP solution under the scenario in which both cooperative and hydrodynamic effects are dominating is presented. The mathematical model that is able to depict of magnetophoresis kinetics of MNP solution in this regime is particularly crucial, as most engineering applications involving the magnetophoresis of MNP is fallen into this regime (Leong et al., 2020). With the developed mathematical model, the underlying mechanism and transport behaviour of magnetophoresis of MNP with both cooperative and hydrodynamic effects are dominating can be elucidated and it can be used to predict a particular magnetophoresis process in the real time application.

Before formulating the new mathematical model, several factors that are relevant to the magnetophoresis kinetics such as shape of aggregates, induced convection motions, Brownian motion, magnetic dipole-dipole interactions, viscous drag force, buoyancy force, gravitational force, and magnetophoretic force should be clarified . For instance, De Las Cuevas, Faraudo and Camacho (2008) have observed

the motion of MNPs under an external magnetic field where the cooperative effect is dominating, and they discovered that MNPs will align in the direction of the magnetic field with for formation of elongated aggregates which move along the magnetic gradient, as shown in Figure 2.12. There are two possible aggregations that can be formed by MNPs during magnetophoresis, which are tip-to-tip aggregation and lateral aggregation (Faraudo & Camacho, 2009). Furthermore, Leong et al. (2017) have identified that the MNPs separation rate is only dependent on the magnetic field gradient at the collection plane (the container surface adjacent to the magnet) when the hydrodynamic effect is dominating and the MNP solution is continuously being homogenized by the induced convective current. In this experiment setup (see Figure 3.6), the magnetic field generated by the cylindrical permanent magnet is pointing upward, therefore, it is reasonable to assume that the elongated MNP aggregates that are reaching the MNP collection plane is aligning at the axial direction of the magnet. For the sake of simplicity, several logical assumptions have been made in the mathematical modelling: (1) Gravitational and its corresponding buoyant forces are neglected under low Reynold number flow because it is negligible as compared to the magnetophoretic and viscous drag force experienced by the MNPs during magnetophoresis (about  $\sim 1.63 \times 10^{19}$  times smaller) due to the small mass and volume of MNPs (Leong et al., 2017), (2) Only tip-to-tip aggregation occur during magnetophoresis as it is the most common way of aggregation under the magnetophoresis of MNP solution under homogeneous magnetic field (Faraudo & Camacho, 2009), (3) The hydrodynamic is overwhelming which causing the MNP solution appears to be homogeneous at all time (see Figure 4.5) and the separation rate is only dependent on the magnetic field gradient or magnetophoretic velocity of the MNP aggregates at the collection plane (Leong et al., 2017), (4) MNPs are dispersed uniformly at the beginning of the experiment, and (5) Cluster of MNPs (PSS-functionalized MNPs prior to the aggregation) are in the perfect spherical shape with hydrodynamic diameter of  $d_{H,0}$ .

### 4.3.1 Aggregation Kinetics

In this subsection, the aggregation kinetics of MNPs subjected to magnetophoresis is

modelled mathematically. First, it is important to define some important terminology being used in the following mathematical modelling. MNP cluster is the PSS-functionalized MNP which consists of a number of MNPs linked together by the long-chain PSS molecules. It is the form of MNPs exist in the MNP solution prior to the magnetophoresis and can be viewed as an individual magnetic species suspended in the solution without undergoing aggregation. However, in the experiment being conducted in this study, aggregations of MNP clusters are imperative since the aggregation parameter is larger than unity (see APPENDIX Section A) for more detailed calculation). Under this scenario, the magnetic dipole interactions should overwhelm the thermal energy which is leading to the aggregation of MNP clusters to form elongated aggregates. Here, MNP aggregate is the term to describe the magnetic species that consists of two or more MNP clusters that are held together by the magnetic dipole interaction. The significance of magnetic dipole interaction is greatly affected by the interparticle distance which is related to MNP concentration. As the MNP concentration increases, the number of MNPs per unit volume increases while reducing the distance amongst particles resulting in higher possibility of particle interactions. For each successful aggregation, the number of magnetic species in the solution will decrease with the formation of a larger MNP aggregate.

To depict the aggregation kinetics, it is useful to first ignore the effect of magnetophoresis (the separation and withdrawal of MNP out of the solution) and thus, the number of MNP clusters dispersed in the solution is a constant. This is equivalent to the scenario that the MNP solution is exposed to the magnetic field, which induces the aggregation of MNP clusters but there is no separation of MNPs occurring yet. Let the initial number of individual MNP clusters denoted by a symbol  $n_o$  and the number of magnetic species after  $p$  times of aggregation to be is denoted by a symbol  $n$ , the relationship can be shown in the equation:

$$n = n_o - p \quad (4.1)$$

It should be noted that the magnetic species here is referring to MNP cluster or MNP aggregate as defined previously. The magnetic species in the solution is reducing during the aggregation process, in which the average number of MNP clusters in an aggregate can be determined by the following equation:

$$\bar{s} = \frac{n_o}{n} \quad (4.2)$$

where symbol  $\bar{s}$  is the average number of MNP clusters in a MNP aggregate, which can be obtained through dividing the initial number of MNP clusters in the solution by the real time number of magnetic species in the solution.

To ensure successful aggregation between MNP clusters, the magnetic dipole-dipole interaction energy ( $E_d$ ) must be large enough to overcome the thermal energy (De Las Cuevas, Faraudo and Camacho 2008). Each MNP cluster is assumed to have the same magnetic dipole moment and hydrodynamic diameter. Here, the magnetic dipole-dipole interaction can be computed through the following equation:

$$E_d = -\frac{\mu_o m_o^2}{2\pi d^3} \quad (4.3)$$

where  $\mu_o$  is the permeability of free space in water,  $m_o$  is the magnetic dipole moment of a MNP cluster, and the  $d$  is the separation distance between the MNP clusters. It can be observed from the equation (4.3) that the magnetic dipole-dipole interaction is declining with the distance between two MNP clusters. In conjunction with this situation, the magnetic Bjerrum length is introduced, and it is defined a distance over where the magnetic dipole-dipole interaction energy is equal to the thermal energy (De Las Cuevas, Faraudo and Camacho 2008), which can be mathematically formulated as:

$$\lambda_B = \left( \frac{\mu_o |\bar{m}|^2}{2\pi k_B T} \right)^{\frac{1}{3}} \quad (4.4)$$

If the separation distance between both magnetic species is smaller than magnetic Bjerrum length, the magnetic dipole-dipole interaction is dominating, and the aggregation process can be successful (De Las Cuevas, Faraudo and Camacho 2008). In this context, the aggregation frequency of magnetic species should be derived by relating it to the rate in which the magnetic species come close among each other for the magnetic dipole-dipole interaction to be dominant (the separation distance between



them is lesser than magnetic Bjerrum length  $\lambda_B$ ). In a magnetophoresis in which hydrodynamic effect is dominating, a magnetic species (individual or aggregate) moves in the solution as it is continuously swept by the induced convection flow (Leong et al., 2017). After a period of time  $t$ , the magnetic species will contact another magnetic species after flow through a volume  $V'$  (see Figure 4.10), which is the volume of a magnetic species can sweep through before interacting with another magnetic species. Since MNP aggregation can occur once the interparticle distance between the magnetic species is shorter than the magnetic Bjerrum length (the magnetic dipole energy overwhelms the thermal energy), the equation of this volume can be related to the magnetic Bjerrum length and defined as:

$$V' = (\pi\lambda_B^2 + 2(\bar{s} - 1)d_{H,0}\lambda_B)\bar{v}t \quad (4.5)$$

where  $\bar{v}$  is the average velocity of magnetic species in the solution. Let consider the magnetic species swept through an average volume occupied by one species (which is the inverse of the MNPs concentration,  $\frac{1}{c}$ ), and let  $T'$  represents the time taken to swept through the volume, the following equation will be resulted by incorporating this relationship into equation (4.5):

$$\frac{1}{c} = (\pi\lambda_B^2 + 2(\bar{s} - 1)d_{H,0}\lambda_B)\bar{v}T' \quad (4.6)$$

Furthermore, the aggregation frequency  $f'$  of a magnetic species can be defined as:

$$f' = \frac{Z}{T'} = Z(\pi\lambda_B^2 + 2(\bar{s} - 1)d_{H,0}\lambda_B)\bar{v}c \quad (4.7)$$

where  $Z$  is the fraction of successful aggregation when magnetic species interact with each other. Let symbol  $n$  denotes the number of all the magnetic species suspended in the solution, the total aggregation frequency within the MNP solution  $f_a$  can be mathematically formulated as:

$$f_a = \frac{1}{2}nf' = \frac{1}{2}nZ(\pi\lambda_B^2 + 2(\bar{s} - 1)d_{H,0}\lambda_B)\bar{v}c \quad (4.8)$$

Equation (4.8) includes a factor of 1/2 to prevent the duplicate counting of aggregation frequency in the solution among different species. The number concentration of the magnetic species in the MNP solution subjected to aggregation can be computed through dividing the total magnetic species suspended in the solution by the volume of the solution ( $V$ ), as given by:

$$c = \frac{n}{V} \quad (4.9)$$

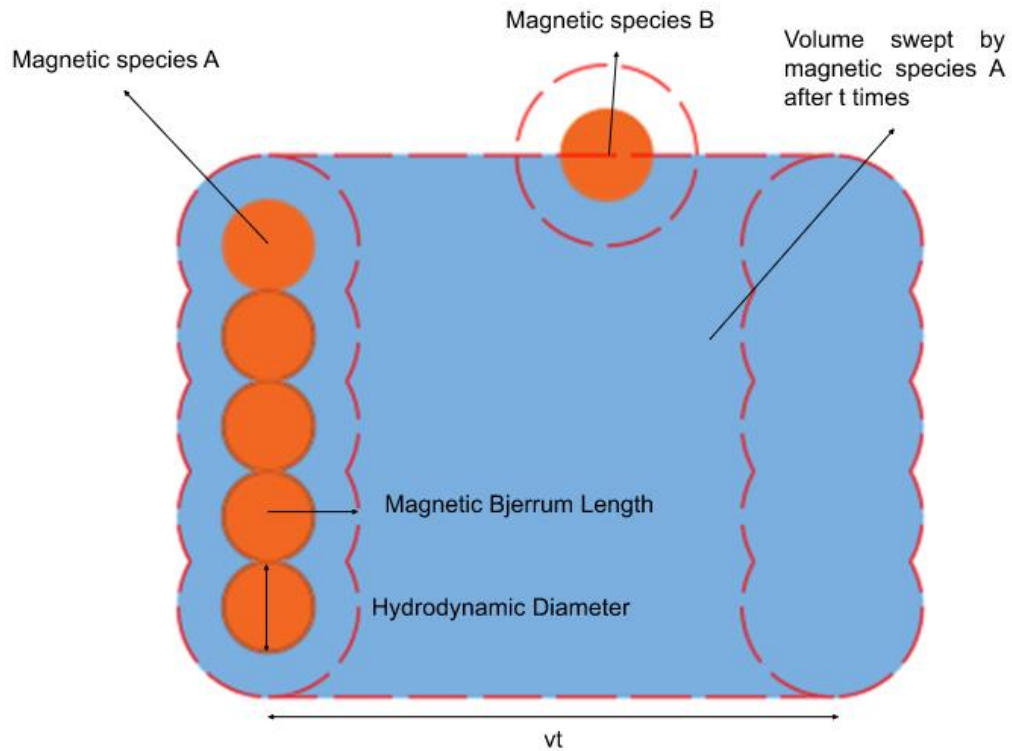


**Figure 4.10: Free Volume Swept Through by the Elongated Aggregate (Magnetic Species A).**

By substituting equation (4.9) into equation (4.8), the aggregation frequency become:

$$f_a = \frac{nZ\bar{v}}{2} (\pi\lambda_B^2 + 2(\bar{s} - 1)d_{H,0}\lambda_B) \left(\frac{n}{V}\right) = \frac{n^2Z\bar{v}}{2V} (\pi\lambda_B^2 + 2(\bar{s} - 1)d_{H,0}\lambda_B) \quad (4.10)$$

Since one aggregation decreases the total number of magnetic species by one, the aggregation frequency can also be stated as:

$$f_a = -\frac{dn}{dt} \quad (4.11)$$

Therefore, the changes of number of magnetic species over time can be expressed as:

$$\frac{dn}{dt} = -\frac{n^2 Z \bar{v}}{2V} (\pi \lambda_B^2 + 2(\bar{s} - 1) d_{H,0} \lambda_B) \quad (4.12)$$

By substituting equation (4.2) into equation (4.12) and rearranging the formula, the equation is expressed as:

$$\frac{dn}{dt} = -\frac{Z \bar{v}}{2V} [(\pi \lambda_B^2 + 2d_{H,0} \lambda_B) n^2 + 2d_{H,0} \lambda_B n_0 n] \quad (4.13)$$

The equation (4.13) is simplified by denoting constants with symbols, such as  $X = \frac{Z \bar{v}}{2V}$ ,

$A = (\pi \lambda_B^2 + 2d_{H,0} \lambda_B)$ , and  $B = 2d_{H,0} \lambda_B n_0$ :

$$\frac{dn}{dt} = -X[An^2 + Bn] \quad (4.14)$$

Through partial fraction integration methods, the equation (4.14) can be solved by integration:

$$\int_{n_0}^n \frac{1}{An^2 + Bn} dn = -X \int_0^t dt \quad (4.15)$$

where  $n_0$  is the initial number of magnetic species in the MNP solution at  $t = 0$ .

For the right-hand side of the equation (4.15):

$$\begin{aligned} -X \int_0^t dt &= -X[t]_0^t \\ &= -X(t - 0) \\ &= -Xt \end{aligned}$$

For the left-hand side of the equation (4.15):

$$\int_{n_0}^n \frac{1}{An^2 + Bn} dn = \int_{n_0}^n \frac{1}{n(An + B)} dn = \int_{n_0}^n \frac{C}{n} dn + \int_{n_0}^n \frac{D}{An + B} dn$$

By comparing both side of the equation above, the following equation yields:

$$1 = C(An + B) + D(n)$$

which gives rise to:

$$C = \frac{1}{B} \text{ and } D = -\frac{A}{B}$$

Hence,

$$\begin{aligned} \int_{n_0}^n \frac{1}{An^2 + Bn} dn &\approx \int_{n_0}^n \frac{1}{B(n)} dn + \int_{n_0}^n -\frac{A}{B(An + B)} dn \\ &\approx \frac{1}{B} \left[ \int_{n_0}^n \frac{1}{B(n)} dn + \int_{n_0}^n -\frac{A}{B(An + B)} dn \right] \\ &\approx \frac{1}{B} [In(n) - In(An + B)]_{n_0}^n \\ &\approx \frac{1}{B} \left[ In\left(\frac{n}{An + B}\right) \right]_{n_0}^n \\ &\approx \frac{1}{B} \left\{ \left[ In\left(\frac{n}{An + B}\right) \right] - \left[ In\left(\frac{n_0}{An_0 + B}\right) \right] \right\} \\ &\approx \frac{1}{B} \left[ In\left(\frac{\frac{n}{An+B}}{\frac{n_0}{An_0+B}}\right) \right] \end{aligned}$$

Let the constant  $\frac{n_0}{An_0+B} = E$ , and equate the left-hand side and right-hand side equation

(4.15):

$$\begin{aligned} -Xt &= \frac{1}{B} \left[ In\left(\frac{\frac{n}{An+B}}{E}\right) \right] \\ Ee^{-BXt} &= \frac{n}{An + B} \\ n(1 - AEe^{-BXt}) &= BEe^{-BXt} \end{aligned}$$

$$n = \frac{BEe^{-BXt}}{1 - AEe^{-BXt}}$$

By substituting the constants into the equation, the equation is given as:

$$n = \frac{(2d_{H,0}\lambda_B n_0)\left(\frac{n_0}{An_0+B}\right)e^{-(2d_{H,0}\lambda_B n_0)\left(\frac{Z\bar{v}}{2V}\right)t}}{1 - (\pi\lambda_B^2 + 2d_{H,0}\lambda_B)\left(\frac{n_0}{An_0+B}\right)e^{-(2d_{H,0}\lambda_B n_0)\left(\frac{Z\bar{v}}{2V}\right)t}} \quad (4.16)$$

Equation (4.16) is the equation that describes the evolution of the number of magnetic species with respect to time during the aggregation process (by assuming the magnetophoretic separation process is not occurring). Figure 4.11 shows the relationship between the number of magnetic species,  $n$  and time,  $t$  (as calculated by using Equation (4.16) for the MNP system (with concentration of 50 mg/L) employed in the current study).

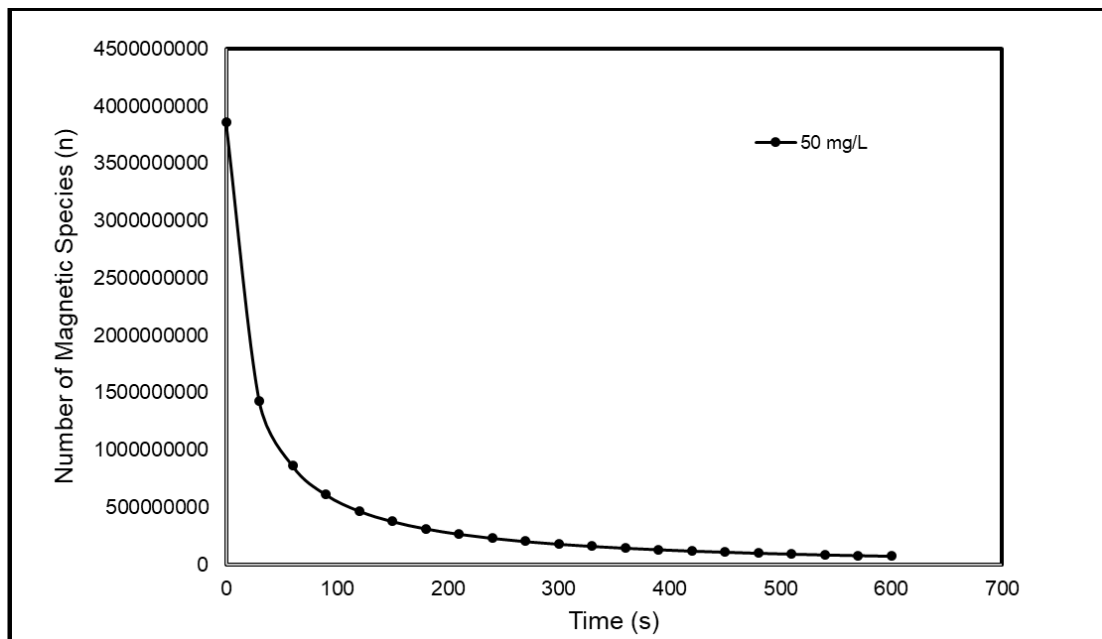


**Figure 4.11: The Relationship Between the Number of Magnetic Species and Time.**

According to Figure 4.9, as time passes, the number of magnetic species decreases very rapidly. This scenario is due to the rapid aggregation of MNPs suspended in the solution upon subjected to the external magnetic field. These magnetic species can exist as either an individual MNP cluster or an aggregate

comprising multiple individual MNP clusters. Additionally, Yavuz et al. (2006), Faraudo and Camacho (2009), and De Las Cuevas, Faraudo and Camacho (2008) also reported the aggregation of MNPs during magnetophoresis process. For instance, the initial number of magnetic species in the solution is  $3.86 \times 10^9$ , which has been decline by 8 times ( $4.68 \times 10^8$ ) after subjected to the aggregation for 120 seconds. This has proven the rapid aggregation of MNPs during magnetophoresis of the MNP system used in the current study, which is consistent with the experimental observation demonstrated in the previous section.

### 4.3.2 Magnetophoresis Kinetics

In this subsection, the aggregation kinetics derived in the previous subsection is incorporated into the magnetophoretic separation kinetics, with the aim to describe the phenomenon in which the MNPs are depleted and separated from the solution with the simultaneous occurrence of MNP aggregation. Leong et al. (2017) have studied on the kinetics of magnetophoresis in which hydrodynamic effect is dominating but cooperative effect is insignificant and discovered that the MNP separation kinetics is only dependent on magnetic field gradient at the surface of the MNP collection plane. The equation to depict the time-evolution of the number of magnetic species in the MNP solution is given as:

$$\frac{dn}{dt} = -\frac{\alpha}{V}n \quad (4.17)$$

where  $\alpha$  is the separation factor at the MNP collection plane ( $z = 0$ ) which can be formulated as:

$$\alpha = v_{z|z=0}A_s \quad (4.18)$$

where  $v_{z|z=0}$  is the velocity of MNPs at the collection plane, and  $A_s$  is the surface area of the collection plane. The magnetophoretic force ( $F_{mag}|_{z=0}$ ) induced on a magnetic species (either MNP cluster with  $\bar{s} = 1$  or MNP aggregate with  $\bar{s} > 1$ ) at the

collection plane can be defined as:

$$F_{mag}|_{z=0} = \bar{m}_0 \frac{\partial B}{\partial z}|_{z=0} \quad (4.19)$$

However, there is a viscous drag force ( $F_d|_{z=0}$ ) that acting in the opposite direction of the magnetophoretic force and can be formulated as:

$$F_d|_{z=0} = 3\pi\eta d_{H,0} v_z|_{z=0} \quad (4.20)$$

where  $\eta$  is the viscosity of the MNP solution. Then, the velocity of magnetic species can be computed by equating Equations (4.19) and (4.20):

$$v_z|_{z=0} = \frac{\bar{m}_0}{3\pi\eta d_{H,0}} \frac{\partial B}{\partial z}|_{z=0} \quad (4.21)$$

Thus, the rate of change of number of magnetic species due to the removal of MNPs at the collection plane ( $\frac{dn}{dt}|_c$ ) can be formulated by incorporating the equations (4.18) and (4.21) into equation (4.17):

$$\frac{dn}{dt}|_c = -\frac{m_0 A_s}{3\pi\eta d_{H,0}} \frac{\partial B}{\partial z}|_{z=0} \left(\frac{n_o}{n}\right) (n) = -\frac{m_0 A_s}{3\pi\eta d_{H,0}} \frac{\partial B}{\partial z}|_{z=0} n_o \quad (4.22)$$

On the other hand, the rate of change of number of magnetic species due to the aggregation process ( $\frac{dn}{dt}|_a$ ) is expressed by the following equation (see equation (4.13) in subsection 4.3.1:

$$\frac{dn}{dt}|_a = -\frac{Z\bar{v}}{2V} [(\pi\lambda_B^2 + 2d_{H,0}\lambda_B)n^2 + 2d_{H,0}\lambda_B n_o n] \quad (4.23)$$

The total rate of change of number of magnetic species during the magnetophoresis process is given by the sum of rate of change of number of magnetic species due to aggregation process and the rate of separation of magnetic species at the collection plane, which is mathematically formulated as:

$$\frac{dn}{dt} = \frac{dn}{dt}\bigg|_c + \frac{dn}{dt}\bigg|_a$$

$$\frac{dn}{dt} = -\frac{m_0 A_s}{3\pi\eta d_{H,0}} \frac{\partial B}{\partial z}\bigg|_{z=0} n_o - \frac{Z\bar{v}}{2V} [(\pi\lambda_B^2 + 2d_{H,0}\lambda_B)n^2 + 2d_{H,0}\lambda_B n_o n] \quad (4.24)$$

The individual magnetic cluster are changing with time as well because the magnetic species is captured on the collection plane as time pass by, therefore, the number of individual clusters changing with time can be defined as:

$$\frac{dn_o}{dt} = \bar{S} \frac{dn}{dt}\bigg|_c = -\frac{m_0 A_s}{3\pi\eta d_{H,0}} \frac{\partial B}{\partial z}\bigg|_{z=0} n_o \left(\frac{n_o}{n}\right) = -\frac{m_0 A_s}{3\pi\eta d_{H,0}} \frac{\partial B}{\partial z}\bigg|_{z=0} \left(\frac{n_o^2}{n}\right) \quad (4.25)$$

In this case, the initial number of magnetic species and the number of magnetic species are functions of time, which will vary with time due to continuous capture of the magnetic species on the collection plane. By solving the equations (4.24) and (4.25) through numerical methods simultaneously, the kinetic profile of magnetophoresis can be evaluated. The MNPs concentration  $c$  can be computed by dividing  $n_o$  by the volume of solution,  $V$ :

$$c = \frac{n_o}{V} \quad (4.26)$$

### 4.3.3 Analysis on the Simulation Results from the Mathematical Model

In this subsection, a comparison will be made between the predicted and experimental results, and an analysis will be carried out to identify and examine the underlying factors responsible for any discrepancies observed between the two sets of results.

Figure 4.12 and Figure 4.13 demonstrated the overall trends of the predicted and experimental measured magnetophoresis kinetics of MNP solutions of different concentrations, are consistent among with each other. As compared to the model prediction that demonstrates smooth decay curve, some minor fluctuations are observed for the experimental result in Figures 4.12 and 4.13 owing to two main factors. The first factor is the relatively lower precision and stability of the customized



UV-vis spectrophotometer built from the arduino system to measure the concentration of the MNP solution. In fact, it is a low cost UV-vis spectrophotometer built by only simple components. Secondly, the hydrodynamic effect is also responsible for the fluctuations in the magnetophoresis kinetic profiles recorded experimentally. In this context, the hydrodynamic effect induces convection flows in the solution which promotes the homogenisation of the solution, ensuring that the concentration of magnetic species remains constant throughout the solution (Leong et al., 2017). However, the homogeneization of MNP solution is not perfect throughout the entire timescale of magnetophoresis experiment. At a particular moment during the experiment, more magnetic species may be carried by the convection flows towards the measurement spot, resulting in more significant blockage of light from penetrating through the solution and causing temporary increase in the detected concentration as well as the slight fluctuations. Despite these fluctuations, the customized UV-vis spectrophotometer is still an effective tool to measure the magnetophoresis kinetics of MNP solution as the fluctuation range is very small as compared to the overall decay/change of the concentration throughout the entire magnetophoresis process.

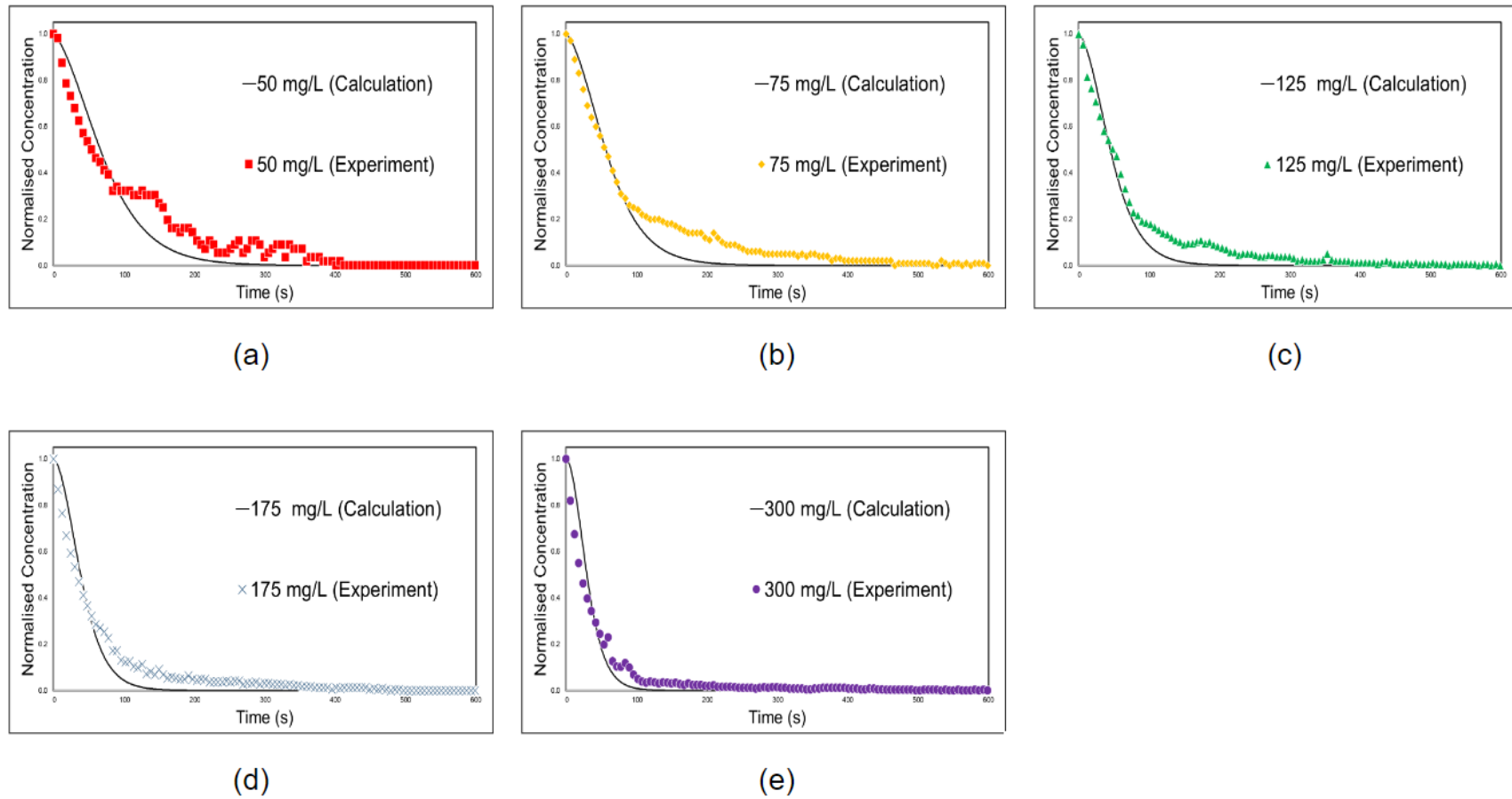


**Figure 4.12: Magnetophoresis Kinetics Profile with Concentrations (a) 50 mg/L, (b) 75 mg/L, (c) 125 mg/L, (d) 175 mg/L, and (e) 300 mg/L. The Solid Lines Denote the Magnetophoresis Kinetic Predicted by the Mathematical Model while Markers Denote the Experimental Result.**

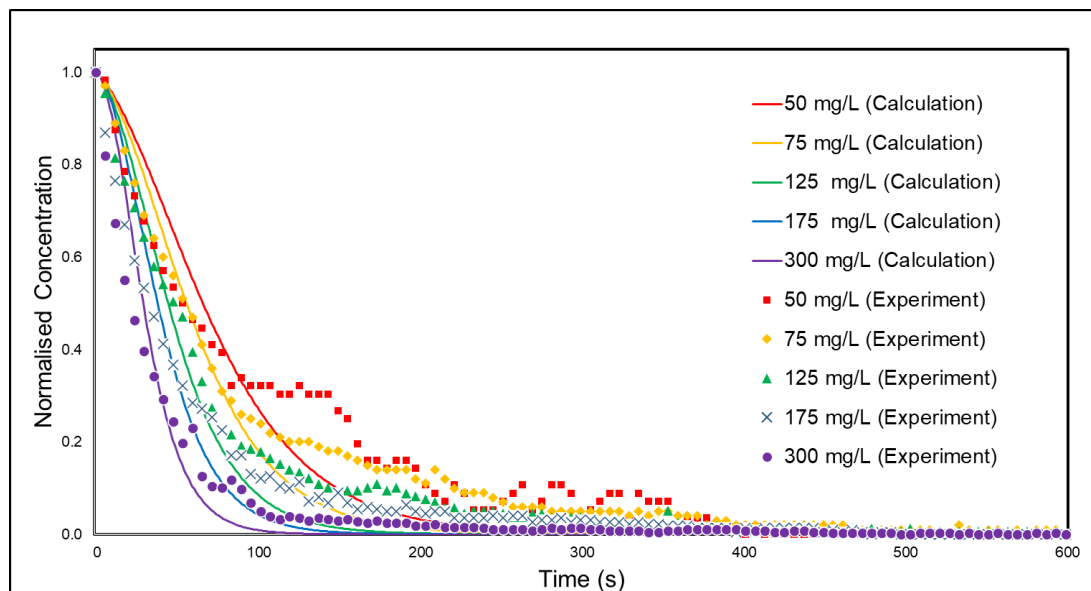


**Figure 4.13: Magnetophoresis Kinetic Profile (Normalised Concentration Against Time Graph) of MNP Solution (with Concentration 50 mg/L, 75 mg/L, 125 mg/L, 175 mg/L, 300 mg/L) Subjected to an External Magnetic Field Created by NDFeB Magnet. The Solid Lines are the Magnetophoresis Kinetic Predicted by the Mathematical Model while Markers are the Experiment Result.**

In addition, it also can be observed from the model prediction that the normalized concentration drops slower just after the initiation of magnetophoresis (with the lower slope) and it drops more rapidly after sometime (the slope become steeper). This is because MNP cluster appears as individual clusters which are subjected to slower separation at the beginning, and after being exposed to the magnetic field for a longer moment, the more aggregation processes have been completed which leads to the formation of the larger aggregate that can be separated from the solution more rapidly, this findings is consistent with the experiment data of Yavuz et al. (2006). De Las Cuevas, Faraudo and Camacho (2008) reported the same phenomom in the magnetophoresis experiment, which the separation rate is faster at higher concentraions. There, in all cases in Figure 4.11 (all concentrations), the concentration decline is slower for model predicted as compared to the experimental observation at the beginning of the magnetophoresis. After a period of time, when the concentration of magnetic species falls below a range, the separation rate resulted from

the model prediction surpasses the experimental measurement. In particular, it is obvious from Figure 4.11 that the actual experimental separation rates (with concentrations 50 mg/L, 75 mg/L, 125 mg/L, 175 mg/L, and 300 mg/L) are faster than the model prediction at the beginning of magnetophoresis. This is because, in real-life experiments, functionalized MNPs are typically stored in vials for a period of time before being subjected to the experiment. During this time, some MNPs may form aggregate, resulting in aggregates that consists of more than two magnetic species that have a higher magnetic susceptibility and experience a stronger magnetophoretic force, leading to a faster separation rate (Lim et. al, 2014). Hence, not all of the MNPs dispersed in the cuvette are individual clusters at the beginning of the experiment.

In addition, there is a more apparent discrepancy between the predicted and experimental results when the normalised concentration of the MNP solution falls below certain levels. The experiment observation shows the slower decline in the normalized concentration toward the end of the magnetophoresis. The deviations of the experimental result from the model magnetophoresis kinetic profile at 50 mg/L concentration are the most significant after the normalised concentration drop below 0.3. For the magnetophoresis experiment conducted under the higher concentrations (75 mg/L, 125 mg/L, 175 mg/L, and 300 mg/L), the noticeable deviation starts to develop after the normalised concentrations drop below 0.2. The number of magnetic species in solution is related to the normalised concentration, low normalised concentration indicates low number of magnetic species remaining in the solution. The cooperative effect is more pronounced at higher concentrations, resulting in a faster separation rate, whereas at low concentrations, this effect diminishes, becoming less significant (De Las Cuevas, Faraudo and Camacho 2008). The concentration of the MNP solution plays a critical role in the intensity of the hydrodynamic effect since the effect is influenced by the non-uniform magnetic susceptibility per unit volume, which is similar to the natural convection that arises due to the non-uniform density of the solution (Leong et al., 2015). The reason for this discrepancy is that the mathematical model accounts for cooperative and hydrodynamic effects throughout magnetophoresis. In contrast, in real experiments, when the normalised concentration drops below certain levels, the hydrodynamic and cooperative effects are weakened as there are not enough magnetic species in the solution to form these effects (the

aggregation parameter and the magnetic Grashof number are less than unity). On the one hand, Andreu et al. (2011) have identified that the cooperative effect is triggered when the dimensionless aggregation parameter exceeds unity. On the other hand, the onset criteria for the hydrodynamic effect is achieved when the dimensionless magnetic Grashof number exceeds unity (Leong et al., 2015). When the concentration of the MNP solution used in the experiment is higher, the deviation between the experimental and theoretical results is less significant. This is due to the fact that under the same normalised concentrations, higher concentration solutions have a greater number of magnetic species remaining in the solution. Consequently, the cooperative and hydrodynamic effects are more prominent in higher concentration solutions compared to lower concentration solutions, which causes the model prediction to be closer to the experimental results for magnetophoresis conducted under the higher concentration.

Moreover, Figure 4.14 illustrates the average number of MNP clusters present in a magnetic species throughout the experiment. The results indicate an initial increase in the number of clusters with time and flatten after 100 seconds for all concentrations (75 mg/L, 125 mg/L, 175 mg/L, and 300 mg/L). However, at higher concentrations, there is a higher average number of MNP clusters in a magnetic species, due to the intensive cooperative effect and aggregation of MNP clusters. This trend is consistent with the findings of De Las Cuevas, Faraudo and Camacho (2008), who also demonstrated a higher degree of cooperative effect during the magnetophoresis operated at higher concentrations. As the magnetophoresis process progresses, the number of magnetic species suspended in the solution decreases as they are captured on the collection plane. Since this is a batch process, the number of magnetic species remains constant, resulting in a reduction in the number of individual MNP clusters over time. Therefore, there are no available MNP clusters for aggregation towards the end of the magnetophoresis (such as  $t = 100$  s for this case). Another possible explanation for this phenomenon is using the concept of the surface energy, in which the aggregates of this size have reached a minimum energy state that is most favourable thermodynamically, leading to the aggregates to maintain their size in such a most stable state (Chong et al., 2020).

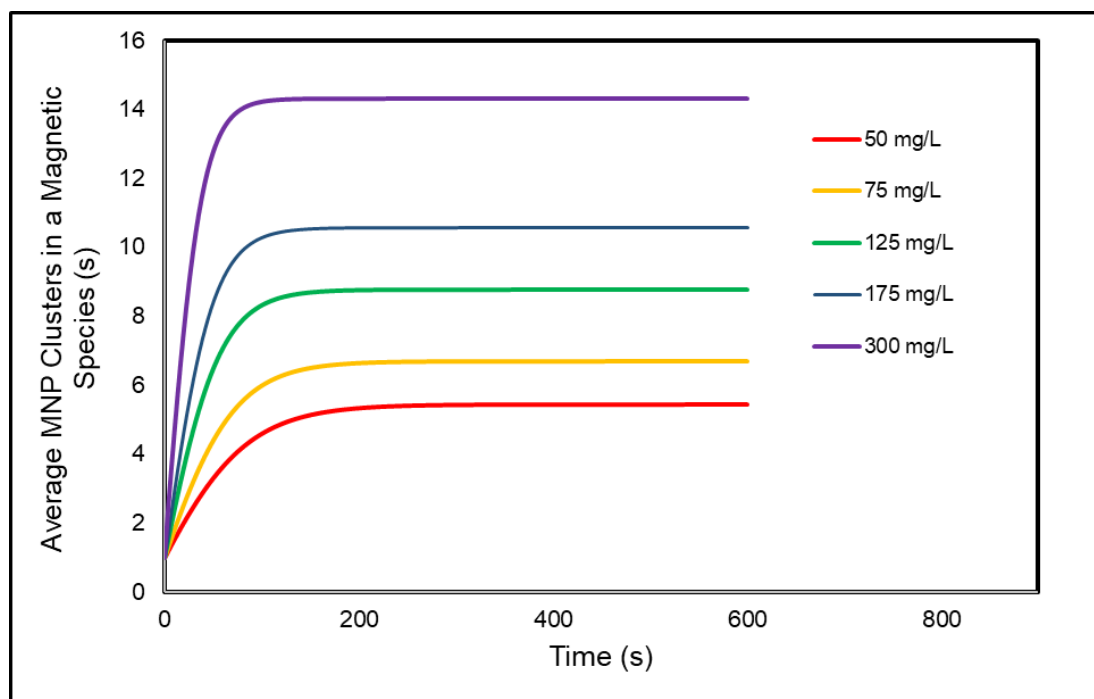


**Figure 4.14: Average MNP Clusters in a Magnetic Species.**

## CHAPTER 5

### CONCLUSION

#### 5.1 Conclusion

The ultimate goal of this project is to understand the transport mechanism of the magnetophoresis process in which cooperative and hydrodynamic effects are dominant. One of the three objectives of this article focuses on enhancing the colloidal stability of MNPs by functionalizing their surfaces with polyelectrolytes, which is serving as the model system to be used in the subsequent investigations. MNPs are naturally colloidally unstable and tend to form aggregation (Chong et al., 2020), which makes MNPs inefficient for various engineering applications such as drug delivery, magnetic resonance imaging (MRI), and environmental remediation. By coating polyelectrolytes to their surfaces, the MNPs become more stable and can resist aggregation. The colloidal stability is related to the surface interactions including electrostatic, van der Waals, and steric forces. The first stage of this research aims to identify the ideal conditions for functionalization to achieve maximum colloidal stability of the resulted MNP system by promoting physical interactions between the MNPs and polyelectrolytes (Bolívar & Gonzalez, 2018). To determine the optimal conditions for functionalization, the functionalization of MNPs was conducted under four different ratios of MNPs to PSS, which are 1:0.5, 1:1, 1:2, and 1:4. The functionalized MNP systems were subjected to sedimentation and DLS tests to assess the colloidal stability of them. The analysis showed the MNP system functionalized under the MNP to PSS ratio of 1:1 has the smallest hydrodynamic diameter and remained suspended in the solution for the longest duration. Hence, this result reveals

that the MNP to PSS ratio of 1:1 is the optimal functionalization condition that can produce MNPs that exhibit the highest colloidal stability, and the MNP system functionalized under this condition is used as the model system in the subsequent study on the magnetophoresis kinetics.

The next objective of this study is to investigate the magnetophoresis kinetic profile of the MNP solution at various concentrations. The kinetics of magnetophoresis were analysed using a self-made UV-vis spectrophotometer. The results of the experiment showed that there was a positive correlation between the concentration of the MNP solution and the separation rate. Specifically, at higher concentrations of MNPs, the separation rate was faster, indicating that the rate of magnetophoresis was influenced by the concentration of the solution. This was attributed to the stronger cooperative and hydrodynamic effects, which have a significant impact on the magnetophoresis kinetics. The experimental findings were consistent with the hydrodynamic theory proposed by Leong et al. (2015) and the cooperative theory proposed by De Las Cuevas, Faraudo and Camacho (2008), as these effects were revealed to speed up the separation rate.

Last but not least, the final objective of this study is to develop a mathematical model to predict the magnetophoresis kinetics of MNP solution of different concentrations, under the situation where both cooperative and hydrodynamic effects are dominating. The model was developed by assuming the homogeneity of the MNP solution throughout the entire magnetophoresis process owing to the overwhelming of magnetophoresis induced convection. In addition, the MNPs are assumed to undergo tip-to-tip aggregation during the magnetophoresis process. The results of the model prediction were compared with the experimental results and showed a good fit in overall, suggesting that the model was able to accurately predict the behaviour of the MNP solution subjected to magnetophoresis in which both cooperative and hydrodynamic effects are dominant.

In conclusion, the outcomes of this study have successfully achieved all the objectives proposed at the beginning of this project. The results lead to a better understanding on the transport mechanism of magnetophoresis of MNP solution under



cooperative and hydrodynamic regimes. In addition, this study also gives rise to a mathematical model that is able to predict the behaviour of magnetophoresis in this regime up to good accuracy.

## 5.2 Recommendations and Improvements

There are several recommendations to improve and further extend this research in the future:

1. There are more factors that can potentially affect the effectiveness of MNP functionalization such as temperature and functionalization duration. These factors were not investigated in the current study but can be explored in the future research to improve the effectiveness of MNP functionalization process.
2. Besides varying the particle concentration, the magnetophoresis kinetic profile of MNPs also can be evaluated under various operating conditions, such as different temperature, viscosity, and magnetic field strength. This is because these factors also have the high potential to affect the magnetophoresis kinetics of MNPs.
3. Additionally, there are several aspects of the mathematical model that could be improved in future studies. First, an important consideration is the inclusion of lateral aggregations in the model, which were not accounted for in the model developed in the current study. Lateral aggregations can occur during the experiment and can influence the behaviour of MNPs during the magnetophoresis process. Various conditions in real-life application also should be considered in developing the model to improve the accuracy of it to capture the behaviour of MNPs during magnetophoresis. This includes taking into account the complex geometries of the collection site, which may not always be a simple, rectangular shape like the surface of the cuvette used in the present study. Therefore, by incorporating more realistic factors into the model, a more robust and accurate mathematical model for the magnetophoresis kinetics can be developed for a wide range of applications.

## REFERENCES

- Adair, J., Suvaci, E. and Sindel, J., 2001. Surface and Colloid Chemistry. *Encyclopedia of Materials: Science and Technology*, pp.1-10.
- Andreu, J., Camacho, J., Faraudo, J., Benelmekki, M., Rebollo, C. and Martínez, L., 2011. Simple analytical model for the magnetophoretic separation of superparamagnetic dispersions in a uniform magnetic gradient. *Physical Review E*, 84(2).
- Andreu, J., Camacho, J. and Faraudo, J., 2011. Aggregation of superparamagnetic colloids in magnetic fields: the quest for the equilibrium state. *Soft Matter*, 7(6), p.2336.
- Akbarzadeh, A., Samiei, M. and Davaran, S., 2012. Magnetic nanoparticles: preparation, physical properties, and applications in biomedicine. *Nanoscale Research Letters*, 7(1).
- Al Harraq, A., Lee, J. and Bharti, B., 2020. Magnetic field-driven assembly and reconfiguration of multicomponent supraparticles. *Science Advances*, 6(19).
- Alfredo Reyes Villegas, V., Isaías De León Ramírez, J., Hernandez Guevara, E., Perez Sicairos, S., Angelica Hurtado Ayala, L. and Landeros Sanchez, B., 2020. Synthesis and characterization of magnetite nanoparticles for photocatalysis of nitrobenzene. *Journal of Saudi Chemical Society*, 24(2), pp.223-235.
- Bolívar, W.M. and Gonzalez, E.E. (2018) 'Study of agglomeration and magnetic sedimentation of glutathione@Fe<sub>3</sub>O<sub>4</sub> nanoparticles in water medium', *DYNA*, 85(205), pp. 19–26.

- Chong, W.H. *et al.* (2020) “Study on the enhancement of colloidal stable poly(sodium 4-styrene sulfonate) coated magnetite nanoparticles and regeneration capability for rapid magnetophoretic removal of organic dye,” *Journal of Chemical Technology & Biotechnology*, 95(12), pp. 3093–3104.
- Chung, E., Leon, L. and Rinaldi, C., 2020. *Nanoparticles for biomedical applications*. Oxford: Elsevier.
- De Las Cuevas, G., Faraudo, J. and Camacho, J., 2008. Low-Gradient Magnetophoresis through Field-Induced Reversible Aggregation. *The Journal of Physical Chemistry C*, 112(4), pp.945-950.
- Dasari, A., Xue, J. and Deb, S., 2022. Magnetic Nanoparticles in Bone Tissue Engineering. *Nanomaterials*, 12(5), p.757.
- Faraudo, J. and Camacho, J. (2009) “Cooperative magnetophoresis of superparamagnetic colloids: Theoretical aspects,” *Colloid and Polymer Science*, 288(2), pp. 207–215.
- Floyd, K., Eberly, A. and Hadjifrangiskou, M., 2017. Adhesion of bacteria to surfaces and biofilm formation on medical devices. *Biofilms and Implantable Medical Devices*, pp.47-95.
- Gubin, S., Koksharov, Y., Khomutov, G. and Yurkov, G., 2005. Magnetic nanoparticles: preparation, structure and properties. *Russian Chemical Reviews*, 74(6), pp.489-520.
- Gómez-Pastora, J. *et al.* (2022) ‘Magnetic separations’, *Particle Separation Techniques*, pp. 221–266.
- Gul, S., Khan, S., Rehman, I., Khan, M. and Khan, M., 2019. A Comprehensive Review of Magnetic Nanomaterials Modern Day Theranostics. *Frontiers in Materials*, 6.
- HEDDLE, T. (1971) ‘Electric fields’, *Calculations in Fundamental Physics*, pp. 167–186.

- Helseth, L. and Skodvin, T., 2009. Optical monitoring of low-field magnetophoretic separation of particles. *Measurement Science and Technology*, 20(9), p.095202.
- Horikoshi, S. and Serpone, N., 2013. Introduction to Nanoparticles. *Microwaves in Nanoparticle Synthesis*, pp.1-24.
- Lim, J. *et al.* (2010) ‘Magnetophoresis of nanoparticles’, *ACS Nano*, 5(1), pp. 217–226.
- Lim, J.K. *et al.* (2013) “Characterization of magnetic nanoparticle by Dynamic Light Scattering,” *Nanoscale Research Letters*, 8(1).
- Lim, J. *et al.* (2014) ‘Magnetophoresis of iron oxide nanoparticles at low field gradient: The role of Shape Anisotropy’, *Journal of Colloid and Interface Science*, 421, pp. 170–177.
- Leong, S., Ahmad, Z. and Lim, J., 2015. Magnetophoresis of superparamagnetic nanoparticles at low field gradient: hydrodynamic effect. *Soft Matter*, 11(35), pp.6968-6980.
- Leong, S., Yeap, S. and Lim, J., 2016. Working principle and application of magnetic separation for biomedical diagnostic at high- and low-field gradients. *Interface Focus*, 6(6), p.20160048.
- Leong, S., Ahmad, Z., Low, S., Camacho, J., Faraudo, J. and Lim, J., 2020. Unified View of Magnetic Nanoparticle Separation under Magnetophoresis. *Langmuir*, 36(28), pp.8033-8055.
- Langford, A., Bruchsaler, M. and Gupta, M., 2022. Suspension properties and characterization of aluminum-adjuvanted vaccines. *Practical Aspects of Vaccine Development*, pp.225-266.
- Miller, C., 1924. The Stokes-Einstein law for diffusion in solution. Proceedings of the Royal Society of London. Series A, Containing Papers of a Mathematical and Physical Character, 106(740), pp.724-749.

- Mody, V., Singh, A. and Wesley, B., 2013. Basics of magnetic nanoparticles for their application in the field of magnetic fluid hyperthermia. *European Journal of Nanomedicine*, 5(1).
- Meng, X., Ryu, J., Kim, B. and Ko, S., 2016. Application of Iron Oxide as a pH-dependent Indicator for Improving the Nutritional Quality. *Clinical Nutrition Research*, 5(3), p.172.
- Mohammed, L., Gomaa, H., Ragab, D. and Zhu, J., 2017. Magnetic nanoparticles for environmental and biomedical applications: A review. *Particuology*, 30, pp.1-14.
- Munaz, A., Shiddiky, M. and Nguyen, N., 2018. Recent advances and current challenges in magnetophoresis based micro magnetofluidics. *Biomicrofluidics*, 12(3), p.031501.
- Nikam, D.S. *et al.* (2014) 'Colloidal stability of polyethylene glycol functionalized  $\text{Co}_0.5\text{Zn}_0.5\text{Fe}_2\text{O}_4$  nanoparticles: Effect of pH, sample and salt concentration for hyperthermia application', *RSC Advances*, 4(25), p. 12662.
- Novák, P. and Havlíček, V., 2016. Protein Extraction and Precipitation. *Proteomic Profiling and Analytical Chemistry*, pp.51-62.
- Patel, S., Patel, M., Patel, A., Chougule, M. and Choudhury, H., 2018. Solid Lipid Nanoparticles for Targeted Brain Drug Delivery. *Nanotechnology-Based Targeted Drug Delivery Systems for Brain Tumors*, pp.191-244.
- Piacenza, E., Presentato, A. and Turner, R., 2018. Stability of biogenic metal(loid) nanomaterials related to the colloidal stabilization theory of chemical nanostructures. *Critical Reviews in Biotechnology*, 38(8), pp.1137-1156.
- Ramos, A.P. (2017) 'Dynamic light scattering applied to nanoparticle characterization', *Nanocharacterization Techniques*, pp. 99–110.

- Savliwala, S., Chiu-Lam, A., Unni, M., Rivera-Rodriguez, A., Fuller, E., Sen, K., Threadcraft, M. and Rinaldi, C., 2020. Magnetic nanoparticles. *Nanoparticles for Biomedical Applications*, pp.195-221.
- Taira, S. *et al.* (2009) 'Functionalized magnetic nanoparticles as an in vivo delivery system', *Micro and Nano Technologies in Bioanalysis*, pp. 571–587.
- Teague, J., Allen, M. and Scott, T., 2018. The potential of low-cost ROV for use in deep-sea mineral, ore prospecting and monitoring. *Ocean Engineering*, 147, pp.333-339.
- Tan, Y.W. *et al.* (2022) "Low-gradient magnetic separation of magnetic nanoparticles under continuous flow: Experimental Study, Transport Mechanism and Mathematical Modelling," *ELECTROPHORESIS*, 43(21-22), pp. 2234–2249.
- Wilczewska, A., Niemirowicz, K., Markiewicz, K. and Car, H., 2012. Nanoparticles as drug delivery systems. *Pharmacological Reports*, 64(5), pp.1020-1037.
- Wakayama, N.I. (1997) 'Magnetic buoyancy force acting on bubbles in nonconducting and diamagnetic fluids under microgravity', *Journal of Applied Physics*, 81(7), pp. 2980–2984.
- Yeap, S., Ahmad, A., Ooi, B. and Lim, J., 2012. Electrosteric Stabilization and Its Role in Cooperative Magnetophoresis of Colloidal Magnetic Nanoparticles. *Langmuir*, 28(42), pp.14878-14891.
- Yeap, S.P. *et al.* (2014) "On size fractionation of iron oxide nanoclusters by low magnetic field gradient," *The Journal of Physical Chemistry C*, 118(41), pp. 24042–24054.
- Yeap, S., Lim, J., Ooi, B. and Ahmad, A., 2017. Agglomeration, colloidal stability, and magnetic separation of magnetic nanoparticles: collective influences on environmental engineering applications. *Journal of Nanoparticle Research*, 19(11).

Yang, Y., Chawla, A., Zhang, J., Esa, A., Jang, H. and Khademhosseini, A., 2019. Applications of Nanotechnology for Regenerative Medicine; Healing Tissues at the Nanoscale. *Principles of Regenerative Medicine*, pp.485-504.

## APPENDIX

### SECTION A

#### Calculation of Aggregation Parameter and Magnetic Grashof Number

The saturation magnetization value,  $M_s$ , of bare MNPs and PSS-functionalized-MNPs are 70.41 emu/g and 69.48 emu/kg, respectively (Tan et al., 2022). It is justifiable to rely on the findings of this study because the magnetic nanoparticles used in the research were obtained from the same manufacturer and functionalized with PSS coating and similar hydrodynamic diameter (around 250 nm). Additionally, the PSS content in the magnetic nanoparticles was only about 1 percent, which had minimal impact on the degree of magnetization. Assuming that the magnetic response of PSS-functionalized-MNPs is solely due to the presence of MNPs and not PSS, the mass fraction of MNPs in PSS-functionalized-MNPs can be calculated using the following method:

Mass fraction of MNP in PSS-functionalized-MNPs cluster:

$$\begin{aligned} \text{mass fraction of MNP} &= \frac{69.48 \frac{\text{emu}}{\text{kg}}}{70.41 \frac{\text{emu}}{\text{kg}}} \times 100\% \\ &= 98.68 \text{ wt}\% \end{aligned}$$

Mass fraction of PSS in PSS-functionalized-MNPs cluster = 100 – 98.68

$$\text{mass fraction of PSS} = 100 - 98.68$$



$$= 1.32 \text{ wt}\%$$

Let assume the packing factor of the MNP clusters (spherical in shape) is 0.74 (only 74 vol% of the cluster is occupied by MNP and PSS), The density of the particle is assumed to be following the density of magnetite, which is given by  $5180 \text{ kg/m}^3$  and the density of MNP is  $5180 \text{ kg/m}^3$  and density of PSS is  $810 \text{ kg/m}^3$ . The volume fraction of MNPs in the cluster can be calculated:

Volume fraction of MNP in PSS-functionalized-MNPs cluster

$$\begin{aligned} & \frac{\frac{0.9868}{5180 \frac{\text{kg}}{\text{m}^3}}}{\frac{0.9868}{5180 \frac{\text{kg}}{\text{m}^3}} + \frac{0.0132}{810 \frac{\text{kg}}{\text{m}^3}}} \times 0.7 \\ & = 0.6820 \end{aligned}$$

Due to same materials (PSS and nano powders) are employed for the experiment, the value of volume fraction of a MNP reported by the literature (Tan et al., 2022) should be almost similar to this study. Therefore, it can be concluded that the volume fraction of MNPs for this study is approximately 0.6820.

### **Aggregation Parameter, $N^*$**

Based on the Dynamic Light Scattering (DLS) result, a hydrodynamic diameter of  $D_{h,0} = 276 \text{ nm}$  was selected for the PSS-functionalized-MNPs with a MNP to PSS ratio of 1:1.

Volume of MNP in one PSS-functionalized-MNPs cluster,  $V$

$$\begin{aligned} & = \frac{\pi D_{h,0}^3}{6} \times 68.20\% \\ & = \frac{\pi (276 \times 10^{-9})^3}{6} \times 0.6820 \\ & = 7.5077 \times 10^{-21} \text{ m}^3 \end{aligned}$$

Mass of MNP in one PSS-functionalized-MNPs cluster,  $m_p$

$$\begin{aligned}
&= 7.5077 \times 10^{-21} m^3 \times 5180 \text{ kg}/m^3 \\
&= 3.8890 \times 10^{-17} \text{ kg}
\end{aligned}$$

The dimension of magnet used in the experiment is: radius,  $r = 0.75$  cm and height,  $h = 2$  cm. Therefore, at the surface of the magnet ( $y = 0$ ),

$$\begin{aligned}
B &= \frac{B_r}{2} \left[ \frac{y + h_{mag}}{\sqrt{(y + h_{mag})^2 + r_{mag}^2}} - \frac{y}{\sqrt{y^2 + r_{mag}^2}} \right] \\
&= \frac{1.45}{2} \left[ \frac{0 + 0.02}{\sqrt{(0 + 0.02)^2 + 0.0075^2}} - \frac{0}{\sqrt{0^2 + 0.0075^2}} \right] \\
&= 0.6788 \text{ T} \\
H &= \frac{B}{\mu_0} = \frac{0.6788}{1.257 \times 10^{-6}} = 5.40 \times 10^5 \text{ A}/m
\end{aligned}$$

Then, the magnetic dipole moment carried by one PSS-functionalized-MNPs cluster is with the saturation magnetization value,  $M_s$ , of pure MNP is 70.41 emu/g:

$$\begin{aligned}
m_o &= m_p M_{p,m} \\
&= (3.8890 \times 10^{-17}) \left( 70.41 \text{ A} \cdot \frac{m^2}{kg} \right) \\
&= 2.9016 \times 10^{-15} \text{ A m}^2
\end{aligned}$$

Finally, the aggregation parameter  $N^*$  of MNP solution at concentration of 50 mg/L at ambient temperature can be computed as follows:

$$\begin{aligned}
\Gamma &= \frac{\mu_0 m_o^2}{2\pi D_{h,0}^3 k_B T} \\
&= \frac{1.257 \times 10^{-6} \times (2.9016 \times 10^{-15})^2}{2\pi \times (276 \times 10^{-9})^3 \times 1.381 \times 10^{-23} \times 298} \\
&= 19467
\end{aligned}$$

$$\phi_0 = \frac{c}{\rho_p} = \frac{0.05}{51800.6820} = 1.4153 \times 10^{-5}$$

$$\begin{aligned}
N^* &= \sqrt{\phi_0 e^{\Gamma-1}} \\
&= \sqrt{(1.4153 \times 10^{-5}) e^{12167-1}} \\
&= 1.3195 \times 10^{2638}
\end{aligned}$$

The extremely huge value of  $N^*$  indicates that the MNP system employed in this study is indeed a cooperative system with remarkable aggregation effect, which has been considered in the modelling of the magnetic separation process.

### Magnetic Grashof Number, $Gr_m$

The formula of the magnetic Grashof number is given as the following equation:

$$Gr_m = \frac{\nabla B (\partial M_{(m)} / \partial c)_H (c_s - c_\infty) L_c^3}{\rho_f \eta_k^2}$$

The dimension of magnet used in the experiment is: radius,  $r = 0.75$  cm and height,  $h = 2$  cm. Using a step size of 0.001, which is at ( $y = 0.001$  m),

$$\begin{aligned}
B &= \frac{B_r}{2} \left[ \frac{y + h_{mag}}{\sqrt{(y + h_{mag})^2 + r_{mag}^2}} - \frac{y}{\sqrt{y^2 + r_{mag}^2}} \right] \\
&= \frac{1.45}{2} \left[ \frac{0.001 + 0.02}{\sqrt{(0.001 + 0.02)^2 + 0.0075^2}} - \frac{0.001}{\sqrt{0.001^2 + 0.0075^2}} \right] \\
&= 0.5869 \text{ T} \\
\nabla B &= \left| \frac{0.5869 - 0.6788}{0.001} \right| \\
&= |-91.86| \\
&= 91.86 \frac{\text{T}}{\text{m}}
\end{aligned}$$

Then, at the surface of the magnet, MNPs are assumed at their saturation magnetization, thus, the value of  $\partial M_{(m)}/\partial c$  is 70.41 A m<sup>2</sup>/kg. Besides, at the beginning of the experiment, the concentration at the surface of the collection plane  $c_s$  is assumed to be zero. The density solution and the kinematic viscosity of solution are 1000 kg/m<sup>3</sup> and 0.000001 m/s<sup>2</sup>. The characterization length  $L_c$  can be calculated by the following equation:

$$\begin{aligned} L_c &= \frac{\text{Area of the cuvette surface}}{\text{Perimeter of the cuvette surface}} \\ &= \frac{0.0001296 \text{ m}^2}{0.04 \text{ m}} \\ &= 3.24 \times 10^{-3} \text{ m} \end{aligned}$$

Thus, the magnetic Grashof number of MNP solution at concentration of 50 mg/L at ambient temperature can be computed as follows:

$$\begin{aligned} Gr_m &= \frac{(91.86)(70.41)(0 - 0.05)(3.24 \times 10^{-3})^3}{(1000)(0.000001)^2} \\ &= |-10999.32| \\ &= 10999.32 \end{aligned}$$

The value of the magnetic Grashof number is far larger than unity, indicating that the presence of hydrodynamic effect during the experiment.

## SECTION B

### Magnetophoresis Kinetic Profile Calculation

The MNPs used in this experiment was magnetite nanopowders purchased from Nanostructured & Amorphous Materials, Inc. The particles were spherical in shape with mean diameter of ~30 nm and synthesized via wet chemistry method. MNPs were functionalised and diluted in deionized (DI) water to prepare MNP solutions with different concentrations. PSS were coated on the surface of MNPs during the functionalised process, therefore, the MNPs particle core size is larger than pure MNPs, which is about 276 nm as measured by dynamic light scattering (DLS). Based on the DLS data, the magnetic cluster with hydrodynamic size of 276 nm is the smallest magnetic species which can be found in the MNP solution at the beginning of the experiment, assuming there is no aggregation of MNP clusters (It should be reminded that it is difficult to find individual particle with diameter of 30 nm in the solution since almost all particles have been functionalised by PSS permanently during the synthesise process). Therefore, it should be emphasised that the term ‘individual MNPs’ represents the particle cluster in the suspension before undergoing further aggregation and magnetophoresis which has hydrodynamic diameter of 276 nm. Here, we can calculate the magnetic dipole moment of individual particle  $m_0 = 2.9016 \times 10^{-15} \text{ A m}^2$ . The volume of MNPs solution used is fixed at 3 mL for all concentration range, thus,  $V = 3 \text{ mL} = 3 \times 10^{-6} \text{ m}^3$ .

For  $c$  mg/L of MNPs solution, there are  $(x \times \frac{10^{-6} \text{ kg}}{1 \text{ mg}} \times \frac{1 \text{ L}}{10^{-3} \text{ m}^3} = 10^{-3}x)$  kg of MNPs in  $1 \text{ m}^3$  of solution. Hence, the number of individual particles in  $1 \text{ m}^3$  of  $x$  mg/L MNPs solution is given by particles per  $\text{m}^3$  of solution. Since the volume of MNPs solution subjected to magnetophoresis in this experiment was fixed at 3 mL (or

$3 \times 10^{-6} \text{ m}^3$ ), the initial number of individual MNP clusters within the solution with concentration of  $x \text{ mg/L}$  can be computed by:

$$n_o = \frac{(c)(10^{-3})(V)}{m_p} = \frac{c(10^{-3})(3 \times 10^{-6})}{(3.8890 \times 10^{-17})(3 \times 10^{-6})} = 2.5714 \times 10^{13} \text{ } c \text{ particles}$$

Here,  $n_o(t = 0) = n(t = 0)$  because all magnetic species exist as individual particles at the beginning of experiment before particle aggregation taking place. Also, the fraction of successful aggregation  $Z$  is taken as 0.01 (1%) as it can be fixed into our experimental result.

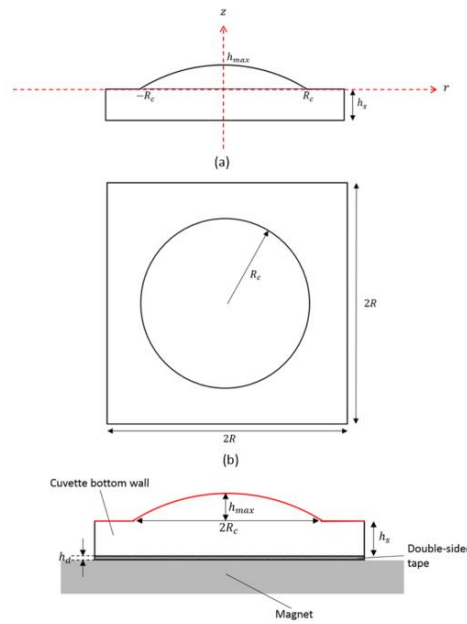


**Figure A: Surface of the Collection Plane at Different Point of View (Leong et al., 2017).**

According to (Leong et al., 2017) calculation, the area of MNPs collection plane  $A_s$  was taken as  $1.2696 \text{ cm}^2$  and average magnetic field gradient on the collection plane  $\left. \frac{\partial B}{\partial z} \right|_{z=0}$  was  $91.86 \text{ T/m}$ . The average velocity  $\bar{v}$  of the magnetic species was assumed as  $5 \times 10^{-5} \text{ m/s}$ , which is the approximation for the magnitude of convective flow within MNPs solution subjected to magnetophoresis according to the COMSOL simulation reported by (Leong et. al., 2015).

After defining the value of all parameters, Equations (4.23) and (4.24) were solved numerically by using EXCEL. A time interval of 1 second was applied in the differential equation calculations, which provided us with reliable result. Decreasing the step size beyond this point did not significantly alter the result, indicating that our level of accuracy was adequate. The simulation was done by the magnetophoresis of the MNPs solution with the following concentrations: 25 mg/L, 75 mg/L, 125 mg/L, 175 mg/L and 300 mg/L.